

**UNCLASSIFIED**

**260955**

**AD**

**DEFENSE DOCUMENTATION CENTER**

**FOR**

**SCIENTIFIC AND TECHNICAL INFORMATION**

**CAMERON STATION, ALEXANDRIA, VIRGINIA**



**UNCLASSIFIED**

NOTICE: When government or other drawings, specifications or other data are used for any purpose other than in connection with a definitely related government procurement operation, the U. S. Government thereby incurs no responsibility, nor any obligation whatsoever; and the fact that the Government may have formulated, furnished, or in any way supplied the said drawings, specifications, or other data is not to be regarded by implication or otherwise as in any manner licensing the holder or any other person or corporation, or conveying any rights or permission to manufacture, use or sell any patented invention that may in any way be related thereto.

WADC TECHNICAL REPORT 58-343  
VOLUME II

260955

CATALOGED BY ASTIA  
AS AD No. \_\_\_\_\_

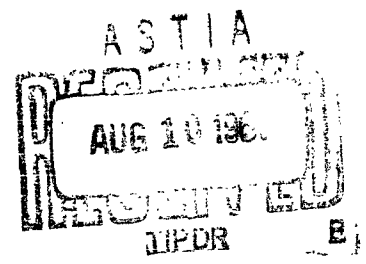
# METHODS OF SPACE VEHICLE NOISE PREDICTION

*Peter A. Franken*  
and

*The Staff of Bolt Beranek and Newman Inc.*

XEROX

SEPTEMBER 1960



WRIGHT AIR DEVELOPMENT DIVISION

## NOTICES

When Government drawings, specifications, or other data are used for any purpose other than in connection with a definitely related Government procurement operation, the United States Government thereby incurs no responsibility nor any obligation whatsoever; and the fact that the Government may have formulated, furnished, or in any way supplied the said drawings, specifications, or other data, is not to be regarded by implication or otherwise as in any manner licensing the holder or any other person or corporation, or conveying any rights or permission to manufacture, use, or sell any patented invention that may in any way be related thereto.



Qualified requesters may obtain copies of this report from the Armed Services Technical Information Agency, (ASTIA), Arlington Hall Station, Arlington 12, Virginia.



This report has been released to the Office of Technical Services, U. S. Department of Commerce, Washington 25, D. C., for sale to the general public.



Copies of WADD Technical Reports and Technical Notes should not be returned to the Wright Air Development Division unless return is required by security considerations, contractual obligations, or notice on a specific document.

WADC TECHNICAL REPORT 58-343  
VOLUME II

## **METHODS OF SPACE VEHICLE NOISE PREDICTION**

*Peter A. Franken*  
*and*  
*The Staff of Bolt Beranek and Newman Inc.*

*SEPTEMBER 1960*

Flight Dynamics Laboratory  
Contract No. AF33(616)-6217  
Project No. 1370  
Task No. 13786

WRIGHT AIR DEVELOPMENT DIVISION  
AIR RESEARCH AND DEVELOPMENT COMMAND  
UNITED STATES AIR FORCE  
WRIGHT-PATTERSON AIR FORCE BASE, OHIO

## FOREWORD

This report was prepared for the Flight Dynamics Laboratory, Wright Air Development Division, Wright-Patterson Air Force Base, Ohio. The research and development work was accomplished by Bolt Beranek and Newman Inc., Cambridge, Massachusetts, and Los Angeles, California, under Air Force Contract No. AF33(616)-6217, Project No. 1370, "Dynamic Problems in Flight Vehicles," Task No. 13786, "Methods of Noise Prediction Control and Measurement." Mr. D. L. Smith of the Dynamics Branch, Flight Dynamics Laboratory, Aeromechanics Division, Directorate of Advanced Systems Technology, is Task Engineer. This report is denoted Volume II, following WADC TR 58-343, "Methods of Flight Vehicle Noise Prediction." This report is intended as a critical summary of practical information now available, and an investigation of problems not reported in the existing literature. It is anticipated that this report will be revised as newer methods and procedures are developed. The work which was initiated in May 1957 will, therefore, continue.

Major contributions to this report were made by Drs. I. Dyer, M. A. Heckl, E. M. Kerwin, Jr., and E. E. Ungar, of Bolt Beranek and Newman Inc. This assistance is gratefully acknowledged.

WADC TR 58-343  
Volume II

## ABSTRACT

Possible sources of noise in space vehicles are reviewed. Information is summarized describing the various fluctuating pressure fields that may exist at the vehicle exterior. The response of the vehicle structure to these pressure fields and the resulting radiation of noise to the internal spaces are studied analytically. The need for new theoretical and experimental knowledge in specific areas is emphasized.

The effects of rocket engine noise on communication and hearing are considered in detail. General comments are made concerning vehicle and equipment design for noise control.

## PUBLICATION REVIEW

This report has been reviewed and is approved.

FOR THE COMMANDER:

*for*   
JOHN P. TAYLOR  
Colonel, USAF  
Chief, Flight Dynamics Laboratory

iii

WADC TR 58-343  
Volume II

## TABLE OF CONTENTS

<u>Section</u>	<u>Page</u>
INTRODUCTION TO VOLUME II . . . . .	182
VI. NOISE SOURCES . . . . .	186
A. Rocket Engine Noise . . . . .	186
1. Test Stand Operation . . . . .	186
2. Effects of Forward Motion . . . . .	190
3. In-Silo Operation . . . . .	191
4. Correlation Properties of Rocket Noise . . . . .	193
APPENDIX TO VI A -- EFFECTS OF MOTION ON WAVE PROPAGATION . . . . .	195
B. Pressure Fluctuations in a Turbulent Boundary Layer . . . . .	198
1. Spectrum Shape and Characteristic Dimensions for Subsonic Boundary Layers . . . . .	198
2. Roughness-Induced Noise . . . . .	200
3. Supersonic Boundary Layers . . . . .	202
4. Summary . . . . .	203
C. Wake Noise . . . . .	204
D. Base Pressure Fluctuations . . . . .	207
E. Oscillating and Moving Shocks . . . . .	210
F. Flow Over Cavities . . . . .	214
G. Flight Through a Turbulent Atmosphere . .	216
1. Subsonic Flight Speeds . . . . .	216
2. Supersonic Flight Speeds . . . . .	218
3. Retro-rocket Turbulence . . . . .	220
H. Pressure Due to Micro-Meteorite Impacts .	221
I. Discussion . . . . .	223

TABLE OF CONTENTS

<u>Section</u>	<u>Page</u>
VII. STRUCTURAL RESPONSE . . . . .	225
A. Response of Plates to Moving Shocks . . .	226
1. Shock Moving at Constant Velocity . .	228
2. Sinusoidally Oscillating Shock . . .	232
B. Response of Plates to Temporally Random Pressure Fields: Atmospheric Turbulence, Rocket Noise . . . . .	234
1. Response to Atmospheric Turbulence .	234
2. Response to Sound . . . . .	237
a. Response of Resonant Structures to Sound . . . . .	237
b. Sound Transmission Through Finite Cylinders . . . . .	238
C. Response of Plates to Pressures That Are Random in Space and Time . . . . .	241
1. General Solution . . . . .	242
2. Response to Boundary Layer Pressure Fluctuations . . . . .	243
a. Response at Coincidence . . . . .	245
b. Response Below and Above Coincidence . . . . .	247
3. Response to Micro-Meteorites . . . . .	248
VIII. NOISE IN INTERNAL SPACES . . . . .	255
A. Structural Radiation and Acoustic Damping . . . . .	256
1. "Equivalent" Transmission Loss . . .	258
2. Sound Radiation and Structural Damping . . . . .	259
B. Ventilation Noise Within Space Vehicles .	261



TABLE OF CONTENTS

<u>Section</u>	<u>Page</u>
IX. THE EFFECTS OF NOISE ON MAN: NUMERICAL	
EXAMPLE . . . . .	267
A. Example -- Space Vehicle Noise Levels . .	268
B. Effects of Noise on Communication . . . .	272
1. Intelligibility of Received Speech	
During Launch . . . . .	273
2. Intelligibility of Transmitted	
Speech During Launch . . . . .	275
3. Temporary Threshold Shift Following	
Subsonic Boost . . . . .	276
C. Hearing Damage Risk . . . . .	276
X. DESIGN CONSIDERATIONS . . . . .	279
REFERENCES FOR VOLUME II . . . . .	285
ERRATA IN VOLUME I . . . . .	291
ILLUSTRATIONS - FIGURE 75 THROUGH 118	293

## LIST OF FIGURES

<u>Figure</u>	<u>Title</u>
75	Source Location as a Function of Strouhal Number
76	Geometry for Rocket-Deflector Configuration
77	Correction for Changes in Ambient Temperature and Pressure
78	Reference Free Field Sound Pressure Level at Missile
79	Sound Pressure Level Change as a Function of Mach Number
80	Change in Sound Pressure Level of Large Rockets
81	Differences Between Highest Noise Levels in Unlined I-Tube Silo and Above Ground
82	Differences Between Highest Noise Levels in Launch Duct of Unlined Double-U Silo and Above Ground
83	Angular Correlation Around Missile
84	Effects of Forward Motion: Source and Receiver Geometry
85	Effects of Forward Motion: Changes in Angle and Observed Wavelength
86	Effect of Forward Motion on Near-Field Sound Pressure Level Contours of Contemporary Turbojet Engine
87	Boundary Layer Turbulence Spectra
88	Velocity Fluctuations in Supersonic Boundary Layers
89	Qualitative Comparison of Noise Radiation from a Jet and from a Wake
90	Measured Acoustic Power of F-100 Aircraft in Flight (Reference 6.13)

## LIST OF FIGURES

<u>Figure</u>	<u>Title</u>
91	Sketch of Flow in a Supersonic Wake
92	Typical Static Pressure Distribution over a Supersonic Vehicle
93	Frequency of Shock Oscillations on Spiked Bodies (Reference 6.23)
94	Frequency of Sound Radiated in Cavity Flow (Reference 6.26)
95	Plate Subject to Discontinuous Pressure
96	Steady and Varying Pressure Distributions
97	Proposed Shape of Random or Grazing Incidence Transmission Loss of Cylinder (Broad-Band Noise Excitation)
98	Characteristic Transmission Loss and Radial Resonance Frequency of Cylindrical Steel or Aluminum Shells
99	Radiation Factor for Travelling Waves on an Infinite Plate
100	Radiation Factor for Travelling Waves on a Finite Plate
101	Effect of Fluid Flow on Radiation Factor for Standing Waves on an Infinite Plate
102	Fan Noise Spectra
103	End Reflection Loss at the Open End of Square Ducts
104	Grille Noise for Core Area of 1 Square Foot
105	Relative Sound Pressure Level in a Room
106	"Free Space" Rocket Noise Levels at Launch

## LIST OF FIGURES

<u>Figure</u>	<u>Title</u>
107	Detail of Double Wall Construction in Example
108	Double Wall Resonance Frequency
109	$TL_0$ for Panels near and Above the Coincidence Frequency, $f_c$
110	Approximate Transmission-Loss Increase ( $\Delta TL$ ) Due to Acoustical Blankets
111	$C_2$ , Correction to $TL_0$ for Maximum Effect of Standing Waves in Medium-Sized Receiving Space
112	$C_3$ , Correction to $TL_0$ for Reverberation in Large Receiving Spaces
113	Noise Reduction of Double Wall in Example (See Figure 107 for Wall Detail)
114	Intelligibility of Received Speech During Boost
115	Intelligibility as a Function of Articulation Index
116	Noise Attenuation of Present-Day High-Altitude Helmet, Headset Cushion and Differential Microphone
117	Intelligibility of Transmitted Speech During Boost
118	Hearing Damage Risk During Boost

## INTRODUCTION TO VOLUME II

The present report is denoted Volume II, following WADC TR 58-343, "Methods of Flight Vehicle Noise Prediction." The numbering system of pages, figures, equations, and sections started in TR 58-343 is continued in this report. Although this procedure may be somewhat unconventional, it serves to emphasize to the reader the interdependence of the material in the two volumes and should avoid possible confusion arising from duplication of numbers.

This report is not intended to be either a collection of engineering formulas or an exhaustive detailed report of results available in the literature. Rather, the report is intended as a critical summary of practical information now available, and an investigation of problems not reported in the existing literature. An important feature of this report is the assembly of general analytical formalisms useful in studying the response of structures to various forcing fields, and the reradiation of noise by the excited structures.

The general procedure for determining noise in space vehicles may be summarized as follows:

1. Describe the forcing field.
2. Calculate the structural response.
3. Determine the internal noise.

Review of the incomplete information now available indicates that four potential sources of noise in space vehicles appear predominant:

1. Rocket engine noise
2. Flow noise (turbulence in boundary layers, wakes, and cavity flow)

3. Separation and staging transients
4. Mechanical equipment

Under certain circumstances, moving shocks and wake noise may become significant sources, but no definite experimental evidence of the importance of these sources exists.

Table A is an index to the source and response information contained in this report:

TABLE A

		Source Data	Response Calculation
Primary Sources	Rocket Engine Noise	VI A	III (Plates) VII B 2 (Cylinders)
	Boundary Layer Turbulence	VI B	VII C 2
	Base Turbulence	VI D	VII C 3
	Cavity Flow Fluctuations	VI F	VII C 3 (Turbulence)
	Staging Transients	VI A (silos) ignition)	
	Mechanical Equipment	II C VIII B	VII A
	Moving Shocks	VI E	VII A
	Wake Noise	VI C	III (Plates) VII B 2 (Cylinders)
	Atmospheric Turbulence	VI G	VII B 1
	Micro-meteorites	VI H	VII C 3

In addition to the sources listed in Table A, engine vibrations and unsteady thermal stresses could under some circumstances become noise sources. These subjects have not been studied in this report.

Study of this source and response information shows that at present theory is often idealized and that experimental results are often incomplete. Many important questions remain to be answered, and definitive prediction procedures cannot be formulated. It is important that these uncertainties be emphasized, so that predictions based on current information are interpreted properly.

In order to determine the internal noise, two steps are required. First, the mean square velocity of the surface bounding the region of interest is converted into a mean square pressure radiated into a perfectly absorbing space. This step is described in Part A of Section VIII. Then the mean square internal pressure is adjusted to account for geometry and absorption, as described in Section IV.

Certain material in Volume I (Sections I - V) has been replaced by more current and complete information in the present volume. Table B lists these replacements.

TABLE B

Subject	Part of Volume I Replaced	Part of Volume II Containing Replacement
Rocket engine noise	II A 4	VI A
Effects of forward motion on jet noise	II A 5	VI A (Appendix)
Boundary layer noise	II B 1	VI B
Atmospheric turbulence	II B 2	VI G

A list of minor errata in Volume I is given at the end of the present volume. Errata are not listed for those parts of Volume I that are being replaced.

References are numbered serially within each Section and are listed following Section X.

SECTION VI  
NOISE SOURCES

A. Rocket Engine Noise

Section II presented a procedure for estimating rocket engine noise along a vehicle surface. On the basis of new and improved information that has become available since the preparation of Section II, these procedures have been revised and up-dated. In addition to test stand and in-flight operation, the material has been extended to cover in-silo operation. Some comments on the correlation of noise at different positions on a vehicle surface are also included.

1. Test Stand Operation

The sound pressure level\* in octave bands over the surface of a rocket-powered vehicle during static firing on a test stand is given by:

$$\text{SPL} = 10 \log \frac{1}{2} \text{mv}^2 + \text{SPL}_0 - 20 \log R - \Delta B \quad (87)$$

where  $1/2 \text{mv}^2$  is the mechanical stream power of the rocket exhaust in watts,  $\text{SPL}_0$  is the reference sound pressure level in an octave band for R equal to 1 foot, R is the distance from the point in question on the vehicle surface to the noise source location in the jet stream, and  $\Delta B$  is the correction for ambient conditions.

The various steps in the procedure to determine SPL in octave bands from the above equation are summarized as follows:

---

\* Sound pressure level is defined as

$$\text{SPL} = 20 \log_{10} \frac{p}{p_0} \quad \text{db}$$

where p is the rms sound pressure in microbars, and  $p_0$  is the reference sound pressure of 0.0002 microbar.

1. Compute the mechanical stream power of the rocket, which is given by  $1/2 mv^2$  in watts, where  $m$  is the mass flow of the rocket and  $v$  is the expanded jet velocity, the ratio of thrust to mass flow. In MKS units,  $m$  is in kilograms/second and  $v$  is in meters/second.
  
2. Find the average source distance  $x_0$ , which is the distance from the rocket nozzle to the average location of the noise source of frequency  $f$ . For a rocket nozzle of diameter  $D$ , the average source distance in terms of  $x_0/D$  is given as a function of Strouhal number  $\frac{fD}{v}$  by the lower curve in Figure 75. This curve applies for a vehicle mounted vertically firing into a bucket deflector that is open at the two ends only and located approximately 15 feet below the rocket nozzle.

Data are also available for a vehicle-deflector configuration where the deflector was located approximately 40 feet from the rocket nozzle and was an open curved scoop. Except for the higher values of Strouhal number, it is seen that the source distance  $x_0$  for this latter configuration is 3 to 5 times greater. Indications are that the nozzle-deflector distance a may appreciably influence the noise generation in the jet stream, and consequently affect the location of the noise sources. We suggest the use of the lower curve in Figure 75, since it will give results that are conservative for most practical vehicle-deflector configurations.

3. Compute the source-to-receiver distance  $R$  appropriate to the geometry (see Figure 76). For cases in which the exhaust stream extends directly back of the vehicle along the longitudinal axis of the vehicle, or where  $x_0$  is less than  $a$ :

$$R = x + x_0 \quad (88)$$

where  $x$  is the distance from the rocket exhaust nozzle plane to the observation point, and  $x_0$  has been obtained in Step 2 above.

When  $x_0$  is greater than  $a$ , i.e., downstream from the deflector,  $R$  is given as follows:

$$R = [(x + a)^2 + (x_0 - a)^2]^{1/2} \quad (89)$$

4. Determine the correction for ambient temperature and pressure changes,  $\Delta B$ , from Figure 77. (This is Figure 32 of Volume I, repeated here for convenience.)  $\Delta B = 0$  db for the reference conditions of  $520^\circ$  R and 14.7 pounds/sq. in.
5. Determine the reference free field sound pressure level,  $SPL_0$ , in octave bands from Figure 78.  $SPL_0$  is given as a function of the Strouhal number,  $\frac{fD}{v}$ .
6. Combine the results of Steps 1 through 5 in Equation (87) to obtain the sound pressure level in octave bands that would exist at the point in question in the absence of a rigid surface. If the levels actually existing at the external surface of the vehicle are

desired, these levels should be increased by approximately 6 db in the frequency range given by:

$$\frac{fD}{v} \geq \frac{c_a D}{\pi v D_{veh}} \quad (90)$$

where  $c_a$  is the ambient speed of sound and  $D_{veh}$  is the vehicle diameter. At lower frequencies, there is no pressure doubling effect, and hence no correction to be applied.

Several workers have suggested on physical grounds that the velocity appearing in the Strouhal number (see Steps 2 and 5) should be  $c_a$  rather than  $v$ . At present, this choice cannot be clearly resolved.

It was suggested in Section II that the broadness of the rocket noise spectrum may be due to the presence of multiple nozzle configurations usually found in large vehicles. However, noise spectra from single-engine (4 ft in diameter) firings are just as broad as data from a rocket with two nozzles, each about 4 ft in diameter, spaced 10 ft on centers. These results suggest that rocket noise may be inherently broader in spectrum shape than turbojet noise, although more comparative data on single- and multiple-nozzle operations should be gathered to clarify this situation. However, in the above procedure, use  $D$  as the diameter of a single nozzle even for multiple-nozzle operation. In calculating the mechanical stream power, use the total mass flow of all of the engines in simultaneous operation.

Little quantitative information is now available on the effects of water spray at the exhaust deflector. Qualitatively, water spray has been found to reduce the noise levels

only when the water mass flow is greater than the exhaust gas mass flow.

## 2. Effects of Forward Motion

Following vehicle lift-off, the noise levels over the surface of the vehicle can be affected in several ways. These effects of forward motion include changes in wave propagation, operating conditions, wave number  $k$ , noise radiation (hemispherical to spherical), and angle between the jet stream and the vehicle axis.

The effects of motion on the wave propagation in the medium between the source and the receiver have been taken into account in a simple way, as described by Powell<sup>6.1/</sup>. The sound pressure level at the vehicle surface is reduced by forward motion at a subsonic Mach number  $M$ . The amount of this reduction is given by the quantity  $\Delta\text{SPL}_m$ , which is approximately:

$$\Delta\text{SPL}_m = 20 \log (1 - M) \quad (91)$$

At supersonic speeds, no rocket noise can propagate to the space vehicle surface. A plot of  $\Delta\text{SPL}_m$  as a function of  $M$  is given in Figure 79.\*

Changes in rocket engine operating conditions, such as mass flow and rocket exhaust velocity, occur during flight and affect the amount of noise produced. For given values of mass flow  $m$  and exhaust gas velocity  $v$  relative to the values for the vehicle at rest,  $m_0$  and  $v_0$ , the change in

\* The effects of motion on wave propagation are discussed in more detail in the Appendix to this Section.

sound pressure level,  $\Delta$ SPL, can be determined directly from Figure 80.

As the vehicle moves away from the ground, there is a gradual transition from hemispherical to spherical radiation of sound. This effect reduces the noise levels by 3 db. There is also an increase in angle between the jet stream direction and the vehicle axis since, as the missile moves away from the deflector, less of the jet stream is deflected. This effect reduces the noise level by the order of 3 db. In addition, there are important changes in the exhaust flow, which are seen as changes in the noise source positions such as are shown in Figure 75.

Each of these effects should be taken into account when estimating the noise level over the surface of a vehicle in motion by suitably modifying the prediction procedure described in the previous section.

### 3. In-Silo Operation

Noise levels over the surfaces of missiles fired from underground silos are significantly higher over most of the frequency range than for static operation of the same missile on a test stand. The increase in sound pressure level varies with frequency, distance from the exhaust nozzles, and silo configuration. From preliminary data obtained during firings from two different types of silos, an I-tube silo (see Figure 81) and a double-U silo (see Figure 82), the increase in sound pressure level can range as high as 20 to 25 db.

A summary of measured sound pressure level differences for above- and below-ground operation is given in Figures 81 and 82. Since the sound pressure level on the missile surface varies during emergence from the silo, the data are

given in terms of the differences between the highest noise levels measured on the missile surface in an unlined (hard-wall) silo during launch and at the same point on the missile surface during test stand operation. The data for an I-tube silo are presented in Figure 81 and show that, at any given frequency, the sound pressure level differences are essentially the same on the missile surface 3 to 50 ft from the exhaust nozzle plane. The greatest differences occur at the lower frequencies (5 to 50 cps). Above 1000 cps, there is essentially no change in sound pressure level.

In contrast, the results from missile firings in a double-U silo show that the sound pressure level differences vary with observation position on the missile surface. Data obtained at 3 ft, 52 ft, and 77 ft from the exhaust nozzle plane all show about 10 to 20 db increase in sound pressure level below about 10 cps. However, above this frequency the sound pressure level differences increase with increasing distance from the exhaust nozzle plane.

Several physical factors enter into the complicated situations depicted by Figures 81 and 82:

1. The confining silo geometries permit higher order modes to exist that would not be present for above-ground firings; that is, sound is reflected from the silo walls.
2. The exhaust flow pattern, and thus the nature of the noise sources, is changed considerably as the missile moves away from the deflector.
3. In the I-tube silo, the noise sources are very close to the missile surface. Also, attenuation

of sound in the hot turbulent gas in the silo is greater than in a cool stationary medium. This increase in attenuation is expected to be pronounced at higher frequencies.

Ignition of a rocket engine is accompanied by a pressure pulse. When the engine is in a silo, the pulse is confined to essentially one-dimensional propagation, and the amplitude is increased over its above-ground value. Pulse amplitudes of the order of 5 to 10 psi have been observed in silos. The pulse is believed to be associated with the rapidly changing rates of heat and mass flow at ignition.

It should be emphasized that relatively few in-silo measurements are available at this time, and that the data given here are preliminary and should be used only as guideposts.

#### 4. Correlation Properties of Rocket Noise

The properties of the rocket noise field around a space vehicle should be described not only in terms of amplitude behavior but also in terms of correlation behavior. Correlation is a measure of the average phase relationships between the instantaneous pressures measured at two points. A correlation of plus one indicates that the two pressures are always in phase; a correlation of minus one indicates that the two pressures are always  $180^\circ$  out of phase; and a correlation of zero indicates that the two pressures are always  $90^\circ$  out of phase or, equivalently, are in phase as often as they are completely out of phase in any long period.

In the usual case in which the vehicle is highly symmetrical about a central axis, the rocket noise correlation is conveniently given in terms of a longitudinal

correlation along the vehicle axis, and an angular correlation in a plane perpendicular to the vehicle axis. In this case sound propagates at grazing incidence along the vehicle, and thus the longitudinal correlation is approximately of the form  $\cos k (x - x')$ , where  $x$  and  $x'$  are the longitudinal coordinates of the two observation points, and the points are at the same angular position around the vehicle. Measured longitudinal correlations show reasonable agreement with this cosine form, but because of the finite measurement bandwidth and the finite extent of the noise source in the exhaust stream, the measurement curves show smaller oscillations at higher frequencies than are predicted.

Figure 83 shows the correlation of rocket noise measured at different angular positions on a vehicle surface.  $\Phi$  and  $\Phi'$  are the angular coordinates (measured in radians) of the two observation points, and the points are in the same plane perpendicular to the vehicle axis.  $r$  is the vehicle radius. The general behavior of Figure 83 is explained as follows: At low frequencies the noise sources are sufficiently far from the measurement stations that the noise appears to be coming from one source, and the pressures in a plane are well correlated. At high frequencies the noise sources are so close to the measurement stations that the noise reaching different points around the vehicle comes from different, uncorrelated sources. Additional data may be expected to show the more detailed behavior of the angular correlation as a function of distance from the exhaust plane.

APPENDIX TO VI A  
EFFECTS OF MOTION ON WAVE PROPAGATION

The motion of a noise source may change the nature of wave propagation in the medium between the source and the receiver. In order to study the effects of wave propagation changes, we must choose a mathematical model of the moving medium. The model used in Section II was a simple source and receiver connected rigidly and moving at a constant subsonic speed. Experimental evidence indicates, however, that with exhaust noise one does not observe the significant increase in SPL that is expected upstream of rigidly connected sources moving near Mach 1. Accordingly Powell<sup>6.1/</sup> has suggested that the rigid connection hypothesis leads to conservative results, and that the hypothesis that the vehicle moves away from the sources is more realistic. In the following discussion we present a quantitative procedure based on this second hypothesis. It is entirely possible that further refinements will be needed to include other physical effects in this procedure.

A special case of considerable interest occurs when the source and receiver lie on a line in the direction of motion and the source is downstream of the receiver. In this case the forward motion does not change the effective angle between the source and the receiver, and the major effect is a decrease in SPL given by:

$$\Delta\text{SPL}_m = 20 \log (1 - M) \quad (91)$$

where M is the vehicle Mach number. This is the result reported by Powell and mentioned earlier in the text.

More generally one may be concerned with arbitrary source and receiver positions. Then the source directivity characteristics may become important, because motion changes the effective angle between source and receiver. It is often convenient to use source directivity curves such as Figure 16 in Volume I of WADC TR 58-343 for a turbojet engine, and to assume that the forward motion moves the receiver from its actual position R to an apparent position R' on a line parallel to the direction of motion. This change in position is shown in Figure 84 for the receiver either upstream or downstream of the source. The motion changes the angle  $\theta$  into the angle  $\Phi$ .

Using the geometry of Figure 84, we may determine the relationship between  $\theta$  and  $\Phi$ . The sound wave travels distance  $r$  at velocity  $c$  in the same time that the receiver is convected over distance  $\Delta x$  at velocity  $V$ , or

$$\frac{r}{c} = \frac{\Delta x}{V} \quad (92)$$

Also, from the triangle whose hypotenuse is  $r$ ,

$$r^2 = y^2 + (x + \Delta x)^2 \quad (93)$$

Since by definition

$$\tan \theta = \frac{x}{y}, \quad \tan \Phi = \frac{x + \Delta x}{y}, \quad M = \frac{V}{c} \quad (94)$$

we obtain

$$\tan \Phi = \frac{1}{(1 - M^2)} [\tan \theta + M \sqrt{1 - M^2 + (\tan \theta)^2}] \quad (95)$$

Associated with this motion there occurs a change in wavelength perceived by the receiver, so that

$$\lambda/\lambda_0 = 1 - M \sin \Phi, \quad (96)$$

where  $\lambda$  is the perceived wavelength at vehicle Mach number  $M$ , and  $\lambda_0$  is that observed at rest.

Plots of Equations (95) and (96) for several values of  $M$  appear in Figure 85. The right-hand graph gives the apparent angle  $\Phi$  in terms of the angle  $\theta$  and Mach number  $M$ ; the left-hand graph may then be used to find the change in observed wavelength. It may be seen that at supersonic speeds no jet noise propagates upstream of the noise source (positive values of  $\Phi$ ). [It should be noted that at very high speeds pressure fluctuations other than jet noise (such as boundary layer noise) may become significant.]

As an example, the angular transformation of Figure 85 has been applied to the near-field noise contours of a contemporary turbojet engine for the value of Mach 0.8. Both sets of contours are shown in Figure 86, where the broken lines represent sound pressure levels during static operation and the solid lines the estimated sound pressure level contours for  $M = 0.8$ . In making the transformation shown in Figure 86, the simplifying assumption that the sound sources are located near the jet exhaust nozzle has been made. For greater refinement one may transform contours of noise measured in bands of frequency, specifying the corresponding noise source location at some position downstream of the nozzle.

## B. Pressure Fluctuations in a Turbulent Boundary Layer

Several experimental programs have been performed to study the pressure field in a turbulent boundary layer. 6.2-6.12/ Considerable difficulty has been encountered in obtaining meaningful results, because of the small dimensions generally associated with boundary layers that can be observed in well-controlled experiments. Consequently not all of these programs have provided significant quantitative information.

### 1. Spectrum Shape and Characteristic Dimensions for Subsonic Boundary Layers

The root-mean-square pressure fluctuation at a rigid plane surface over which a subsonic boundary layer is moving has been found to be directly proportional to the free stream dynamic pressure,  $[1/2]\rho U_{\infty}^2$ . The larger the transducer diameter  $D$ , the smaller the measured rms pressure  $p$ , because the very small-scale pressure fluctuations cancel each other over the transducer surface. From the experimental data extrapolated to an infinitesimal transducer, a generally accepted value for the proportionality is

$$p \doteq 6. \times 10^{-3} \left[ \frac{1}{2} \rho U_{\infty}^2 \right] \quad (97)$$

Some experimentally obtained spectra  $S(f)$  of boundary layer turbulence are shown in Figure 87. The spectra are plotted in dimensionless form. Figure 87 shows the effects of transducer size on the measured results: larger transducers do not detect as much energy in the smaller higher frequency eddies as do the smaller transducers.

The solid line in Figure 87 shows the shape of a spectrum that is relatively simple and that fits the data reasonably well:

$$S(f) = S(0) \frac{1}{1 + \left(\frac{f}{f_0}\right)^2} \quad (98)$$

On the basis of the experimental data, it appears that this assumed spectrum will tend to overemphasize the higher frequencies where the data fall off faster than  $1/f^2$ . The characteristic frequency of the assumed spectrum  $f_0$  is related to the characteristic dimensions of the turbulence by

$$f_0 \doteq 0.1 \frac{U_\infty}{\delta^*} \quad (99)$$

where  $\delta^*$  is the displacement boundary layer thickness.  $\delta^*$  is the order of 1/10 of the boundary layer thickness defined in Figure 35 of WADC TR 58-343.

On the basis of cross-correlation data such as are given in Reference 6.10, we observe that boundary layer turbulence is convected at a velocity  $v$  which is related to the free stream velocity  $U_\infty$  by

$$v \doteq 0.8 U_\infty \quad (100)$$

As it is convected, the turbulence decays with a characteristic decay time (measured in a frame of reference which moves along with the turbulence) given by

$$\theta \doteq 30 \frac{\delta^*}{U_\infty} \quad (101)$$

One value of the characteristic length scale of the turbulence in the direction of convection can be obtained from the cross-correlation data. A second value of this scale can be obtained from the spectrum  $S(f)$ , because

$$l \doteq \frac{v}{2\pi f_0} \quad (102)$$

As might be expected, these two values of the scale  $l$  do not show precise agreement. Also, the value of  $l$  may vary somewhat, depending on the particular analytical form which is chosen to fit the spectrum or correlation data and on other details of the data-fitting processes. An average value of the scale is given by

$$l \doteq 25^* \quad (103)$$

No quantitative information is now available on the length scale measured perpendicular to the direction of convection. We assume for the present that this scale is of the order of  $l$ .

It should be pointed out that the data given here were obtained in the absence of longitudinal pressure gradients, and that preliminary measurements in water indicate that the presence of such a gradient causes a marked change in the boundary layer spectrum. Additional data are clearly needed.

## 2. Roughness-Induced Noise

Up to this point in our discussion we have considered only the turbulent pressure fluctuations that are generated in high speed flow over a smooth rigid surface. It is clear that similar pressure fluctuations will be generated when the surface is rough. Some preliminary studies of these roughness-induced pressure fluctuations have been

reported by Skudrzyk.<sup>6.11/</sup> The spectrum associated with these pressures peaks at a characteristic frequency  $f_r$  given by the approximate relation

$$f_r \doteq \frac{0.1U_\infty}{h} \quad (104)$$

where  $h$  is the average roughness height. From Skudrzyk's results we may draw the tentative conclusion that the roughness-induced boundary layer noise becomes approximately equal to the smooth-plate boundary layer noise in a frequency band around  $f_r$  for a critical free stream velocity  $U_r$  given by

$$U_r \doteq 750 \cdot \frac{\nu}{h} \quad (105)$$

where  $\nu$  is the kinematic viscosity of the fluid. The units of  $\nu$  are  $\text{ft}^2/\text{sec}$  in the English system. For air near standard temperatures and pressures, the critical velocity is related to the roughness size by

$$U_r \doteq \frac{0.13}{h} \quad (106)$$

where  $h$  is measured in feet. For conditions other than standard temperatures and pressures, the kinematic viscosity can be obtained from the relation

$$\nu = 1.7 \times 10^{-4} \left( \frac{T}{T_{\text{stand}}} \right)^{1.7} \left( \frac{P_{\text{stand}}}{P} \right) \text{ft}^2/\text{sec} \quad (107)$$

For velocities above the critical velocity the roughness-induced noise depends strongly on the nature

of the surface. The increase in roughness noise with velocity can be related to the velocity ratio

$$\left(\frac{U}{U_r}\right)^n$$

where  $n$  is an exponent between 3 and 6, the lower values of  $n$  corresponding to smooth painted metals and the higher values of  $n$  corresponding to very densely pitted surfaces.

In order to obtain an idea of the roughness dimensions involved in typical metal surfaces, we note that rolled surfaces will have a roughness size of the order of  $10^{-5}$  to  $10^{-4}$  feet. For these dimensions, the critical velocity  $U_r$  would be the order of 10,000 ft/sec at standard temperature and pressure. However, during re-entry the pitting of the surface may increase the roughness size and reduce the critical velocity  $U_r$  by several orders of magnitude. Since the highest velocity presently contemplated for vehicles in the atmosphere is about 3000 ft/sec, it appears that roughness-induced noise will be important only during pitting conditions. When the pitting dimensions are known, they may be used to obtain estimates of the critical velocity and the rate of increase of roughness-induced noise above the critical velocity.

### 3. Supersonic Boundary Layers

At the present time there is little detailed information concerning boundary layer pressures occurring in supersonic flow. Recent measurements of velocity fluctuations in equilibrium supersonic boundary layers<sup>6.12/</sup> lend some support to the belief that the supersonic case is not too grossly different from the subsonic case. From Reference 6.13

we may estimate the rms pressure fluctuations  $p$  in the supersonic case to be

$$p \doteq \left( \frac{\Delta v}{U_\infty} \right)^2 \left[ \frac{1}{2} \rho U^2 \right] \quad (108)$$

in which it is assumed that the velocity fluctuations  $\Delta v$  travel at the local mean velocity. Figure 88 shows measurements of  $\Delta v/U$  obtained from Reference 6.12, from which we may conclude that the fluctuating pressure is of the order of 0.3% of the dynamic pressure. This value is in rough accord with the subsonic value, although somewhat less. Unpublished data from Chen also indicate a higher value for supersonic flow than for subsonic flow and show important qualitative changes in the spectrum shape.

#### 4. Summary

We repeat here in convenient form the expressions for average values of the parameters which describe the subsonic boundary layer pressure field:

$$20 \log \frac{p}{0.0002} \doteq 20 \log \left[ \frac{1}{2} \rho U_\infty^2 \right] + 84 \text{ db} \quad (109)$$

where  $p$  is measured in dynes/sq cm and  $\frac{1}{2} \rho U_\infty^2$  is measured in lbs/sq ft.

Typical spectrum shapes are given in Figure 87, where

$$S(f) = \frac{2p^2}{\pi f^3} \quad (110)$$

and

$$f_0 \doteq 0.1 \frac{U_\infty}{\delta^*} \quad (99)$$

$$e \doteq 30 \frac{\delta^*}{U_\infty} \quad (101)$$

$$l \doteq 25^* \quad (103)$$

$$v \doteq 0.8 U_\infty \quad (100)$$

### C. Wake Noise

The turbulent flow in the wake of a vehicle may give rise to noise radiation. Since no direct data are available on this noise source, we must appeal to qualitative arguments for its estimation. We restrict attention here to vehicle Mach numbers less than unity; for  $M \geq 1$ , sound radiated by the wake cannot reach the vehicle.

Qualitatively the wake of a subsonically moving vehicle is composed of a region of high shear, flow separation, and concomitant turbulence. This is much the same situation that exists in the jet stream of a gas reaction motor, and we may speculate that the noise radiation characteristics of the two are similar. Figure 89 depicts in qualitative terms the situation in a jet stream and in a wake. In the case of jet radiation the velocity profile is directed away from the jet engine, and the most intense radiation is in the general downstream direction. In case of wake turbulence the velocity profile is directed towards the moving vehicle, and by analogy we might expect the most intense radiation to be in the general upstream direction.

The implications of the qualitative picture described above are essentially borne out by measurements on turbojet aircraft in flight.<sup>6.13, 6.14/</sup> Figure 90 shows one of these measurements, from which we can see that the power radiated in the general upstream direction increases with increasing

Mach number. However, we must emphasize that additional data are required to establish more fully the mechanism of noise radiation in turbulent wakes.

We proceed to estimate the order-of-magnitude of wake noise based on the proposed mechanism. The total mechanical power associated with the wake may be estimated to be the product of the wake drag and the forward speed of the vehicle. Consequently, we may write the acoustic power,  $P_w$ , radiated from the wake as a fraction of the mechanical power:

$$P_w = \eta Dv = \eta c_D \frac{1}{2} \rho A v^3 \quad (111)$$

where  $D$  is the wake drag

$c_D$  is the drag coefficient associated with the wake

$\rho$  is the undisturbed air density

$A$  is the projected area in the flight direction

$v$  is the vehicle speed.

The quantity  $\eta$  is the order of  $10^{-4} M^5$ , based on the analogy with subsonic jet noise radiation<sup>6.15/</sup>. The drag coefficient  $c_D$  is of the order of unity or less, depending upon the shape of the vehicle trailing surface. We note that Equation (111) implies an eighth power dependence of power on velocity, in good agreement with the measurements shown in Figure 90.

We may compare the wake radiation with the radiation of noise by rocket engines and turbojet engines. The corresponding acoustic powers for these cases are given by

$$P_r = \eta_r \frac{1}{2} \rho_r A_r (v_r - v)^3, \quad \eta_r \sim 10^{-2} \quad (112)$$

$$P_t = \eta_t \frac{1}{2} \rho_t A_t (v_t - v)^3, \quad \eta_t \sim 10^{-4} (M_t - M)^5$$

where the subscripts r and t refer to rockets and turbojets, respectively. The terms  $\rho$ , A,  $v_r$  and  $v_t$  refer to the exhaust stream, and the Mach numbers are based on the speed of sound in the undisturbed medium.

With the use of order-of-magnitude values for the  $\rho$  and A terms of Equations (111) and (112), and with the use of typical values of the Mach numbers ( $M \leq 1$ ,  $M_r \sim 7$ , and  $M_t \sim 2$ ), we find that the acoustic power of a wake is much less than that of a rocket engine, and comparable to that of a turbojet engine.

From the estimated power we may determine the sound pressure on the vehicle due to wake noise. To do this we must take account of the radiation directivity, the spectrum, and the effect of forward motion. As discussed previously, wake noise has a directional characteristic that is reversed from that of jet noise. Also the spectrum is expected to shift in accordance with the different speed-to-dimension ratios. Finally, the forward speed effect as given in Equation (91) is expected to apply. With these factors in mind we would conclude: In the case of a missile in powered flight, wake noise is less important than rocket noise. On the other hand, in free subsonic flight of a re-entry vehicle, wake noise may be important. In the case of an aircraft at high subsonic speeds, wake noise may be quite important relative to turbojet noise.

No measurements are available on the correlation of wake noise over vehicle surfaces. However, we may reasonably expect the correlations to be qualitatively similar to those of jet noise.

Sound radiation from the wake of cylinders placed transverse to flow has been calculated and measured

recently, 6.16, 6.17/ and displays the general behavior assumed here for noise of vehicle wakes. With transverse cylinders, however, there are additional strong components of radiation associated with fluctuating lift and drag forces. These components are related to the nearly periodic shedding of large scale vortices from the cylinder, rather than to the turbulent portion of the wake. With the very much higher Reynolds numbers and grossly different geometries associated with flight vehicles, vortex shedding does not appear to be of importance in flight vehicle noise environments. However, this general question needs to be clarified further and placed on quantitative grounds.

#### D. Base Pressure Fluctuations

Noise radiated by the wake of a flight vehicle was discussed in the foregoing section. Here we consider the pressure fluctuations associated with wake turbulence that may be felt directly by the base of the vehicle without intermediate sound radiation. These pressure fluctuations may be expected to contribute to the noise environment of the vehicle for both subsonic and supersonic flight speeds, inasmuch as sound propagation is not a factor. There are not direct data available relevant to this noise environment, and we are forced to speculate about its magnitude.

The situation in the wake of a subsonic vehicle was discussed qualitatively in the last section. The supersonic case is more complex because of the existence of shock waves. In Figure 91 we give a qualitative picture of the flow expected at the base of a supersonic flight vehicle, 6.18/ As in the subsonic case there is a region of relatively dead air in a small volume immediately behind the base. The boundary layer over the vehicle surface thickens past

the base and forms a turbulent wake a short distance downstream. The qualitative form of the shear profile at the base is expected to be similar to that at the boundary of a supersonic jet issuing into still air.<sup>6.18/</sup>

Because of the similarity between the flow at the base and the flow issuing from a jet, we might speculate that the order-of-magnitude of the base pressure fluctuations can be estimated from jet pressure fluctuations. Of interest here are pressure fluctuations measured very close to a jet where the aerodynamic rather than the acoustic field predominates. The pressure fluctuations,  $\Delta p$ , close to a turbulent jet (i.e., in the near field) may be written as<sup>6.19/</sup>

$$\Delta p = \frac{k}{2} \rho v^2 \left( \frac{r_0}{r} \right)^3 \quad (113)$$

where  $\rho$  is the density and  $v$  is the velocity in the jet. The quantity  $r_0$  is a characteristic dimension of the jet, and  $r$  is the distance from the jet. The proportionality constant  $k$  is of the order of  $10^{-2}$ . We may rewrite Equation (113) in a somewhat more convenient form for estimating, by analogy, the base pressure fluctuations:

$$\Delta p = \frac{k\gamma}{2} p_b M^2 \left( \frac{r_0}{r} \right)^3 \quad (114)$$

Here  $p_b$  is the static base pressure and  $\gamma$  the ratio of specific heats. For subsonic flight  $p_b$  is approximately equal to the free stream static pressure,  $p_\infty$ . For supersonic flight  $p_b$  is about 40% of  $p_\infty$  over a wide range of Reynolds numbers and Mach numbers of interest.<sup>6.18, 6.20/</sup>

With the use of the foregoing we may estimate the magnitude of the base pressure fluctuations. We see most directly from Equation (113) that the base pressure fluctuations are expected to maximize at a condition equivalent to the maximum free stream dynamic pressure of the vehicle, a condition that generally occurs in supersonic flight. A typical set of conditions for maximum free stream dynamic pressure of a large missile is  $p_{\infty} = 150 \text{ lbs/ft}^2$  (60,000 ft) and  $M = 3$ . For a conservative estimate let us take  $r$  to be the same order as  $r_0$ . Then the base pressure fluctuations in this case will be of the order of or less than  $4 \text{ lbs/ft}^2$ , corresponding to a pressure level of 140 db. We see that the base pressure fluctuations may be of considerable magnitude and may be comparable to the magnitude of some of the other environments discussed previously.

The wake diameter in the turbulent region is about 50% of the base diameter, over a wide range of flow conditions.<sup>6.18/</sup> Thus the characteristic dimensions and velocities of wakes are not much different from those of usual jet systems. Pressing the analogy with jet pressure fluctuations further, we may, therefore, expect the spectrum of the base pressure fluctuations to maximize in the audio frequency range.

Not much can be said about the space-time correlation of the pressure fluctuations, except that its scale may be a sizeable fraction of the base area. Consequently, this pressure field may couple quite well to the vehicle structure.

It must be emphasized that the foregoing estimates must be regarded as pure speculation. Because of the possible importance of this environment it is evident that measurements and additional studies of base pressure fluctuations would be extremely helpful.

## E. Oscillating and Moving Shocks

In supersonic flight abrupt changes in static pressure may occur at some points in the vehicle surface. Motions of these pressure discontinuities constitute a noise environment.

A distribution of static pressures likely to be encountered on the surface of a typical rocket vehicle traveling at supersonic speeds is sketched in Figure 92. Abrupt increases in pressure occur at locations where the surface is sharply concave, and sudden pressure decreases occur where the surface is sharply convex. The static pressure increases outside of the boundary layer occur over extremely short distances--in fact, over distances of the order of the mean free path of the molecular motions of the fluid  $\frac{6.21}{\rho c}$  (about  $10^{-5}$  in. in air at standard conditions). The pressure decreases are considerably less abrupt than the increases; they occur over distances of the order of several inches. The sudden pressure increases are called (compression) shocks; the pressure decreases are often called expansion shocks even though they are not abrupt enough to be considered shocks in the strictest sense of the word.

The values of the pressures indicated in Figure 92 are of the correct order-of-magnitude for Mach numbers in the range of 5 to 10. (The pressure difference across a shock is not, in general, strongly affected by Mach number for Mach numbers in this range.) Thus, pressure increases across a shock may easily be of the order of the atmospheric pressure at altitude.

The interaction between an attached shock and a boundary layer usually thickens this layer locally and makes the pressure increase felt by the vehicle surface

less abrupt. Because of the boundary layer the surface pressure rise occurs over distances of the order of an inch or two, instead of over the  $10^{-5}$  in. in absence of the boundary layer.<sup>6.21, 6.22/</sup> The magnitudes of the pressure differences, however, are virtually unaffected by the boundary layer.<sup>6.22/</sup>

When attached shocks are observed in wind tunnels by use of any of the several well known optical devices, they are often found to oscillate. Thus pressure fluctuations of the order of the atmospheric pressure at altitude will be felt in the vicinity of the shocks. For example, at 60,000 ft the atmospheric pressure is about 150 lbs/ft<sup>2</sup>, so that the level of the pressure fluctuations will be about 175 db. Since it is clear that such motions of pressure discontinuities are likely to induce important vibrations in the skin structures of high speed flight vehicles, it is unfortunate that very little is known about the characteristics of these shock oscillations, such as their lineal extent and spectral composition. It is evident that this environment warrants further study.

Shock oscillations of a somewhat different sort have been observed in the presence of flow separation spikes which are often mounted at the front of supersonic vehicles in order to reduce drag. The drag reduction in this case is obtained by essentially replacing the drag associated with a blunt bow shock by the lesser drag associated with a conical shock attached to the spike, although in general both shocks are observed. The bow shock has a tendency to detach and spread the spike shock; under some conditions (depending mostly on Mach number and relative spike length) this spreading continues to the point where the bow shock is weakened so much that the spread spike shock can no

longer be maintained. The spike shock then collapses, and the cycle is repeated, resulting in periodic flow fluctuations.<sup>6.23, 6.24/</sup>

The effects of spike length and Mach number on the frequency of this type of shock pulsation<sup>6.23/</sup> may be visualized from Figure 93. At Mach 2 a one-diameter long spike is found to produce shock oscillations at a frequency of about 3,000 cps, if the ambient air temperature is  $70 \pm 30^{\circ}\text{F}$  ( $530^{\circ}\text{R}$ ). The surface pressure fluctuations associated with these shock pulsations may be quite significant. For example, at Mach 4.3 and with a spike-to-diameter ratio of  $4/3$ , a maximum octave band pressure level of 163 db was measured<sup>6.24/</sup> at the front of a blunt body like that shown in Figure 93, near the base of the spike. This maximum occurred in the 600-1200 cps range; a nearly uniform decrease of 5 db/octave was observed on both sides of the maximum.

The spike shock pulsations are strongly influenced by the shape of the nose cone. It appears that less blunt configurations have less tendency to set up such oscillations; in fact, hemispherical noses are known to give rise to no shock pulsations at all. More information is needed about the shock-induced fluctuations of pressure on the lateral surfaces of the vehicles, especially for curved nose configurations, so that the responses of the structures can be evaluated more realistically. Also, the effects of Reynolds number and geometric scaling need further investigation before the presently available results, obtained from small wind-tunnel models, can be applied with confidence to full scale craft.

Shocks sweeping across vehicle surfaces may also cause these to vibrate. Such relative motions of shock and vehicle may occur due to explosions, or when one vehicle passes through a shock wave generated by another. The intensities of explosions and of the attendant shocks cover such a wide range that no meaningful order of magnitude can be assigned to the shock strengths. However, the pressure increase experienced by one vehicle passing through the bow shock wave created by another vehicle is given by 6.13/

$$\frac{\Delta p}{p_{\infty}} = 0.53 \delta \frac{(M^2 - 1)^{1/8}}{(y/L)^{3/4}} \quad (115)$$

where  $p_{\infty}$  is static pressure in undisturbed atmosphere  
 $\Delta p$  is observed pressure increase  
 $y$  is distance between two vehicles, measured normal to flight path  
 $\delta = D/L$  is fineness ratio  
 $D$  is maximum diameter  
 $L$  is length  
 $M$  is Mach number.

} of vehicle  
 } producing  
 } shock

The foregoing relation applies strictly only for relatively large distances between the two vehicles, i.e.,  $\frac{y}{L} > 100$ , but may be used to give reasonably reliable estimates for  $\frac{y}{L}$  as low as 5 in some cases. It shows that for high Mach numbers the pressure rise varies nearly as  $M^{1/4}$  and thus is not strongly dependent on Mach number, and that the pressure rise varies inversely as only the  $3/4$  power of distance. As an example of the pressure jumps one may encounter, a vehicle with fineness ratio 0.15, length 100 ft, traveling at Mach 3 at 60,000 ft causes a  $\Delta p$  of about 3 lb/ft<sup>2</sup> to be observed on another vehicle

1000 ft away. The pressure jump is a transient which sweeps over the receiving vehicle at a speed determined by their relative motions.

#### F. Flow over Cavities

Many instrumentation and equipment installations on a space vehicle require that the side of the vehicle be cut to form a cavity. When air flows over this cavity, significant fluctuations in pressure may exist along the cavity, forcing the surface into motion. These fluctuations have been observed by several investigators, but little quantitative information exists for subsonic flow conditions, and no quantitative information has been found in unclassified publications for supersonic flow conditions.

Several kinds of pressure fluctuations have been observed with flow over a cavity. One kind is aperiodic fluctuations associated with the turbulent flow in the cavity. Such turbulence is similar to boundary layer or base turbulence discussed earlier. Roshko<sup>6.25/</sup> reports turbulent pressure fluctuations of the order of 5% of the free stream dynamic pressure  $\frac{1}{2}\rho U_\infty^2$ , for flow of 75 ft/sec over a cavity approximately four inches square. This value is seen to be an order-of-magnitude higher than is found for boundary layer turbulence, and is indicative of the highly turbulent flow in the cavity.

A second kind of pressure fluctuation is associated with a directional sound wave that may be emitted from the cavity. The mechanism of sound generation is not understood, but is thought to involve an interaction with the vortex flow in the cavity. Krishnamurty has measured the frequency of the sound produced by flow over small cavities (dimensions of the order of 0.1 inches).<sup>6.26/</sup> His results for laminar

and turbulent boundary layer flows are shown in Figure 94. In the case of turbulent boundary layer flow, sound was observed at two different frequencies, which were harmonically related. Levels of the order of 160 db were observed in some cases.

A third kind of pressure fluctuation is the sound wave that may be set up if the cavity is set into an "organ pipe" resonance. Flow over the cavity lip causes the air column to resonate. The resonance frequency is given by the condition that the length of the air column is an odd multiple of the wavelength, or

$$f_{\text{res}} = \frac{c}{4L} (2n + 1) \quad n = 0, 1, 2, \dots \quad (116)$$

where  $c$  is the speed of sound in the cavity, and  $L$  is the length of the cavity. The amplitude of this sound wave is strongly dependent on the details of the flow conditions at the cavity lip.

A final kind of pressure fluctuation arises from the oscillating shock patterns that may occur in supersonic flow over cavities. Such fluctuations have been discussed qualitatively earlier. No details of these shock motions are available, but it is clear that they may give rise to pressure fluctuations of the order of the ambient static pressure.

## G. Flight Through a Turbulent Atmosphere

### 1. Subsonic Flight Speeds

When a flight vehicle moves through a turbulent atmosphere at subsonic speeds, the random pressure fluctuations in the turbulence are felt directly by the surfaces of the vehicle. Because the mean scale  $D$  of the turbulence is much larger than overall vehicle dimensions, it is often assumed in aerodynamic gust loading problems that the vehicle moves as a rigid body in response to the turbulence. However, there is a wide range of turbulent "eddy" sizes having values larger and smaller than the mean scale  $D$ . Eddies whose sizes are comparable to or smaller than the vehicle length  $L$  give rise to a random pressure field that will excite vibrations of individual panels on the vehicle surface, rather than excite motion of the entire vehicle.

In order to characterize this random pressure field, we require a value of the rms pressure fluctuation  $\Delta p$  and the temporal scale  $\tau$ . The static pressure  $p$  at the surface of a body is related to the ambient pressure  $p_0$  and to the free stream density  $\rho$  and velocity  $v$  by

$$p = p_0 + c \frac{1}{2} \rho v^2 \quad (117)$$

where the coefficient  $c$  is a function of vehicle geometry, flow conditions, and measurement position. (See for example, Reference 6.27). Then the pressure fluctuation will be approximately

$$\Delta p \sim c \rho v (\Delta v) \quad (118)$$

$\Delta v$  is an "effective" component of the turbulent velocity associated with eddies comparable to or smaller than  $L$ . Based on the data in Reference 6.28, the maximum value of  $\Delta v$  is an order-of-magnitude less than the rms turbulent velocity, or about 1/2 ft/sec in the lower atmosphere. The maximum magnitude of  $c$  is the order of unity, and it may take on positive, negative, and zero values.

Equation (118) may now be used to obtain an estimate of the upper limit of  $\Delta p$ . For example, for a density of  $2 \times 10^{-4}$  slugs/cu ft, corresponding to an altitude of 60,000 ft, and a forward velocity of 1000 ft/sec,  $\Delta p \leq 0.1$  lbs/sq ft or a maximum pressure level of 108 db. This is clearly an upper limit, because the value of  $\Delta v$  will decrease with increasing altitude. Also much lower values of  $\Delta p$  will occur at observation positions where steady flow results show a vanishing value for  $c$ . Thus,  $\Delta p$  may vary by orders-of-magnitude over the vehicle.

The predominant pressure fluctuations experienced by a vehicle moving through atmospheric turbulence result from vehicle motion through the turbulent velocity fluctuations. Therefore, a characteristic circular frequency  $\omega_0$  of the pressure field associated with the smaller eddies will be

$$\omega_0 \doteq \frac{v}{L} \quad (119)$$

Using a value of  $L$  of 100 ft and a forward speed of 1000 ft/sec, we obtain  $\omega_0$  equal to  $10 \text{ sec}^{-1}$ . We may speculate that the corresponding octave band spectrum will increase 3 db per octave at very low frequencies, peaking around  $f_0 = \omega_0/2\pi$  cps, and decrease very rapidly above this peak. For the example just considered, the frequency of

the maximum is about 2 cps. Frequencies in the audible range, therefore, are well down on the spectrum "tail," and levels in this range will be well below the overall value of 108 db obtained previously. More information on the spectrum shape above  $f_{\max}$  is required to make quantitative estimates of the pressure levels at audible frequencies.

Some of the pressure fluctuations in atmospheric turbulence are independent of the vehicle motion. These pressure fluctuations are of the order of  $\frac{1}{2} \rho (\Delta v)^2$ , and are generally negligible compared with those given by Equation (118).

## 2. Supersonic Flight Speeds

When a flight vehicle moves supersonically, it is surrounded by a set of pressure discontinuities or shocks. (This situation has been discussed in Part E and is illustrated in Figure 92.) When atmospheric turbulence is convected through one of these shocks, it produces sound pressures downstream of the shock, and these pressures excite the vehicle structure.

The analysis of Ribner<sup>6.29/</sup> can be used to estimate the overall level of shock-turbulence sound. For the case of a supersonic vehicle we may assume that the ambient pressure  $p_0$  downstream of the shock is constant, independent of the convection speed of the turbulence. Ribner's results for the sound pressure  $p$  downstream of the shock then take on the form

$$\frac{p}{p_0} = b(M_u) \frac{\Delta v}{v} \quad (120)$$

where  $M_u$  is the Mach number upstream of the shock and  $b(M_u)$  is a proportionality factor. The value of  $b(M_u)$  varies very slowly with Mach number, and is approximately 0.6. In an intense turbulent field, such as exists at a jet interface, the ratio  $\Delta v/v$  may be of the order of  $10^{-1}$ . For turbulence in the atmosphere, we speculate that this ratio may be the order of  $10^{-3}$ . Using this latter figure, we obtain 108 db for the sound pressure level downstream of a shock at 60,000 ft ( $p_0 = 150$  lbs/sq ft).

The pressure estimated with the use of Equation (120) is acoustic in that it propagates in the flow as well as convects with the flow. (In contrast, the pressure fluctuations estimated by Equation (118) for the subsonic case are not acoustic.) In the supersonic case there are also non-acoustic pressure fluctuations. These pressure fluctuations are about an order-of-magnitude  $\frac{(20 \text{ db})}{6.29}$  greater than those estimated by Equation (120).

The space-time correlation of the shock-turbulence sound may be estimated from the sound propagation speed and the convection speed. The spectrum is not known, but noise measurements in wind tunnels suggest that the spectrum will maximize in the audio frequency range, in contrast to the situation expected in the subsonic case.

Comparison with the environments discussed earlier indicates that the pressures associated with flight through a naturally turbulent atmosphere are of somewhat less importance. This is so for both subsonic and supersonic flight. However, we must emphasize again that much of the above is in the realm of speculation; hard facts are not available for substantiation. Furthermore, the atmosphere

may be more turbulent than that assumed; a source of additional turbulence that may be of importance is mentioned in the next paragraphs.

### 3. Retro-rocket Turbulence

One proposed method of decelerating a space vehicle consists of firing a rocket in the direction of the forward flight path. As the vehicle decelerates, it may move through a portion of the rocket exhaust stream. The turbulent velocity fluctuations in the exhaust stream can move over and excite the vehicle surfaces, and thereby act as noise sources.

This method of "retro-firing" deceleration would probably be used in a very low density atmosphere. Therefore, a description of the rocket exhaust turbulence requires some understanding of jet behavior in such atmospheres. Unfortunately, little information of this kind is available. We may speculate that the exhaust stream will expand right at the rocket exit nozzle, so that the pressure inside the stream is equal to the (very low) pressure of the surrounding atmosphere. Also, the interface between the expanded jet and the atmosphere may become hot, because of the high relative velocity between the two media. However, we must have a more quantitative picture of the exhaust flow in order to estimate the importance of retro-firing operation as a noise source. Thus, there is a need for experiments to determine the steady and the fluctuating quantities of a rocket exhaust in a low density atmosphere.

## H. Pressure Due to Micro-Meteorite Impacts

Although the existence of cosmic debris or meteoritic dust outside the earth's atmosphere has been indirectly deduced many years ago, it has been only since the advent of high-altitude rockets and satellites that this dust has been sampled and made the subject of more direct study.<sup>6.30-6.34/</sup> With orbital and space flights a reality, the possible noise induced by the continued encounter of vehicles with micro-meteorites naturally becomes one of the many matters of concern.

Relative abundances, masses, radii, and velocities, of micro-meteorites at the edge of the earth's atmosphere are given in the table on the following page, based on one of the most widely accepted estimates.<sup>6.31/</sup> This estimate is based on extrapolation of visual, photographic<sup>6.32/</sup> and radio meteor data, but some of the measurements obtained from satellites and sounding rockets seem to agree with it.<sup>6.32-6.34/</sup> More data concerning the abundance of the smaller particles may soon become available as a result of studies currently in progress. It is of interest to note that meteorites in general have sponge-like structures, with densities of the order of  $0.05 \text{ gm/cm}^3$ .

In the table no account is made of possible shielding by the earth; a factor of one-half should be applied to the number of impacts for vehicles near the earth's surface. Other corrections for distance from the earth cannot be made in absence of precise data on particle and vehicle orbits, but it is likely that the number of meteorites striking a vehicle will decrease with increasing distance from the earth, even if shielding by the earth is taken into account.<sup>6.31/</sup> In view of the limits of present

TABLE VI  
METEOROID DATA

Meteor Visual Mag.	Mass (gm)	Radius (Microns)	Velocity (km/sec)	Impacts on 3m Diameter Sphere per Day+
5	0.25	10,600.	28	$2.22 \times 10^{-5}$
6	$9.95 \times 10^{-2}$	7,800.	28	$6.48 \times 10^{-5}$
7	$3.96 \times 10^{-2}$	5,740.	28	$1.63 \times 10^{-4}$
8	$1.58 \times 10^{-3}$	4,220.	27	$4.09 \times 10^{-4}$
9	$6.28 \times 10^{-3}$	3,110.	26	$1.03 \times 10^{-3}$
10	$2.50 \times 10^{-3}$	2,290.	25	$2.58 \times 10^{-3}$
11	$9.95 \times 10^{-4}$	1,680.	24	$6.48 \times 10^{-3}$
12	$3.96 \times 10^{-4}$	1,240.	23	$1.63 \times 10^{-2}$
13	$1.58 \times 10^{-4}$	910.	22	$4.09 \times 10^{-2}$
14	$6.28 \times 10^{-5}$	669.	21	$1.03 \times 10^{-1}$
15	$2.50 \times 10^{-5}$	492.	20	$2.58 \times 10^{-1}$
16	$9.95 \times 10^{-6}$	362.	19	$6.48 \times 10^{-1}$
17	$3.96 \times 10^{-6}$	266.	18	1.63
18	$1.58 \times 10^{-6}$	196.	17	4.09
19	$6.28 \times 10^{-7}$	144.	16	$1.03 \times 10$
20	$2.50 \times 10^{-7}$	106.	15	$2.58 \times 10$
21	$9.95 \times 10^{-8}$	78.0	15	$6.48 \times 10$
22	$3.96 \times 10^{-8}$	57.4	15	$1.63 \times 10^2$
23	$1.58 \times 10^{-8}$	39.8*	15	$4.09 \times 10^2$
24	$6.28 \times 10^{-9}$	25.1*	15	$1.03 \times 10^3$
25	$2.50 \times 10^{-9}$	15.8*	15	$2.58 \times 10^3$
26	$9.95 \times 10^{-10}$	10.0*	15	$6.48 \times 10^3$
27	$3.96 \times 10^{-10}$	6.30*	15	$1.63 \times 10^4$
28	$1.58 \times 10^{-10}$	3.98*	15	$4.09 \times 10^4$
29	$6.28 \times 10^{-11}$	2.51*	15	$1.03 \times 10^5$
30	$2.50 \times 10^{-11}$	1.58*	15	$2.58 \times 10^5$
31	$9.95 \times 10^{-12}$	1.00*	15	$6.48 \times 10^5$

\* Maximum radius permitted by solar light pressure.

+ Includes all meteorites of mass greater than that indicated in "mass" column.

knowledge this table can be applied with reasonable confidence only for distances up to about  $10^4$  km from the earth.

From the values given in the table on the previous page one may compute that the average total momentum flux (i.e., pressure) due to particles of all sizes amounts at most to about  $2 \times 10^{-9}$  dynes/cm<sup>2</sup> if shielding by the earth is neglected. This value of pressure corresponds to a pressure level of -100 db, which is negligible compared to that due to other sources. The aforementioned pressure, however, is an average over a long time, and it is quite possible that significantly higher pressures are reached for short periods, particularly if there exist orbital positions where concentrations of particles occur. Also, the instantaneous response of the vehicle structure might be quite high for a single impact, although the long-time average would be expected to be quite low.

#### I. Discussion

We have presented a review of some of the noise environments likely to be important for flight vehicles. Although this review is by no means exhaustive in subject matter or complete in detail of information, it does indicate that the noise environments of a flight vehicle are indeed complex and that much is yet to be learned about these environments.

The need for further measurements to clarify and widen our knowledge of environmental noise is obvious. Such measurements may be carried out most directly on vehicles in flight, but such experimentation is relatively difficult and costly. It is anticipated that laboratory

investigations, e.g., of base pressure fluctuations on wind tunnel models, may be extremely useful.

Some phases of the experimental investigations are likely to prove extremely difficult because the noise observed may be due to more than one significant source. For example, the boundary layer and the base pressure fluctuations are both functions of dynamic pressure; measurement of noise on a flight vehicle is apt to show a maximum when the dynamic pressure is at its maximum. However, the contributions of the two aforementioned sources will be indistinguishable unless extreme ingenuity and care are exercised in devising and executing the experiment.

Some sources of structural excitation that we have not discussed in this section may be quite important. These include: combustion instability and other internal engine oscillations that may be transmitted directly to the structure, transients associated with changes in propulsion, transients associated with separation of vehicle sections (e.g., stages), unsteady thermal stresses in structures due to unsteady motions of the vehicle. A careful assessment of the environmental problem of a flight vehicle should include these and possibly other sources, as well as those discussed in the present section.

SECTION VII  
STRUCTURAL RESPONSE

Sound due to external sources can reach the interior of completely enclosed spaces, such as space vehicle compartments, only after being transmitted by the enclosing structures. Thus the noise reaching the interior is a function of the forcing field, of the vibrations of the enclosures in response to these fields, and of the vibration transmission and sound radiation characteristics of the various structures involved. Calculation of the response of vehicle structures to these forcing fields forms a natural part of the study of noise within vehicles.

The different kinds of forcing fields encountered in space vehicles require different approaches to the structural response problem: well-defined forces lead to motions that can be described exactly, but random forces lead to motions that must be described statistically. It is therefore convenient to group these forcing fields in terms of their space and time characteristics, as shown in the following table:

1. Fields with exactly defined space and time characteristics

Examples: Periodic vibrations from mechanical equipment, moving shocks with defined characteristics

2. Fields random in time, but with exactly defined space characteristics

Examples: Non-periodic vibrations from mechanical equipment, rocket noise

3. Fields random in space, but with exactly defined time characteristics
4. Fields random in time and space

Examples: Boundary layer turbulence, dust and micro-meteorite interception.

In the remainder of this Section we will present formalisms adequate for studying the various types of fields listed above and will apply these methods to typical physical examples. The problem of structural response to vibrations of mechanical equipment is not considered here, because it logically forms part of a separate program studying vibration in space vehicles. Also, because no important physical examples of forcing fields appear in group 3 above, this group is not discussed further.

#### A. Response of Plates to Moving Shocks

Vehicles in supersonic flight give rise to shock waves, which are essentially pressure discontinuities. The motion of such discontinuities with respect to structures can cause these structures to oscillate, possibly quite severely. The following discussion describes the response of simple structures to pressure discontinuities, in order to shed some light on underlying physical mechanisms. This material is based on work reported in Reference 7.1, which contains a more thorough discussion of the subject.

Consider a pressure discontinuity (shock wave) propagating across a rectangular plate that is simply supported at all edges. The plate edges are taken at  $x = 0, a$ , and  $y = 0, b$ . Let the position of the discontinuity on the panel be described by some function of time  $\xi(t)$ , and let

the shock front move parallel to the y axis. If the pressure ahead of the discontinuity is assumed constant and equal to the pressure below the panel, it may be taken as the pressure datum. Further, if the pressure behind the discontinuity is assumed uniform and greater than the pressure ahead of the discontinuity by an amount p, the situation might be represented schematically as shown in Figure 95.

The deflection of the rectangular plate may conveniently be expressed as

$$\eta = \sum_{m=1}^{\infty} \sum_{n=1}^{\infty} q_{mn} \sin \frac{m\pi x}{a} \sin \frac{n\pi y}{b} \quad (121)$$

The motion of the plate (starting from rest) may then be described by

$$\begin{aligned} q_{mn} &= N_{mn} J_{mn}(t) \\ N_{mn} &= \frac{4p (1 - \cos n\pi)}{\pi^2 \rho h mn \beta_{mn}^2} = \frac{4p (1 - \cos n\pi)}{\pi^6 B mn \left( \frac{m^2}{a^2} + \frac{n^2}{b^2} \right)^2} \\ J_{mn}(t) &= \beta_{mn} \int_0^t \left[ 1 - \cos \frac{m\pi \xi(t)}{a} \right] \sin \beta_{mn} (t - \tau) d\tau \end{aligned} \quad (122)$$

where  $\rho$  is plate density

$h$  is plate thickness

$\beta_{mn}$  are circular resonance frequencies of the plate

$$\beta_{mn} = \sqrt{\frac{B}{\rho h}} \left[ \left( \frac{m\pi}{a} \right)^2 + \left( \frac{n\pi}{b} \right)^2 \right] = 2\pi f_{mn} \quad (123)$$

$$B = \text{Plate Bending Stiffness} = Eh^3/12 (1 - \nu^2)$$

For given motions  $\xi(t)$  of the shock front one may now compute the panel response by carrying out the indicated integration.

1. Shock Moving at Constant Velocity

For a shock moving uniformly at velocity  $v$  one may choose to measure time from the instant the shock first touches the panel and may substitute  $\xi(t) = vt$  into the last of Equation (122) to obtain

$$J_{mn}(t) = \begin{cases} 1 + \frac{r_{mn}^2 \cos \beta_{mn} t - \cos(r_{mn} \beta_{mn} t)}{1 - r_{mn}^2}, & r_{mn} \neq 1 \\ 1 - \cos \beta_{mn} t - \frac{1}{2} \beta_{mn} t \times \sin \beta_{mn} t, & r_{mn} = 1 \end{cases} \quad (124)$$

where

$$\begin{aligned} r_{mn} &= \frac{m\pi v}{a\beta_{mn}} = \frac{v}{u_{mn}} \\ u_{mn} &= \frac{a\beta_{mn}}{m\pi} = \pi \sqrt{\frac{B}{\rho h}} \frac{a}{m} \left[ \left(\frac{m}{a}\right)^2 + \left(\frac{n}{b}\right)^2 \right] \end{aligned} \quad (125)$$

One finds that  $u_{mn}$  represents the x-ward velocity of propagation of a wave of frequency  $\beta_{mn}$ ;  $r_{mn}$  thus is the ratio of the shock velocity to velocity in the x direction of a flexural wave in the mn mode.

One may observe that  $q_{mn}$  oscillates sinusoidally if  $r_{mn} \neq 1$ , with time-wise maxima given by

$$\frac{|q_{mn}| \max}{2N_{mn}} = \begin{cases} \frac{1}{1 - r_{mn}^2}, & r_{mn} < 1 \\ \frac{1}{1 - \frac{1}{r_{mn}^2}}, & r_{mn} > 1 \end{cases} \quad (126)$$

but oscillates with linearly increasing amplitude if  $r_{mn} = 1$ . In addition one may observe that

$$q_{mn} \sim N_{mn} \sim \left[ mn \left( \frac{m^2}{a^2} + \frac{n^2}{b^2} \right) \right]^{-1} \quad (127)$$

$$\dot{q}_{mn} \sim \beta_{mn} N_{mn} \sim \left[ mn \left( \frac{m^2}{a^2} + \frac{n^2}{b^2} \right) \right]^{-1}$$

whence

$$q_{mn} \sim m^{-6}, \quad \dot{q}_{mn} \sim m^{-4}, \quad \text{for } m \doteq n \quad (128)$$

$$q_{mn} \sim m^{-5}, \quad \dot{q}_{mn} \sim m^{-3}, \quad \text{for } m \gg n, \text{ } n \text{ fixed.}$$

The considerable preponderance of the lower modes is evident from these relations.

The case  $r_{mn} = 1$  corresponds to the condition where the velocity with which the shock travels is equal to the wave velocity of  $mn$  mode, giving rise to an effect which is similar to well-known coincidence phenomena. As usually understood, coincidence refers to a matching between a bending wavelength (or velocity) of a structure and a trace wavelength (or velocity) of a pressure wave incident on a structure, so that the pressure and velocity fluctuations

are in phase over some portion of the structure surface. The pressure field is considered to be sinusoidal in space and time, and the area over which the pressure and velocity fluctuations are in phase is independent of frequency. However, in the present case the pressure is not sinusoidal and the area of coincidence does depend on frequency (and, in fact, is not stationary on the structure), as is discussed subsequently.

One may visualize that the first crossing of a plate edge by the pressure increase causes a small disturbance to emanate from that edge. This disturbance gives rise to flexural waves of all frequencies, which propagate at different velocities (proportional to the square root of frequency). If the shock front moves with the same velocity as one of these bending wave components, it continues to feed energy into this component, since pressure and velocity then are in phase over the front-most half wavelength. The area over which the effective excitation acts is proportional to the wavelength, or inversely proportional to the mode number; the area of excitation is thus inversely proportional to mode number  $n$ . This fact accounts for more rapid decrease in modal amplitude with mode number here than in the more commonly considered coincidence problems.

The previous physical interpretations also account for the limit on the energy (and amplitude) associated with modes which are not in coincidence. It also explains that modes whose velocities match the shock velocity less closely are excited less, because the corresponding bending waves coincide less with the exciting field.

The motion of the panel after passing of the shock may be considered as a free vibration about the new equilibrium position, with new "initial" conditions. The modal amplitudes  $A_{mn}$  of this motion are found to be

$$\frac{A_{mn}}{N_{mn}} \begin{cases} \leq 2 r_{mn}^2, & r_{mn} \ll 1 \\ \leq 2, & r_{mn} \gg 1 \\ = \frac{m\pi}{2}, & r_{mn} = 1 \end{cases} \quad (129)$$

whence the influence of trace-matching on the amplitudes of the residual motions is clearly apparent.

Example of Magnitudes. For a rocket traveling at a reasonably high Mach number in the not too rarified portions of the atmosphere, a pressure difference of 0.1 psi across a shock is not unreasonable. For a 2 ft by 2 ft by 0.05 in. steel panel, one finds

$$\text{from Eq (123): } \beta_{mn} = 52.8 (m^2 + n^2) \text{ radians/sec}$$

$$\text{from Eq (122): } N_{mn} = 0.40 (1 - \cos n\pi)/mn (m^2 + n^2) \text{ in.}$$

$$\text{from Eq (125): } u_{mn} = 400 (m + \frac{n^2}{m}) \text{ in./sec}$$

For a velocity of 5,000 ft/sec = 60,000 in./sec, one obtains

$$\text{from Eq (125): } r_{11} = 75$$

$$\text{from Eq (122): } N_{11} = 0.40 \text{ in.}$$

$$\text{from Eq (129): } A_{11}/N_{11} \doteq 2, \text{ hence } A_{11} = 0.80 \text{ in.}$$

This is a significantly large amplitude. (Similar calculations may explain how sonic booms can cause windows to shatter.) However, for the  $m = n = 75$  mode one finds that the amplitude of the residual vibration is  $1.5 \times 10^{-5}$  in. although trace-matching with this mode occurs.

Similarly, for a velocity of 1600 in./sec, one finds

$$r_{11} = 2.0, A_{11} = 0.75 \text{ in.}$$

$$r_{41} = .94, A_{41} = 0.070 \text{ in.}$$

(For the velocity for which  $r_{41} = 1.0$ , one obtains  $A_{41} = .074$  in.) The preponderance of the (1,1) mode is clearly evident from this illustration.

## 2. Sinusoidally Oscillating Shock

If the shock front oscillates sinusoidally about some mean position  $x = C$  on the panel, the position of the shock front may be expressed as

$$\xi(t) = C + H \sin \omega t \quad (130)$$

where  $H$  denotes the excursion and  $\omega$  the circular frequency of the oscillation. Substitution of Equation (130) into Equation (122) results in

$$J_{mn}(t) = 1 - \cos(\beta_{mn} t) - F_{mn}(t) \quad (131)$$

where

$$F_{mn}(t) = \beta_{mn} \int_0^t \cos\left(\frac{m\pi c}{a} + \frac{m\pi H}{a} \sin \omega \tau\right) \sin \beta_{mn}(t - \tau) d\tau \quad (132)$$

General closed expressions for the integrals indicated in Equation (132) are not available, but fortunately one can introduce approximations which permit some useful information to be extracted. These approximations are discussed in Reference 7.1. The results obtained by using these approximations indicate that  $\omega = \beta_{mn}$  or  $\omega = \frac{\beta_{mn}}{2}$  correspond to resonances, i.e., to driving the system at one of its natural frequencies. The two resonances for each mode indicated by this mathematical result may be explained physically by reference to Figure 96. The pressure distribution may be visualized in terms of a uniform steady pressure and a time-varying pressure component as indicated, and the plate response depends on the time-varying component only. This gives rise to a net normal force  $\Delta F$  (per unit width in the y-direction) and a net moment  $\Delta M$  about  $x = C$ . In the figure the instantaneous excursion is shown as  $\Delta x = H \sin \omega t$ ; then

$$\Delta F = p \Delta x = pH \sin \omega t \tag{133}$$

$$\Delta M = \int_0^{\Delta x} px \, dx = \frac{1}{2} pH^2 \sin^2 \omega t = \frac{1}{4} pH^2 (1 - \cos 2 \omega t)$$

Thus, with  $\omega = \beta_{mn}$  the panel is at resonance with the oscillating force, and with  $\omega = \frac{\beta_{mn}}{2}$  the panel is at resonance with the oscillating moment.

One or the other of these plate resonances may be suppressed for certain values of  $\frac{C}{a}$ . In general, this suppression of resonances can be associated with a mismatching between the symmetry of the driving force and the symmetry of the mode shapes in the vicinity of the  $x = C$  position. For example, for the case where  $C = \frac{a}{2}$ , moment resonances are absent if  $m = 1 + 2\lambda$ , and force

resonances are absent if  $m = 2\lambda$ , where  $\lambda$  is any integer (or zero). This agrees with the fact that forces applied at the plate center can excite only the odd-numbered modes and moments only the even-numbered modes.

Discussions of the cases of randomly oscillating shocks and lightly damped plate structures are contained in Reference 7.1.

B. Response of Plates to Temporally  
Random Pressure Fields:  
Atmospheric Turbulence, Rocket Noise

1. Response to Atmospheric Turbulence

The response of an elastic system to a temporally random field can be obtained by use of the results of Thomson and Barton.<sup>7.3/</sup> The mean square displacement  $\langle w^2 \rangle$  is expressed in terms of a frequency integral

$$\langle w^2 \rangle = \int_0^{\infty} \frac{\text{power spectral density of excitation}}{\text{generalized impedance of elastic system}} df \quad (134)$$

For lightly damped structures the major contributions to the integrals occur near the system resonance frequencies  $f_{mn}$ . If the power spectral density does not change markedly at  $f_{mn}$ , the foregoing may be approximated by

$$\langle w^2 \rangle \doteq \frac{1}{4\eta} \sum_{m,n} \frac{S(f_{mn}) b_{mn}^2 \phi_{mn}^2}{M_{mn}^2 \omega_{mn}^3} \quad (135)$$

where  $\eta$  = damping coefficient (reciprocal of resonance Q)  
 $S(f)$  = power spectral density of exciting pressure p

$$p^2 = \int_0^{\infty} S(f) df^*$$

$$b_{mn} = \text{modal participation of load } p = \frac{p \phi_{mn} dA}{\int p dA}$$

$\phi_{mn}$  = dimensionless eigenfunctions of elastic system

$$M_{mn} = \text{generalized mass} = \int \phi_{mn}^2 dm$$

$$\omega = 2\pi f$$

We shall now apply the foregoing to the case of a plate moving through atmospheric turbulence. In line with the discussion of Part G of Section VI, a possible form for the power spectrum  $s(f)$  is

$$S(f) = \frac{2p^2}{\pi f_0 \left[ 1 + \left( \frac{f}{f_0} \right)^2 \right]} = \frac{4p^2}{\omega_0 \left[ 1 + \left( \frac{\omega}{\omega_0} \right)^2 \right]} \quad (136)$$

where  $p$  is the rms pressure fluctuation,  
 $f_0$  is the characteristic frequency, and

$$\omega_0 = 2\pi f_0 \quad (137)$$

The resonance (circular) frequencies of a rectangular thin plate of dimensions  $L_x$ ,  $L_y$ , and thickness  $h$  are

$$\omega_{mn} = \sqrt{\frac{B}{\rho_p h} \left[ \left( \frac{m\pi}{L_x} \right)^2 + \left( \frac{n\pi}{L_y} \right)^2 \right]} = 2\pi f_{mn} \quad (138)$$

where  $B$  and  $\rho_p$  are the plate bending stiffness and density, respectively.

---

\* The power spectral density  $S(f)$  is the Fourier cosine transform of the autocorrelation function  $R(\tau)$ , which describes the temporal decay of the forcing field.

The coefficient of  $\phi_{mn}^2$  in Equation (135) is the mean square displacement in the mn mode,  $\langle w^2 \rangle_{mn}$ . (This is actually the displacement spectral density, integrated through the resonance at  $f_{mn}$  and averaged in space.) Using Equation (136) we obtain

$$\overline{\langle w^2 \rangle_{mn}} = \begin{cases} 0, & m \text{ or } n \text{ even} \\ \frac{64 \langle p^2 \rangle}{\eta \pi^4 \omega_o^3 \omega_{mn}^3 (\rho_p h)^2 (mn)^2 \left[ 1 + \left( \frac{\omega_{mn}}{\omega_o} \right)^2 \right]}, & m \text{ and } n \text{ odd} \end{cases}$$

Because of the quadratic dependence on mode number in Equation (138), we see that Equation (139) contains a dependence on mode number that is at least as strong as (mode number)<sup>-10</sup>. Therefore, the 1,1 mode is the major contributor to the overall mean square displacement.

In order to calculate the sound pressure within a space vehicle, we must obtain the velocity of the vehicle surfaces in the audible frequency range. The mean square velocity in the mn mode is

$$\overline{\langle v^2 \rangle_{mn}} = \omega_{mn}^2 \overline{\langle w^2 \rangle_{mn}} \quad (140)$$

Numerical Example. From the example in Part G of Section VI, a maximum value of the atmospheric turbulence pressure fluctuation is approximately 0.1 lbs/sq ft, or 48 dynes/sq cm, for a vehicle moving 1000 ft/sec at an altitude of 60,000 ft. For a vehicle 100 ft long, the characteristic circular frequency  $\omega_o$  is 10 sec<sup>-1</sup>. The plate dimensions are as follows:

steel plate 50 cm x 50 cm x 0.3 cm  
(Approx. 20 in. x 20 in. 1.2 in.)

$$\eta = 3 \times 10^{-3}$$

$$\text{From Eq (138): } f_{11} = \frac{\omega_{11}}{2\pi} = 56 \text{ cps}$$

$$\text{From Eqs (139) and (140): } \sqrt{\langle v^2 \rangle}_{11} = 0.14 \text{ cm/sec}$$

## 2. Response to Sound

Random sound waves, or noise, constitute a particular example of pressures that fluctuate randomly in time. The important feature that describes such pressure fluctuations and differentiates them from other random pressure fluctuations is the periodic phase properties of the pressure field. These periodic phase properties define the sound wavelength and are important in determining the response of structures to the pressure fields.

a. Response of Resonant Structures to Sound. If one considers a complicated mechanical structure to be composed of a number of coupled panels, it is clear that many resonances will occur in response to excitation by a broadband sound field. Without a detailed and complicated study, one does not know at what frequencies these resonances will occur or where coincidence effects (matching of panel wavelength to projected sound wavelength) will take place. As a conservative measure, one may assume that these effects may occur at any frequency and thereby calculate the envelope curve of all the individual maximum responses as a function of frequency and excitation.

In line with this simplified point of view, the ratio of the exciting sound pressure  $p$  to the resulting resonant vibration velocity  $v$  normal to the surface of the structure is given by

$$\frac{p}{v} = \frac{2\pi f_r m \eta}{T} \quad (141)$$

where  $f_r$  is the resonance frequency,  $m$  is the mass per unit area of the structure, and  $\eta$  is the damping coefficient. The dimensionless transfer function  $T$  takes account of the inter-panel couplings and coincidence effects; its maximum value is not much greater than unity.

Integration of the response over the frequency band around the particular resonance being considered gives for the mean square velocity

$$\langle v^2 \rangle = \frac{S(f_r) T^2}{8\pi \eta f_r m^2} \quad (142)$$

where  $S(f_r)$  is the spectral density of the exciting sound field at the resonance frequency. Equation (142) is the desired result, relating the incident sound field to the maximum structural response.

b. Sound Transmission Through Finite Cylinders.

Section III has considered primarily the excitation of plane structures by sound waves. Because many space vehicle structures have some degree of cylindrical symmetry, it is of interest to extend the material in Section III to cylinders. Cremer,<sup>7.4/</sup> Smith,<sup>7.5/</sup> and Heckl<sup>7.6/</sup> have studied various aspects of sound transmission through cylindrical shells, and portions of their results will be

referred to here. One case of particular interest, sound transmission near grazing incidence, has not been considered in detail, and a tentative procedure will be proposed for obtaining the transmission loss (TL) for this case.

Some analytical aspects of sound transmission through cylindrical shells were discussed in Part H of Section III. It was pointed out that it is convenient to study the shell motion in terms of angular modes, each denoted by a mode number  $n$ . There exists a characteristic frequency  $f_0$ , called the radial resonance frequency, and defined as

$$f_0 = \frac{c_L}{2\pi a} = \frac{1}{2\pi a} \left[ \frac{Eh}{m(1 - \sigma^2)} \right]^{\frac{1}{2}} \quad (143)$$

where  $c_L$  is the speed of (non-dispersive) longitudinal waves in the shell, and  $a$ ,  $E$ ,  $h$ ,  $m$ , and  $\sigma$  are the radius, Young's modulus, total thickness, mass per unit area, and Poisson's ratio of the shell, respectively. For frequencies above the radial resonance, the shell acts in bending as a thin flat plate of thickness  $h$ . Therefore, in this higher frequency range the material in Section III on TL of flat plates is directly applicable to the study of thin cylinders. For frequencies below the radial resonance, the shell may be described adequately by membrane theory.

By Fourier analysis, a signal may be broken up into an integral or sum of periodic components. Therefore, we may Fourier-analyze the pressure fields exciting the cylinder, determine the response of the cylinder to any Fourier component, and finally Fourier-synthesize the response to determine the transmission properties of the shell. For one such Fourier component, the pressure

field outside a cylinder may be written in terms of angular modes as

$$p = \sum_n p_n \cos n\phi e^{-i\omega t} \quad (144)$$

From membrane theory, the transmission impedance  $Z_{tn}$ , the ratio of the exciting pressure to the radial velocity in the  $n^{\text{th}}$  mode, may be found to be (see, for example, Smith, 7.5/ Franken 7.7/)

$$Z_{t0} \doteq -i\omega m \left[ 1 - \left( \frac{\omega_0}{\omega} \right)^2 \right]$$

$$Z_{tn} \doteq -i\omega m \left\{ \frac{n^2(n^2 + 1) - \left( \frac{\omega a}{c_a} \right)^4 \left( \frac{\omega_0}{\omega} \right)^2}{\left[ \left( \frac{\omega a}{c_a} \right)^2 + n^2 \right]^2} \right\}, n > 0 \quad (145)$$

$$\omega = 2\pi f$$

where  $c_a$  is the axial velocity component of the incident wave. The various modal transmission impedances must be combined according to the weighted participation of different angular modes in the forcing field. This gives rise to an average transmission coefficient  $\bar{\tau}$ , related to TL by

$$TL = 10 \log \frac{1}{\bar{\tau}} \quad (146)$$

For the case where the incident sound field is reverberant, that is, where virtually all angles of incidence are possible (random incidence), Heckl 7.6/

has found that the cylinder TL for broad-band noise excitation is given by

$$\begin{aligned} TL &= TL_{\ell} + K \\ K &\doteq \begin{cases} 9 \text{ db, } 0.1 < \frac{f}{f_0} < 0.4 \\ 0 \text{ db, } \frac{f}{f_0} \doteq 1 \end{cases} \end{aligned} \quad (147)$$

Equation (147) is plotted in Figure 97.  $TL_{\ell}$  is one-half the TL given by "normal incidence mass law" at the radial resonance frequency. For steel or aluminum shells,  $TL_{\ell}$  and  $f_0$  may be obtained from Figure 98, using the ratio  $\frac{h}{2a}$ .

Up to this point the important case of sound near grazing incidence has been excluded from the discussion. This case occurs, for example, in a space vehicle with a rocket engine exhausting at the vehicle rear during subsonic powered operation. Based on a small amount of experimental information and some semi-quantitative arguments, it appears that the TL for grazing incidence should not be very different from the TL for random incidence. We therefore propose that the TL given in Figure 97 for random incidence be used also for grazing incidence. It should be emphasized that this is a tentative proposal and that additional theoretical and experimental work is required to establish the accuracy of this procedure.

#### C. Response of Plates to Pressures That Are Random in Space and Time

Many of the fields that may be important in exciting a space vehicle structure consist of pressures that are random both in space and in time. These fields may consist of pressures which are convected along the structure

(boundary layer turbulence) or which are stationary with respect to the structure (base pressure turbulence or dust). A general formalism given by Lyon 7.8/ and more recently by Dyer 7.9/ considers the problem of structural response by a random excitation. (An analogous formalism has been developed by Eringen. 7.10/) This formalism, based on the impulse response concept, may be applied to any elastic system for the most general type of random forcing field. Excitation of plates by turbulent pressures and dust may be conveniently studied by means of this formalism.

### 1. General Solution

The displacement response  $w$  of an elastic system to a forcing function  $p$  can be written as

$$w(\vec{r}, t) = \int_{-\infty}^t dt_0 \int_S dS_0 g(\vec{r}, t | \vec{r}_0, t_0) p(\vec{r}_0, t_0) \quad (148)$$

where  $g$  is the impulse response,  $\vec{r}$  is the position vector, and  $t$  denotes time. Without a subscript these symbols refer to the response; with a subscript  $0$  they refer to the applied impulse. The effects of boundary conditions, initial conditions and radiation losses have been neglected in Equation (148). This step is not restrictive for our interests. In problems involving random processes, we are interested in the response correlation  $\langle ww'^* \rangle$  rather than  $w$  itself. The response correlation may be written as a product of two sums containing the source correlation  $\langle pp'^* \rangle$ .

For any specific problem, three steps are required in principle to apply these results:

1. Determine the eigenfunctions and the resonances of the elastic system.
2. Determine the source correlation  $\langle pp'^* \rangle$ .
3. Perform the indicated integrations and summations.

## 2. Response to Boundary Layer Pressure Fluctuations

The formalism given above is useful in studying excitation by the turbulent pressure fluctuations in the boundary layer on a moving vehicle. Dyer <sup>7.9/</sup> has described an idealized boundary layer pressure field as follows:

1. The pressure field is a stationary random process.
2. The pressure correlation decays with time.
3. The pressure correlation has a spatial extent much smaller than the plate size of interest.
4. The pressure correlation is convected along the surface of the plate in the direction of the free stream velocity.
5. The spatial correlation is homogeneous, depending upon the difference in the spatial coordinates in a frame of reference moving with the mean convection stream.

A convenient and relatively simple correlation function that embodies this description is given by Dyer as

$$\langle p(\bar{r}, t) p^*(\bar{r}', t') \rangle = p^2 \exp \left[ - \frac{\sqrt{(\zeta - v\tau)^2 + \xi^2}}{\ell} - \frac{|\tau|}{\theta} \right] \quad (149)$$

where  $\ell$  is the mean statistical radius of a turbulent "eddy"

$p^2$  is the mean square pressure

$\theta$  is the mean statistical lifetime of a turbulent "eddy"

$v$  is the convection speed

$$\zeta = x - x'$$

$$\xi = y - y'$$

$$\tau = t - t'$$

The spectral density  $S(f)$  is the Fourier transform of the correlation function, or for Dyer's correlation function,

$$\begin{aligned}
 S(f) &= 2 \int_{-\infty}^{\infty} \langle pp'^* \rangle_r = \frac{1}{r} \exp[2\pi i f \tau] d\tau \\
 &= \frac{2p^2}{\pi f_0} \frac{1}{1 + \left(\frac{f}{f_0}\right)^2}
 \end{aligned}
 \tag{150}$$

where

$$2\pi f_0 = \frac{v}{l} + \frac{1}{\theta} \tag{151}$$

Experimental data indicate that the characteristic frequency  $f_0$  is determined mainly by the "eddy passage frequency"  $\frac{v}{l}$  and is practically independent of the lifetime  $\theta$  (see Part B of Section VI).

The eigenfunctions and resonance (circular) frequencies of a simply supported uniform rectangular thin plate of dimensions  $L_x$ ,  $L_y$ , and  $h$  are

$$\phi_{mn} = \frac{2}{\sqrt{L_x L_y}} \sin \frac{m\pi x}{L_x} \sin \frac{n\pi y}{L_y}$$

(152)

$$\omega_{mn} = \frac{c_L h}{\sqrt{12}} \left[ \left(\frac{m\pi}{L_x}\right)^2 + \left(\frac{n\pi}{L_y}\right)^2 \right] = 2\pi f_{mn}$$

where  $c_L$  is the speed of (non-dispersive) longitudinal waves in the plate ( $\omega_{mn}$  is identical to  $\beta_{mn}$  given in the previous discussion on plate excitation by moving shocks). Applying

the general solution outlined above to such a plate excited by boundary layer turbulence, and simplifying the spatial dependence of the correlation function slightly, Dyer finds that the displacement correlation in the  $mn^{\text{th}}$  mode may be written as

$$\langle w(\vec{r}, t) w^*(\vec{r}', t') \rangle_{mn} = \frac{\pi \ell_p^2}{2 \omega_{mn}^2 M^2} \phi_{mn}(\vec{r}) \phi_{mn}(\vec{r}') I_{mn}(\tau) \quad (153)$$

a. Response at Coincidence. We now assume that the mean convection speed  $v$  is comparable to the velocity of free waves in the plate  $c_B$ , where  $c_B^4 = \omega^2 \left[ \frac{B}{M} \right]$ , and  $B$  is the plate bending stiffness. This assumption holds generally for a boundary layer of air, such as exists around a space vehicle.

If the pressure field is correlated only over a distance that is small compared to the wavelength of  $m^{\text{th}}$  plate mode, we do not expect convection effects to be important. In this case the pressure field cannot readily excite plate motions that are coherent over a large scale. The results discussed in (3) below may often be appropriate for such a pressure field. If the pressure field is correlated over a distance that is greater than the  $m^{\text{th}}$  modal wavelength, maximum response occurs for

$$\frac{m\pi v}{L_x} = \omega_{mn} \quad (154)$$

Dyer's analysis shows that the mode number  $m$  is restricted by

$$m\pi > \frac{L_x}{v\theta} \gg 1 \quad (155)$$

Then a maximum response occurs when the convection speed  $v$  has the particular value  $v_0$ , where

$$v_0 = c_B \left[ 1 + \left( \frac{nL_x}{mL_y} \right)^2 \right]^{\frac{1}{2}} \quad (156)$$

This condition is called hydrodynamic coincidence. The value of the time correlation integral for zero time delay  $I_{mn}(0)$  is of special interest because it enters into the expression for the mean square displacement. At hydrodynamic coincidence (maximum response) we find

$$I_{mn}(0) \doteq \frac{\theta}{a_{mn}(a_{mn}\theta + 1)}, \quad \omega_{mn}\theta > 1 \quad (157)$$

where  $a_{mn}$  is the modal damping. In the important limits of very small viscous damping  $\beta_0$  or very small hysteretic damping  $\eta$ ,  $a_{mn}$  is

$$a_{mn} \doteq \frac{\eta\omega_{mn}}{2}, \quad \frac{\beta_0}{\omega_{mn}M} \ll \eta \quad (158)$$

$$a_{mn} \doteq \frac{\beta_0}{2M}, \quad \eta \ll \frac{\beta_0}{\omega_{mn}M}$$

respectively. For low damping

$$I_{mn}(0) \doteq \frac{\theta}{a_{mn}}, \quad \omega_{mn}\theta > 1, \quad a_{mn}\theta \ll 1 \quad (159)$$

From Equation (153) the mean square displacement in the  $mn^{\text{th}}$  mode is

$$\overline{\langle w^2 \rangle}_{mn} = \frac{\pi l^2 p^2}{2\omega_{mn}^2 M^2 L_x L_y} I_{mn}(0) \quad (160)$$

As an example of practical importance, consider the case of low damping with viscous damping negligible compared to hysteretic damping: Equation (160) becomes

$$\overline{\langle w^2 \rangle}_{mn} = \frac{\pi l^2 \theta p^2}{\gamma \omega_{mn}^3 M^2 L_x L_y} \quad (161)$$

If the mean convection speed is close to but not quite equal to the hydrodynamic coincidence speed, we have for the case of low damping

$$I_{mn}(0) = \frac{\theta}{a_{mn} [1 + (\alpha_m \theta - \omega_{mn} \theta)^2]}, \quad \begin{matrix} \omega_{mn} \theta > 1 \\ a_{mn} \theta \ll 1 \end{matrix} \quad (162)$$

where we have defined a "convection frequency"

$$\alpha_m = \frac{m\pi v}{L_x} \quad (163)$$

b. Response Below and Above Coincidence. The case in which the mean convection speed is much smaller than the coincidence speed corresponds to  $\alpha_m \ll \omega_{mn}$ . As a simplification, we consider two special cases which cover the entire range of interest. For low damping or low frequencies

$$I_{mn}(0) = \frac{2\theta}{a_{mn} [1 + (\omega_{mn} \theta)^2]}, \quad a_{mn} \theta \ll 1 \quad (164)$$

and for high frequencies

$$I_{mn}(0) \doteq \frac{2}{\omega_{mn}^2} \left[ 1 + \frac{1}{a_{mn}\theta} + \frac{1}{1 + (\alpha_m \theta)^2} \right], \quad \omega_{mn}\theta \gg 1 \quad (165)$$

For a convection speed much greater than the coincidence speed, we have  $\alpha_m \gg \omega_{mn}$  and

$$I_{mn}(0) \doteq \frac{2\omega_{mn}^2 \theta^3}{a_{mn} [1 + (\alpha_m \theta)^2] [(\omega_{mn}\theta)^2 + (a_{mn}\theta)^2]} \quad (166)$$

For low damping this reduces to

$$I_{mn}(0) \doteq \frac{2\theta}{a_{mn} [1 + (\alpha_m \theta)^2]}, \quad a_{mn}\theta \ll 1 \quad (167)$$

### 3. Response to micro-meteorites

A source correlation which exhibits coherence over a very small spatial and temporal extent may be appropriate in describing the forcing field created by micro-meteorite dust interception (or small-scale stationary turbulence). A simple correlation function that has these properties is

$$\langle pp'^* \rangle = 4\pi l^2 \theta p^2 \delta(\zeta) \delta(\xi) \delta(\tau) \quad (168)$$

where  $l$  is the mean distance over which the forcing field is correlated

$\theta$  is the mean time over which the forcing field is correlated

$p^2$  is the mean square pressure

$\delta$  is the Dirac delta function, defined as

$$\int_{-\infty}^X \delta(x) dx = \begin{cases} 1, & X > 0 \\ 0, & X < 0 \end{cases}$$

$$\zeta = x - x'$$

$$\xi = y - y'$$

$$\tau = t - t'$$

The elastic system to be investigated is a simply supported uniform rectangular thin plate of dimensions  $L_x$ ,  $L_y$ , and  $h$ , and surface mass density  $M$ . The appropriate eigenfunctions and resonance frequencies were given in the previous discussion on plate excitation by boundary layer turbulence.

With small hysteretic damping assumed, the modal displacement correlation is

$$\begin{aligned} \langle ww'^* \rangle &= \frac{2\pi \ell^2 \theta_p^2}{\eta \omega_{mn}^3 M^2 L_x L_y} \cdot \cos \omega_{mn}(t - t') \\ &\cdot \exp \left[ -\eta \omega_{mn} |t - t'| / 2 \right] \\ &\cdot 2 \sin \frac{m\pi x}{L_x} \sin \frac{n\pi y}{L_y} \cdot 2 \sin \frac{m\pi x'}{L_x} \sin \frac{n\pi y'}{L_y} \end{aligned} \quad (169)$$

Specializing to the mean square response, that is, setting  $x = x'$ ,  $y = y'$ , and  $t = t'$ , and performing a spatial average, we obtain for the mean square displacement in the  $mn^{\text{th}}$  mode

$$\overline{\langle w^2 \rangle}_{mn} = \frac{2\pi \ell^2 \theta_p^2}{\eta \omega_{mn}^3 M^2 L_x L_y} \quad (170)$$

Comparison of Equation (170) with the corresponding result for a source correlation function that decays exponentially with delay time but is constant with spatial separation (see previous discussion on atmospheric turbulence) shows that:

1. The present result does not decrease as rapidly with increasing modal frequency, because the source correlation  $\delta(\tau_0)$  contains more high frequency excitation than does  $\exp\left[-\frac{\tau_0}{\theta}\right]$ .
2. The present result does not decrease as rapidly with increasing mode number, because the source correlation  $\delta(\zeta_0) \delta(\xi_0)$  contains more high mode excitation than does a correlation that is constant in space.

Comparison of Equation (170) with the corresponding result for a source correlation function that decays exponentially with delay time but is convected (see previous discussion on boundary layer turbulence) shows that the mean square response to micro-meteorites is twice the mean square response to convected turbulence of the same amplitude and at hydrodynamic coincidence.

For the micro-meteorite excitation, the mean square velocity in the mn mode is then given by

$$\begin{aligned} \overline{\langle v^2 \rangle}_{mn} &= \omega_{mn}^2 \overline{\langle w^2 \rangle}_{mn} \\ &= \frac{2\pi l \theta p^2}{\eta \omega_m^2 L_x L_y} \end{aligned} \tag{171}$$

Numerical Example. The values of the various quantities to be substituted in the equation for  $\langle v^2 \rangle$  are chosen from Whipple's data<sup>6.31/</sup>:

Average particle diameter  $D = 10^{-3}$  cm  
Average particle velocity  $V = 2 \times 10^6$  cm/sec  
Average particle mass =  $2.5 \times 10^{-5}$  gm  
Total momentum flux  $F = 10^{-9}$  gm-cm/sec/sec on 1 sq cm  
of plate surface  
Plate length and width  $L_x = L_y = 50$  cm  
Plate thickness  $h = 0.3$  cm steel  
Plate damping  $\eta = 3 \times 10^{-3}$   
( $c_L$ ) steel =  $5 \times 10^5$  cm/sec

The mean values of quantities associated with the pressure field are evaluated as follows:

Pressure  $p \doteq 2F$   
 $\theta \doteq \frac{D}{V} = 5 \times 10^{-10}$  sec  
 $l \doteq D$

When these values are used, we obtain for the root mean square velocity at the lowest plate resonance

From Eq (171)  $\sqrt{\langle v_{11}^2 \rangle} \doteq 10^{-18}$  cm/sec

From Eq (152)  $f_{11} = \frac{\omega_{11}}{2\pi} = 56$  cps

The resulting velocity is clearly very small.

An Upper Bound. Another approach may be used to determine an upper limit on micro-meteorite noise. The response of an infinite undamped plate to the impact of a mass  $m$  at velocity  $u$  was analyzed by Cremer<sup>7.11/</sup> by means of classical plate theory. He showed that the

plate velocity at the point of impact has a spectrum

$$V_o(\omega) = \frac{u}{\pi \sqrt{\omega^2 + \left(\frac{Z}{m}\right)^2}} \quad (172)$$

where  $\omega$  denotes circular frequency and  $Z$  the driving point impedance of the plate. The latter may be expressed as

$$Z = 4h^2 \sqrt{E\rho/3(1 - \mu^2)} \quad (173)$$

in terms of the plate thickness  $h$ , Young's modulus  $E$ , density  $\rho$ , and Poisson's ratio  $\mu$ .

The plate motion is subject to an inherent space-wise decay, and thus the velocity spectrum at points removed from the point of impact has a lower absolute value than that at the impact point. Since  $V_o(0) \geq V_o(\omega)$  from Equation (172) the velocity spectrum can certainly not exceed

$$V_o(\omega) \leq \frac{mu}{\pi Z} \quad (174)$$

The velocity encountered in a given frequency band  $\Delta\omega$  due to an impulse of magnitude  $mu$  thus is over-estimated by

$$V \leq \Delta\omega \cdot V_o(\omega) = \frac{mu\Delta\omega}{\pi Z} \quad (175)$$

If no energy dissipation would occur at all, the plate would continue to vibrate indefinitely as described above, and the velocity would remain at the previously established value. Additional impacts then would at most contribute linearly to the velocity (assuming their occurrence in proper phase). If an average of  $n_j$  particles of mass  $m_j$  and velocity  $u_j$  impinge on the plate in unit time, the

resulting velocity at time t after initial exposure will be grossly over-estimated by

$$v \leq \frac{\Delta\omega}{\pi Z} (\sum n_j \cdot m_j \cdot u_j) t \quad (176)$$

In order to obtain a more reasonable estimate, one should multiply the value given by Equation (176) by a factor  $\alpha$  representing roughly the ratio of the area vibrating near maximum amplitude to the total exposed area.

The quantity in the parentheses of the foregoing equation denotes the momentum flux through a given area due to particles of all sizes. From Whipple's data, 6.31/ this amounts to approximately 1 gm cm/sec/day on a surface of one square meter.  $\Delta\omega$  may be taken as  $5 \times 10^4$  rad/sec corresponding roughly to the frequency range of human hearing. From Equation (173) one may express the impedance of a steel plate as

$$Z_{\text{steel}} \doteq 3 \times 10^5 h^2 \text{ dyne sec/cm} \quad (177)$$

where the plate thickness h is to be in cm. (For an aluminum plate the impedance would be less by a factor of 3; or

$$Z_{\text{al}} \doteq 10^5 h^2 \text{ dyne sec/cm} \quad (178)$$

For a steel plate one may estimate that the velocity increases at most at the rate of

$$v/t \leq 6. \times 10^{-8} \frac{A}{h^2} \text{ cm/sec/day} \quad (179)$$

for an exposed area of  $A$  square meters and plate thickness of  $h$  cm and with an assumed value  $\alpha = 10^{-6}$  (which most probably is highly conservative). With an area of  $10^3 \text{ m}^2$  and a plate of 3 mm thickness, this means that after a one-day exposure the velocity would reach  $7 \times 10^{-4} \text{ cm/sec}$ .

This estimate is extremely pessimistic, of course. Structural damping would certainly have a strong effect over periods exceeding a few minutes, so that even if the other assumptions (e.g., all particles impacting at proper instant for in-phase addition of vibration) could be met, the actual velocity is likely to be at least an order-of-magnitude less than calculated. In view of this estimate and of the fact that at every stage of the calculation the worst possible condition was assumed, one may conclude that micro-meteorite impacts as described by Whipple's table are not likely to produce significant acoustic noise levels inside orbital vehicles. However, the information currently available on micro-meteorite dust fields is limited to observations very close to the earth. Denser dust fields may well exist in other parts of the solar system that may become of interest in the future. When these additional data on other dust fields are available, the formalisms outlined here will be useful in evaluating the possible structural excitation by these fields.

SECTION VIII  
NOISE IN INTERNAL SPACES

Section VII has considered the problem of determining the velocity of a structure excited by various fluctuating pressure fields. We must now use this velocity to determine the noise in an internal space. It is convenient first to calculate the pressure that would exist if the vibrating surface were to radiate into a perfectly absorbing space. This pressure can be used to determine an "equivalent" transmission loss ( $TL_{equiv}$ ) for the structure. Having determined  $TL_{equiv}$  in this way, one may then proceed with the material in Section IV (in Volume I of WADC TR 58-343) to determine the needed corrections for geometry, internal absorption, etc., to obtain the noise reduction (NR).

Since noise spectra are usually measured in bands of arbitrary width, it will be necessary to convert the modal mean square responses calculated in Section VII into these bandwidths. At the lowest resonances of a panel there will generally be only a few resonances per band of interest, and this number of resonances can be readily calculated from the expression for the (circular) resonance frequency  $\omega_{mn}$ . For example, for a square plate that is simply supported, the ratio of the two lowest resonance frequencies is 2:5, so that an octave band containing the lowest resonance frequency ( $\omega_{11}$ ) will not contain any other resonance.

At higher panel resonances it becomes awkward to compute the number of resonances  $\Delta N$  per frequency band  $\Delta\omega$ . In this case an approximate formula (which becomes more accurate at higher frequencies) is

$$\Delta N = \frac{\sqrt{3} L_x L_y}{2\pi c_L h} \Delta_0 \quad (180)$$

for a panel of dimensions  $L_x$ ,  $L_y$ , and  $h$ .  $c_L$  is the speed of longitudinal waves. It is interesting to note that the quantity  $\langle \dot{w}^2 \rangle_{mn} \Delta N$  does not contain plate length and width explicitly, if the values of  $\langle \dot{w}^2 \rangle_{mn}$  obtained in Section VII for boundary layer turbulence or micro-meteorites are used.

#### A. Structural Radiation and Acoustic Damping\*

The energy of vibration in a steady state flexural wave field on a plate is  $1/2 mSV^2$ , where  $m$  is the plate surface mass,  $S$  is the plate area, and  $V$  is the velocity amplitude. The acoustic power radiated from one side of such a plate into an adjacent medium is  $1/2 \rho c_0 SV^2 \cdot s$ , where  $\rho$  and  $c_0$  are the density and speed of sound in the adjacent medium.  $s$  is the radiation factor, the ratio of power radiated by the plate to power radiated by a flat piston vibrating with the same amplitude. (Strictly speaking, at very low frequencies a flat piston becomes a poor radiator, and the actual power radiated is less than  $1/2 \rho c_0 SV^2 \cdot s$ .)

The radiation factor  $s$  for infinite plates is plotted in Figure 99, as a function of the frequency ratio  $f/f_c$ .  $f_c$  is the critical frequency, at which the flexural wave speed in the plate equals the speed of sound in the adjacent medium. We recall from Equation (61) that for steel, aluminum, glass and other materials with approxi-

---

\* Material in this discussion is based on a paper by Edward M. Kerwin, Jr., presented at the WADC - University of Minnesota Conference on Acoustic Fatigue, 30 September-2 October 1959, and published in the Proceedings of that conference.

mately the same ratio of Young's modulus to density, we have approximately

$$c_B \doteq 51\sqrt{hf} \text{ ft/sec} \quad (61)$$

where  $c_B$  is the flexural wave speed in a plate of thickness  $h$  inches. For the infinite plate there is no radiation when the speed of propagation  $c_B$  is less than  $c_o$ , the speed of sound in the adjacent medium. Above the critical frequency the radiation factor rapidly approaches the limiting factor of 1. That is, for frequencies sufficiently greater than the critical frequency, the flexural wave radiates sound energy as well as would a uniform motion of the plate surface.

For finite plates of length  $b$ , the radiation factor has been computed by Gosele,<sup>8.1/</sup> and the results for three values of plate size are given in Figure 100 (which is Figure 58 repeated for convenience).  $\lambda_c$  is the wavelength of sound at the critical frequency. Figure 100 shows that below the critical frequency a flexural wave on a plate will radiate poorly; above the critical frequency, a flexural wave on a plate will radiate as well as it would with uniform motion on its surface.

The radiation factor  $s$  is modified by the presence of flow past the panel. Kerwin finds the resulting radiation factor for an infinite plate to be

$$s = \frac{1}{2} \left[ \frac{\left| M_o - \frac{c_b}{c_o} \right|}{\sqrt{\left( M_o - \frac{c_b}{c_o} \right)^2 - 1}} + \frac{M_o + \frac{c_b}{c_o}}{\sqrt{\left( M_o + \frac{c_b}{c_o} \right)^2 - 1}} \right] \quad (181)$$

where  $M_o$  is the Mach number of the fluid flow past the panel, and a term in this equation is by definition zero if the denominator becomes imaginary. The radiation factor given by Equation (181) is plotted in Figure 101 as the function of  $M_o$  for different values of  $\frac{c_b}{c_o}$ . In accordance with the results in the absence of flow, when the relative velocity of a flexural wave and the adjacent medium exceeds the velocity of sound, the radiation efficiency increases. When the Mach number  $M_o$  is high enough so that  $(M_o - \frac{c_b}{c_o})$  exceeds unity, then both the upstream and downstream flexural waves are moving supersonically relative to the medium, and the radiation factor approaches its limiting value of unity.

In summary, the effect of flow past the panel may either increase or decrease the radiation factor. The increases can be significant, but the decreases are by no more than about a factor of two. In the limit of high Mach number, the radiation factor approaches unity.

#### 1. "Equivalent" Transmission Loss

The hypothetical rms sound pressure that would exist inside the space if the walls were perfectly absorbing is given by

$$(p^2)_{\text{perfect absorbing}} = \frac{1}{2} (\rho c_o)^2 v^2 \cdot s \quad (182)$$

In a frequency band  $\frac{\omega}{2\pi}$  wide, we have (in terms of modal velocity)

$$(p^2)_{\text{perfectly absorbing, band around } \omega_{mn}} = (\rho c_o)^2 \overline{\langle v^2 \rangle}_{mn} \Delta N \cdot s \quad (183)$$

where the space-averaged modal velocity amplitude  $\overline{\langle v^2 \rangle}_{mn}$  is used. In other words, the hypothetical sound pressure level in the perfectly absorbing space is

$$128 + 20 \log_{10} (\rho c_0) + 10 \log_{10} \overline{\langle v^2 \rangle}_{mn} \\ + 10 \log \Delta N + 10 \log s$$

where  $\rho c_0$  has the units of slugs/sq ft/sec and  $v$  has the units of ft/sec. (Under standard conditions of temperature and pressure,  $\rho c_0$  is 2.6 slugs/sq ft/sec.)  $TL_{equiv}$  for the plate is then

$$TL_{equiv} = SPL_{out} - 128 - 20 \log_{10} (\rho c_0) - 10 \log_{10} \overline{\langle v^2 \rangle}_{mn} \\ - 10 \log N - 10 \log s \quad (184)$$

where  $SPL_{out}$  is the SPL at the vehicle exterior. In the case of an external noise source, such as rocket engine or wake noise (distinguished here from various kinds of turbulence),  $SPL_{out}$  is the "free space" SPL, the level that would exist in the absence of pressure doubling at the surface. The methods of noise source prediction given in this report for this case of a noise source give the "free space" SPL consistently.

## 2. Sound Radiation and Structural Damping

The important structural motions calculated in Section VII occur at resonances and have generally been found to vary inversely with a measure of the structural damping,  $\eta$ . Ordinarily, we may think of the damping to be determined primarily by the inherent losses in the material or by some applied visco-elastic layer. However, since a

vibrating system radiates energy in the form of sound, it is clear that this sound radiation may constitute an important form of energy loss by the system.

The damping factor (or "loss tangent")  $\eta$  may be defined as

$$\eta = \frac{P_o}{\omega W_o} \quad (185)$$

where  $P_o$  is the average rate of energy removal,  $W_o$  is the total vibrational energy of the system, and  $\omega = 2\pi f$ . If the radiated power from a flexural wave accounts for all of the losses, we have

$$W_o = \frac{1}{2} mSV^2$$

$$P_o = \frac{1}{2} \rho c_o SV^2 \cdot s \quad (186)$$

Combining Equations (185) and (186), we obtain for the damping factor

$$\eta = \frac{\rho c_o s}{\omega m} \quad (187)$$

This evaluation of damping due to acoustic radiation takes into account loading on one side of the plate only. Twice the radiated acoustic power, and, therefore, twice the damping factor, would result from radiation from both sides of the plate. We should remember, however, that in some cases of interest the media on opposite sides of the plate may have different densities and speeds of sound.

## B. Ventilation Noise Within Space Vehicles

Volume I of WADC TR 58-343, "Methods of Flight Vehicle Noise Prediction," dealt in a general way with sources of internal vehicle noise. Since ventilating systems may be among the most significant of such sources, additional information concerning these may be desirable. A complete discussion of ventilating system noise is contained in the Heating, Ventilating, Air Conditioning Guide.<sup>8.2/</sup> For convenience, we will summarize in the following section certain portions of this material which are pertinent to vehicle air conditioning and ventilating systems.

Noise associated with ventilating systems may be divided into two general kinds: air-borne noise transmitted through the ventilating ducts, and structure-borne noise transmitted through the walls, floors, etc. Elimination of the structure-borne noise generally involves conventional vibration isolation of the mechanical equipment. Because of the many different kinds of mechanical equipment involved, it is not possible to present general information on the amount of vibration induced by each type of equipment. Reciprocating equipment will generally be considerably more troublesome than centrifugal or axial flow equipment.

Conventional vibration isolation is usually adequate to remove structure-borne noise problems, except in very critical installations (e.g., where the vibrating mechanical equipment is directly adjacent to an area where quiet is essential).

Air-borne ventilating equipment noise in a vehicle will be predominantly from two sources: the ventilating fans and the diffusion grilles. Simplified engineering

procedures for estimating the noise associated with these two sources are given below. We must emphasize that the material in Reference 8.2 should be consulted for further details and description of the qualifications involved in this simplification.

The sound power level (PWL)\* radiated by a fan through a duct into a room may be estimated as follows:

- 1) Determine the overall PWL in the duct from one of the following equations:

$$\begin{aligned} \text{PWL} &= 100 + 10 \log \text{hp} + 10 \log p \\ \text{PWL} &= 65 + 10 \log q + 20 \log p \\ \text{PWL} &= 135 + 20 \log \text{hp} - 10 \log q \end{aligned} \quad (188)$$

where

hp = rated fan motor horsepower

p = static pressure in inches of water

q = fan discharge in cubic feet per minute

- 2) Use the frequency spectrum of the fan noise given in Figure 102. Two spectrum shapes are given, one for axial flow fans, and one for centrifugal fans. The cross-hatched regions indicate the areas in which most of the experimental data are found.
- 3) Determine the reduction in PWL associated with reflection of sound at the duct opening from

---

\* PWL is defined as

$$\text{PWL} = 10 \log_{10} \frac{w}{w_0} \text{ db}$$

where  $w$  is the total acoustic power radiated in watts, and  $w_0$  is a reference sound power of  $10^{-13}$  watt.

Figure 103. This PWL reduction is plotted as a function of frequency times length of a duct side L, assuming that the duct is square. For rectangular duct openings of dimensions  $L_1$  and  $L_2$ , the effective size L may be taken as  $\sqrt{L_1 L_2}$ . For a round opening use 0.9 x (duct diameter) for the effective size.

Grille noise spectra are generally predominant in the speech interference range of 600 to 4800 cps. A designation of the noise levels in this range is given by the speech interference level (SIL). This quantity is defined as the average of the decibel level in the three octave frequency bands, 600-1200, 1200-2400, and 2400-4800 cps. At frequencies below 600 cps, fan noise usually predominates over grille noise. Therefore, we will generally be interested in grille noise levels in the speech interference range only. The following procedure may be used to obtain an estimate of the PWL radiated into a room due to grille noise:

Obtain the power level in the speech interference range from Figure 104. The core area is the area of the duct opening into which the grille fits, and the core velocity is the air stream velocity in the duct. Figure 104 applies for a core area of 1 sq ft. For a core area of A sq ft, the quantity  $10 \log_{10} A$  db should be added to the values obtained from the figure.

The estimates of PWL obtained above for fan noise and grille noise may be converted into sound pressure levels (SPL) by means of the following simplified procedure:

- 1) Compute the average sound absorption coefficient  $\bar{\alpha}$  for the space of interest from the definition

$$\bar{\alpha} = \frac{\alpha_1 S_1 + \alpha_2 S_2 + \dots + \alpha_n S_n}{S_1 + S_2 + \dots + S_n} \quad (189)$$

where  $\alpha_1$  = average sound absorption coefficient for surface of area  $S_1$  sq ft.

- 2) Obtain an estimate of the room constant R, defined by the equation

$$R = \frac{S\bar{\alpha}}{1 - \bar{\alpha}} \text{ sq ft} \quad (190)$$

where  $S = S_1 + S_2 + \dots + S_n$  = total area of the boundary surfaces of the space of interest, in square feet.

Approximate values of absorption coefficients for surfaces that might be encountered in vehicles are given in the following table.

TABLE VIII-A  
TYPICAL VALUES OF ABSORPTION COEFFICIENTS

Material	Coefficients					
	125 cps	250 cps	500 cps	1000 cps	2000 cps	4000 cps
steel or concrete, painted	0.01	0.01	0.01	0.02	0.02	0.02
glass	0.04	0.04	0.03	0.03	0.02	0.02
3/4" thick acoustical tile, flush mounted	0.10	0.20	0.70	0.85	0.70	0.65
people in wooden seats ( $\alpha S$ per person)	4.0	7.5	11.0	13.0	14.0	11.5

- 3) Use Figure 105 to determine the SPL from the PWL computed earlier. For geometries of interest in vehicles, the directivity factor  $Q$  is generally around 3 to 4. The dimension  $r$  is the distance between the duct opening and the listener.

In the procedures given here, no account has been taken of sound attenuation by duct bends or any acoustical treatment placed in the duct passages. Information contained in References 8.2 and 8.3 may be used to estimate this attenuation, if desired.

Example: A 1/10 hp centrifugal fan provides 70 cu ft/min of air at 1" of water static pressure. The air passes through a 4" square duct through a bar deflection-type grille. The duct opening into which the grille fits is also 4" square. The air is fed into a room with 300 sq ft of exposed steel surface. One man in conventional clothing sits three feet from the duct opening. Find the SPL at the man's position.

The following table summarizes the calculations involved in working this example. [Because of the very small absorption in the space, the observation position is found to lie in the reverberant field of the noise source. Therefore, instead of using Figure 105 in determining the SPL from the computed PWL one may use the formula

$$\bar{SPL} = PWL + 10 \log \left( \frac{4}{R} \right) + 0.5 \text{ db} \quad (191)$$

which is appropriate in the reverberant field.]

TABLE VIII-B  
EXAMPLE OF VENTILATING SYSTEM NOISE

Frequency Band cps	PWL Fan Noise in Duct	End Reflection Losses	PWL Fan Noise in Room	PWL Grille Noise	$\bar{\alpha}$	$10 \log \frac{4}{R} + 0.5$	SPL
20-75	89	20	69			-1 (est.)	68
75-150	84	15	69		0.023	-2	67
150-300	79	12	67		0.035	-4	63
300-600	74	6	68	} 20	0.047	-5	63
600-1200	69	3	66		0.063	-7	59
1200-2400	64	1	63		0.067	-7	56
2400-4800	59	0	59		0.058	-6	53
4800-10,000	54	0	54			-5 (est.)	49

SECTION IX  
THE EFFECTS OF NOISE ON MAN: NUMERICAL EXAMPLE

High intensity noise can affect personnel, equipment, and structures. At the present time there is some information on the effects of noise on personnel, although we shall see that this information is not adequate for specifying very detailed criteria. Still less is known about the effects of noise on equipment and structures. For problems concerning equipment exposed to intense sound fields, tolerable sound levels must presently be established for each type of equipment by laboratory test. In general, experience with electronic components in intense noise fields in the audible frequency range indicates that octave band levels of about 120 db do not cause serious damage, while levels in excess of 140 db or 150 db are quite troublesome.

For problems concerning structural fatigue, empirical relations between maximum stress and fatigue life are available for many types of structures. In general, the mean square stress  $\langle \sigma^2 \rangle$  is related approximately to the mean square velocity  $\langle v^2 \rangle$  by

$$\langle \sigma^2 \rangle \doteq 3(\rho c_L)^2 \langle v^2 \rangle C^2 \quad (192)$$

where  $\rho$  is the density of the structure and  $c_L$  is the speed of longitudinal waves in the structure.  $C$  is a stress concentration factor that allows for local stress increases at such places as rivets, welds, and bends. In a well-designed structure,  $C$  will not be much greater than 3. The value of mean square velocity obtained in Section VII may be substituted into Equation (192), and the resulting stress compared with the empirical relations to determine a

fatigue life. A more detailed description of the effects of noise on equipment and structures must await the results of current research programs.

The source information given earlier in this report will be used to estimate the noise levels in a typical space vehicle configuration. This estimate will be performed in Part A of this Section.

The human-operator function most vulnerable to noise of the type anticipated in space vehicles is speech communication. Although there is some evidence that intense noise affects a person's accuracy at time estimates (Jerison,<sup>9.1/</sup> Hirsh<sup>9.2/</sup>) and increases the probability that a brief visual stimulus will not be seen (Broadbent<sup>9.3/</sup>), noise has very little effect on the performance of most of the tasks for which the space vehicle operator will be responsible (Stevens et al,<sup>9.4/</sup> Kryter<sup>9.5/</sup>). Reception of audio warning or code signals will be less markedly impaired than will speech reception or transmission. In Part B of this Section we will examine the extent of the effects of noise on speech communication. General measures to improve speech communication will be discussed in Section X.

High intensity noise can also damage hearing. In Part C of this Section we will review the current thinking on hearing damage criteria for noise of the type anticipated in space vehicles.

#### A. Example -- Space Vehicle Noise Levels

Limited experimental results indicate at present that one major source of noise in space vehicles is the rocket engine during launch and subsonic boost operations. The

expected duration of this noise is of the order of a minute or less, and the highest rocket engine noise levels occur while the vehicle is at or close to the launch stand (see Section VIA). We will consider this situation in our example. (It should be clear that noise sources other than engines can be significant and that material used in this report can be used to evaluate the other sources.)

Although the particular values used in this example do not correspond to a specific vehicle, they are representative of present-day (1960) designs. The operating conditions and dimensions of interest are as follows:

Rocket Engine (Single Nozzle):

Thrust	400,000 lbs
Nozzle Diameter	4 feet
Vehicle Diameter	10 feet
Weight Flow	1600 lbs/sec

Right-angle flame deflector located 15 ft from nozzle plane.

Manned Compartment:

Length	5 feet
Typical Diameter	5 feet
Sidewall construction - see Figure 107 for double wall detail	
Located 80 feet from rocket engine nozzle plane.	
Medium panel damping and high internal acoustical absorption assumed.	

The procedure given in Section VIA was used to obtain the octave band spectrum shown as a solid line in Figure 106,

representing the "free space" SPL that would occur at 80 feet from the rocket nozzle plane. The broken line in Figure 106 is the corresponding spectrum level. The spectrum level is the SPL measured in one-cycle wide frequency bands. The spectrum level presentation occurs commonly in estimations of speech intelligibility and will be used in discussions later in this section.

An average noise reduction for the side wall shown in Figure 107 is obtained by using material contained in Section III, IV and VII. The following major steps are involved in obtaining the estimate of NR:

1. The radial resonance was calculated from Equation (143) to occur at approximately 1100 cps, using a diameter of 5 ft.
2. A value of  $TL_{\ell}$  of 20 db was obtained from Figure 98, for a ratio of skin thickness to diameter of  $10^{-3}$ .
3. The double wall resonance obtained from Figure 108 (Figure 53 of Volume I, repeated here for convenience) was 140 cps. The surface weights of the leaves were taken to be 0.8 lbs/sq ft (skin) and 2.0 lbs/sq ft (honeycomb). The intervening air space was taken to be 5 inches.
4. The honeycomb stiffness and mass were considered to be controlling factors in determining the plate coincidence frequency  $f_c$ . The value of  $f_c$  was calculated to be approximately 390 cps by means of the general relation:

$$f_c = \frac{(c_o)^2}{2\pi} \sqrt{\frac{M}{B}} \quad (193)$$

where  $c_o$  is the velocity of sound in the external medium,  $M$  is the honeycomb surface mass, and  $B$  is the honeycomb bending stiffness. This coincidence is not seen directly because it occurs in the region where flat plate motion is not important. However, the coincidence determines the panel behavior above the radial resonance.

The TL in this higher frequency region is obtained from Figure 109 (Figure 47 of Volume I). The quantity  $A$  is found to be 27 db. Medium damping of the wall and a surface weight of 2.3 lbs/sq ft are assumed.

5. The improvement in TL due to the presence of approximately 4 inches of a fibrous blanket was obtained from Figure 110 (Figure 51 of Volume I). It is assumed that this glass fiber insulation is a typical aircraft type blanket (very small fiber size). Note that the blanket also largely eliminates the effects of the double wall and radial resonances.
6. For a typical dimension of 5 ft, an average value of the correction factor  $C$  for high internal absorption is -5 db (see Figures 111 and 112, which are Figures 69 and 70 of Volume I).
7. The NR is limited by flanking transmission to approximately 55 db at the highest frequencies. Such a limitation is in line with most values observed in field installations.

The NR estimate is shown in Figure 113.

## B. Effects of Noise On Communication

The solid line in Figure 114 is the estimate of average noise levels within the manned compartment considered in the preceding paragraphs. These levels represent the spectral levels at the vehicle exterior (Figure 106) reduced by the side wall Noise Reduction (Figure 113).

The extent to which the peaks of a speech signal (approximately 12 db above the rms speech levels) exceed the ambient noise determines the intelligibility of the speech. If the speech peaks do not exceed the noise, there is no intelligibility. We may make our discussion of intelligibility more quantitative by a method due to Kryter<sup>9.6/</sup>. This method represents a simplification of the 20 band Articulation Index calculation suggested by Beranek<sup>9.7/</sup>. Kryter's method concentrates on the octave bands contained in the frequency region from 150 cps to 10,000 cps. The ratio of the speech peaks to the noise, in decibels, is determined in each octave band, and is multiplied by some fractional value. The Articulation Index is equal to the sum of these weighted signal-to-noise values, as shown in the following table.

Table IX-A  
METHOD OF CALCULATING ARTICULATION INDEX

Octave Band	Speech Peaks-to-Noise Ratio in Decibels*	Fractional Value of S/N Ratio for Intelligibility	Col 2 x Col 3
150-300 cps	_____	.0017	_____
300-600	_____	.0017	_____
600-1200	_____	.0085	_____
1200-2400	_____	.0119	_____
2400-4800	_____	.0085	_____
4800-9600	_____	.0017	_____
			AI = $\Sigma$

\* S/N ratios of 0 db or less are made 0;  
ratios of 30 db or greater are made 30.

Figure 115 presents average curves relating sentence or word intelligibility to the Articulation Index calculated in this manner.

1. Intelligibility of Received Speech During Launch

The broken line in Figure 114 represents the peaks of a speech signal as received at the headset of a present-day (1959) Air Force interphone, which is considered to be an excellent system of communication. The headset amplifier is operating at full volume but without peak clipping.

Figure 116 shows the typical attenuation of a present-day high-altitude helmet or a present-day earphone cushion. If we assume that the helmet and the earphone cushion combine without any interaction, the resulting attenuation would be twice the value shown in Figure 116. (Ordinarily, this is a somewhat optimistic assumption, but will not affect the

accuracy of our present discussion.) When we apply two times the attenuation shown in Figure 116 to SPL within the space vehicle during launch (the solid line of Figure 114), we obtain the dotted line shown in Figure 114. These levels represent our estimate of the rocket noise at the ear of the occupant.

Using the dotted and broken lines in Figure 114, we can predict the intelligibility of received speech during subsonic boost. The Articulation Index calculated as outlined above exceeds 0.9, corresponding to almost perfect intelligibility for sentences or words.

However, the intense low-frequency noise of the rocket prohibits us from taking this prediction of intelligibility at face value. In the presence of such intense low-frequency noise, the main disrupter of communication is not the "local masking" that has been carefully investigated throughout the last 25 years, but is "upward spread of masking" for which effects are much less definite. Kryter<sup>9.8/</sup> has suggested that such masking by low frequencies be taken into account by drawing a line with a negative slope somewhere between 3 db/octave to 6 db/octave. This negative sloping line provides an envelope under which practically all speech information is masked by the low frequencies. If we do this in Figure 114 we discover that the calculated Articulation Index is approximately 0.2; and word intelligibility is very poor. The overwhelming dependence of this estimate on the upward spread of masking is a circumstance with which present-day psycho-acoustics has had no previous experience. An improved prediction of speech intelligibility is therefore strongly dependent on additional tests.

It appears that this is one of the first times that the

upward spread of masking becomes an important practical problem. Obviously, steps should be taken to make the place of this masking in the theory of intelligibility as firm as the place local masking has now. Kryter's formulation,<sup>9.8/</sup> which is based on the only evidence now available, should be tested empirically. As the experimental basis is developed, the formulation should be refined; the slope of this masking envelope should be reduced as far as possible below the present range of values.

## 2. Intelligibility of Transmitted Speech During Launch

We will now consider the intelligibility of the speech of the space vehicle occupant. The solid line in Figure 117 repeats the estimates of rocket noise during launch. The broken line in Figure 117 is the SPL of the speech peaks recorded inside a helmet.<sup>9.9/</sup> Figure 116 gives an estimate of the attenuation associated with a differential microphone operating inside a present-day high-altitude helmet. When this attenuation is applied to the solid line in Figure 117, we obtain the dotted line in Figure 117, which represents the rocket noise picked up by the differential microphone in the helmet.

In considering the intelligibility of transmitted speech, we are not concerned with remote masking from the intense low-frequency components of the rocket noise. The spectrum of the total signal can be tilted electronically in the transmitter or in the receiver, and, if the receiver is in a quiet location, the gain can be turned down to minimize the upward spread of masking. Therefore, we may use the conventional methods of determining speech intelligibility in terms of the signal-to-noise ratio in the speech range. Comparing the broken and dotted lines in Figure 117, we find almost perfect intelligibility.

### 3. Temporary Threshold Shift Following Subsonic Boost

In addition to the direct effects of the intense rocket noise heard during subsonic boost, we must also consider the possibility of communication interference due to threshold shifts induced by this intense noise and persisting in the later supersonic portions of the vehicle trajectory. In the present example, temporary threshold shift does not appear to pose a serious problem. If received speech is intelligible during the subsonic flight, then it will probably continue to be as intelligible during the following supersonic flight. In addition, recent investigations indicate that a fast recovery process from temporary threshold shift occurs in about two minutes after the removal of the intense noise.<sup>9.10/</sup> Therefore, much of the threshold shift induced by the intense noise will have disappeared by two minutes after the removal of the intense noise (that is, about two minutes after the vehicle is moving sonically). By this time, the high gain in the headset amplifier may be reduced somewhat so that the signal-to-noise ratio permits acceptable intelligibility without causing discomfort.

#### C. Hearing Damage Risk

Damage risk (or "hearing conservation") criteria are usually expressed in terms of SPL in octave bands. Thus, we have replotted the dotted curve in Figure 114 representing the maximum noise at the operator's ear, in terms of octave band levels in Figure 118. As in the case of speech intelligibility, we are faced here with the lack of a well-established criterion. However, we can obtain an idea of what tolerance for intense noise is thought to exist by plotting five different damage risk criterion curves that have been proposed. These five curves are given in Figure 118 and are denoted by Roman numerals as follows:

- I. Kryter, 9.5/ 1950
- II. Rosenblith, Stevens, et al., 9.11/ 1952
- III. Kryter 9.12/ 1959, for persons less than thirty years of age.
- IV. Kryter, 9.12/ 1959, for persons between 30 and 40 years of age.
- V. Air Force Regulation 160-3, 1956

These curves are for an 8-hour exposure each day, five days a week, for thirty years or for life.

It is generally assumed that the level of the noise can be traded for the duration of the exposure. However, no satisfactory information exists at present concerning the appropriate trading relation between intensity and duration of exposure. One relationship that has been used frequently considers that the time integral of sound power (or of sound pressure squared) is the fundamental quantity that should remain invariant for equal damage risk. This is often called the "equal-energy rule." (Some recent evidence has been obtained that indicates that the equal-energy rule becomes over-conservative when short durations of exposure are considered.)

To show the range of values that we might obtain from the various criteria, we will compute the allowed exposure duration per day on the basis of each of the damage risk curves and the equal-energy trading relation. We obtain the following results:

Table IX-B  
 ESTIMATES OF ALLOWED EXPOSURE TO ROCKET NOISE  
 (See Figure 118)

Damage Risk Curve	db Exceeded	Allowed Daily Exposure "Equal-Energy Rule"
I	2	300 min.
II	10	48 min.
III	12	30 min.
IV	16	12 min.
V	5	150 min.

According to the figures in this table, then, the noise of the rocket launching as heard by the operator could be borne between 12 minutes and 300 minutes every working day for 30 years without causing impairment of hearing. Because the noise is associated with the launch operation, the expected duration of the noise is certainly of the order of a minute or less. It appears, therefore, that no serious damage risk is being incurred in this example, but the need for improved criteria for short duration noise is evident.

SECTION X  
DESIGN CONSIDERATIONS

On the basis of discussions in previous sections, we may make some general comments on the design of space vehicles and electronic equipment to be used in these vehicles. These comments are not intended to cover all possible design considerations but should give some idea of available noise control measures.

1. The highest rocket engine noise levels experienced in a space vehicle occur when the vehicle is at or close to the launch or test stand. Variations of the order of 10 db in these maximum noise levels can be effected by changes in the stand configuration, such as changing the position and geometry of the exhaust deflector, changing the amount of water addition, or ducting the exhaust flow. Optimization of the stand configuration by these means provides an important method of noise control. At present it appears that this method has not been fully utilized in the design of launch sites for space vehicles.
  
2. It is possible that proper design of the aerodynamics of a space vehicle can bring about important reductions in the flow noise sources, such as boundary layer noise and cavity noise. For example, if it is possible to forestall the transition of the laminar boundary layer to a turbulent boundary layer, it may be possible to reduce the pressure fluctuations experienced at the vehicle surface. Also, if the roughness height of an oblatting

surface is reduced, we may expect that the boundary layer noise associated with this roughness is also reduced. Such control techniques for flow noise appear to be a fruitful area for future work.

3. The important responses of a structure to various fluctuating pressure fields are in general controlled by the structural damping. At resonances or coincidences, the mean square response is inversely proportional to the damping coefficient  $\eta$ . [See, for example, Equations (139), (142), and (161).] For a given surface weight, it is possible to design damping for a particular frequency range and temperature range of interest. This damping may be brought about through the inherent losses in the structure or through a treatment applied to the structure.
4. With the assumption that the interior of a space vehicle capsule is approximately a right circular cylinder, the capsule occupant should be located near the longitudinal centerline. At the centerline the distribution of noise is a minimum in a two-octave frequency range beginning at the frequency

$$f = \frac{600}{D} \text{ cps} \quad (194)$$

where  $D$  is the capsule diameter in feet. [This condition arises from the fact that all non-zero-ordered Bessel functions are equal to zero at the origin (the center of the cylinder).] Off the centerline, the noise may be 5 to 10 db higher (in the two-octave range). Above and below the

two-octave range, the distribution of noise in the capsule will be approximately uniform. Even if the capsule interior does not form a right circular cylinder but does exhibit circular symmetry about some axis, the occupant should be located on or near the axis of symmetry.

5. Development of a side wall structure with very good noise reduction properties, particularly at the low frequencies, generally necessitates an experimental program. Practical structures are usually quite complex and estimation of their noise reduction performance and possible improvements cannot always be put on a firm basis. It is usual in the development of vehicle structures to proceed with a measurement program to optimize the structural design within limitations imposed by other requirements. For example, the type of insulation for best noise reduction can be selected, and the use of damping materials on the metallic surfaces can be investigated. It must be kept in mind that at low frequencies the noise reduction is influenced by the structure as a whole rather than by details, so that an experimental program must involve a large section of the structure rather than a small section of the wall.
  
6. In order to improve low-frequency noise reduction of a side wall, one possible design may provide structural isolation between the separate skins of the wall. Extreme care must be exercised, however, that the separate skins (together with the structures attached to them) do not resonate in the low-frequency

range near 10 cps. For one thing, such a low resonance may give rise to large mean motions and consequent "bottoming" under constant acceleration. Also such a low resonance would be undesirable in view of the high-impedance motion expected at these frequencies due to bending vibration of the vehicle as a whole. "Double structures" such as these often do have very low frequency resonances unless specific care is taken to avoid them. The use of some special fibers, cork, or cushioning materials, however, may be advantageous as a means of providing structural skins. These materials generally provide very good structural contact at very low frequencies, but begin to provide isolation at about 30 cps to 50 cps. It is conceivable that the noise reduction of the side wall in the range of 20 cps to 200 cps can be increased by as much as 10 db without impairing the vibration performance in the very low frequency range near 10 cps.

7. The weakest acoustical link in the personal equipment worn by the operator is the present-day helmet. This helmet generally lets sound in through the neck seal to such an extent that it provides almost no attenuation below 500 cps or 600 cps. Experiments at the Armour Research Foundation with large spherical helmets of steel and plastic indicate that attenuation greater than 30 db down to 100 cps is possible in principle. However, such structures do not make practical helmets. There is a need for a joint effort between helmet manufacturers and acousticians to design headgear meeting the requirements of

space vehicle environments. Note that improved helmet attenuation will improve both the listening and talking problems simultaneously.

8. As we have seen, a major difficulty in the speech communication situation may occur because of the low frequency rocket noise. It is therefore appropriate to recommend a development of noise-cancelling earphones, since low-frequency noise is amenable to active cancellation. The principle has been developed for certain applications by R.C.A., which already holds a basic patent. A microphone located near to the earphone picks up noise that leaks through into the cavity. The noise is amplified and sent back, out of phase, into the earphone. The circuit is so arranged that the desired signal is not subjected to degeneration. The result is an active enforcement of silence (except for the desired signal) in the vicinity of the earphone. The noise cancellation scheme can provide as much as 20 db of noise suppression at low frequencies. This amount of suppression would remove the difficulties that could arise from upward spread of masking.
  
9. Speech intelligibility can be improved by increasing the level of the received speech signal. The level of received speech in present-day equipment falls far short of the maximum contributory levels. It is therefore important that the designer of electronic equipment take full advantage of the possibilities of tilting the speech spectrum appropriately and increasing the power delivered to the earphone.

10. An important problem associated with the foregoing items concerns the wearability of the personal equipment. In general, it is necessary to have a tight acoustic seal around the ears to provide the attenuation assumed in our earlier discussion. Such a seal rapidly becomes quite painful to the wearer. In addition, there is a problem of helmet comfort, and a problem of keeping a noise-cancelling microphone near enough to the lips to cancel more noise than speech without having it touch the lips or interfere with speech or eating. An important design recommendation is, therefore, that the wearability of helmets, headsets, microphones, and other items of personal equipment be given special attention early in the course of a space vehicle design. This emphasis on wearability has not been considered of much importance in the past; however, the more severe noise environments in present and future vehicles suggest that this problem be considered at the earliest possible stage.

REFERENCES FOR VOLUME II

- 6.1 Powell, A., J. Acoust. Soc. Am., 30, 1048 (1958).
- 6.2 Rogers, O. R., and R. F. Cook, WADC Technical Report 52-341 (1952).
- 6.3 Habel, L. W., and D. R. Bowman, NACA Research Memo L53G06a, (1953).
- 6.4 Mull, H. R. and J. S. Algranti, NACA Research Memo E55K067 (1956).
- 6.5 Dyer, I., J. Acoust. Soc. Am., 28, 782 (Abstract), 1956.
- 6.6 Kraichnan, R. H., J. Acoust. Soc. Am., 29, 65 (1957).
- 6.7 Willmarth, W. W., NACA Technical Note 4139 (1958).
- 6.8 McLeod, N. J., and G. H. Jordan, NACA Research Memo (1958).
- 6.9 Harrison, M., David Taylor Model Basin Report 1260 (1958).
- 6.10 Willmarth, W. W., NASA Memo 3-17-59W (1959).
- 6.11 Skudrzyk, E. J., and G. P. Haddle, J. Acoust. Soc. Am., 32, 19 (1960).
- 6.12 Kistler, A. L., Phys. Fluids, 2, 290 (1959).

- 6.13 von Gierke, H. E., Chapter 33, Handbook of Noise Control, C. H. Harris, Ed., McGraw-Hill Book Co., New York, (1957).
- 6.14 von Gierke, Cole, Eldred, Fass, Hoelt, and Kyrakis, J. Acoust. Soc. Am., 28, 804(A) (1956).
- 6.15 Franken, P. A., Noise Control, 4, 152-160 (1958).
- 6.16 Etkin, Korbacher, and Keefe, University of Toronto Institute of Aerophysics, Report 39 (1956).
- 6.17 Phillips, O. M., J. Fluid Mech., 1, 607-624 (1951).
- 6.18 Chapman, D. R., NACA Report 1051 (1951).
- 6.19 Westervelt, P. J., General Electric Co. General Engineering Laboratory Report 57GL222 (1957).
- 6.20 Kavanau, L. L., J. Aero. Sci., 21, 257-260 (1954).
- 6.21 Shapiro, A. H., The Dynamics and Thermodynamics of Compressible Fluid Flow, Ronald Press Co., New York (1953) Chapters 3, 5, 16, 25.
- 6.22 Hammit, G., J. Aero. Sci., 25, 345-356 (1958).
- 6.23 Daniels, L. E., and H. Yoshihara, WADC Technical Report No. 54-31 (1954).
- 6.24 Rubin, E. S., and E. M. Kerwin, Jr., Proceedings of IX International Congress of Applied Mechanics, Brussels, Belgium, 373-386 (1956).

- 6.25 Roshko, A., NACA Technical Note 3488 (1955).
- 6.26 Krishnamurty, K., NACA Technical Note 3487 (1955).
- 6.27 Cole, R. J., NACA Research Memo L52D30 (1952).
- 6.28 Crane, H. L., and R. G. Chilton, NACA Technical Note 3702 (1956).
- 6.29 Ribner, H. S., NACA Report 1233 (1955).
- 6.30 Hodge, P. W. and J. S. Rinehart, "High Altitude Collection of Extroterrestrial Particulate Matter," Presented at the Madison Meeting of the American Astronomical Society, June 1958.
- 6.31 Whipple, F. L. Proceedings of VIII International Astronautical Congress, Barcelona, 418-427, 1957.
- 6.32 Manring, E. R., "Micrometeorite Measurements from 1958 Alpha and Gamma Satellites," Geophysics Research Directorate, Air Force Cambridge Research Center.
- 6.33 Dubin, M., "Cosmic Debris of Interplanetary Space," Presented at the 2nd OSR Astronautics Conference, Denver, Colorado, April 1958.
- 6.34 Dubin, M., "Direct Measurements of Meteoritic Dust Using Rockets and Satellites," Presented at the 10th General Assembly of the International Astronomical Union, August 1958.
- 7.1 Ungar, E. E., WADD Technical Report No. 60-445 (1960).

- 7.2 Timoshenko, S., Theory of Plates and Shells, McGraw-Hill Book Co., New York (1940), p. 118.
- 7.3 Thomson, W. T. and M. V. Barton, J. Appl. Mech., 24, 248 (1957).
- 7.4 Cremer, L., Acustica, 5, 245 (1955).
- 7.5 Smith, P. W. Jr., J. Acoust. Soc. Am., 29, 721 (1957).
- 7.6 Heckl, M., Akustische Beihefte, 1, 259 (1958).
- 7.7 Franken, P. A., J. Acoust. Soc. Am., 32, 473 (1960).
- 7.8 Lyon, R. H., J. Acoust. Soc. Am., 28, 76 (1956), and 28, 391 (1956).
- 7.9 Dyer, I., J. Acoust. Soc. Am., 31, 922 (1959).
- 7.10 Eringen, A. C., J. Appl. Mech., 24, 46 (1957).
- 7.11 Cremer, L., The Propagation of Structure-Borne Sound, Report No. 1 (Series B), Dept. of Scientific and Industrial Research, London.
- 8.1 Gosele, K., Acustica, 3, 243 (1953), and Akustische Beihefte, 1, 94 (1956).
- 8.2 Chapter 40, Heating, Ventilating, Air Conditioning Guide, 35th Edition (1957).
- 8.3 Doelling, N., Chapter 17, Noise Reduction, L. L. Beranek, Ed., McGraw-Hill Book Co., New York (1960).

- 9.1 Jerison, J. H., and A. K. Smith, WADC Technical Report 55-358, and Psych. Abstr., 31, No. 1, 221 (1957).
- 9.2 Hirsh, I. J., R. C. Bilger, and B. H. Deatherage, Am. J. Psychol., 69, 561 (1956).
- 9.3 Broadbent, D. E., Quart. J. Exptl. Psychol., 6, 1 (1954).
- 9.4 Stevens, S. S., et al, Report of Project II, Committee on Sound Control in Vehicles, National Research Council, Psycho-Acoustic Laboratory, Harvard University, Cambridge, Massachusetts, 31 March 1941.
- 9.5 Kryter, K. D., J. Speech Hear. Disorders, Mongr. Supp. 1, 1 (1950).
- 9.6 Kryter, K. D., D. Flanagan, and C. Williams, Technical Note 59-58, Air Force Cambridge Research Center.
- 9.7 Beranek, L. L., Proc. Inst. Radio Engr., 35, 880 (1947).
- 9.8 Kryter, K. D., Chapter IV of Joint Services Human Engineering Guide for Equipment Designers, McGraw-Hill Book Co., New York, forthcoming.
- 9.9 Radio Corporation of America, "Study of Speech Reception Types." Appendix 5.0 in Study and Investigation of Specialized Electro-Acoustic Transducers for Voice Communication in Aircraft. Final Report, Contract No. AF 33(616)-3710, Task No. 43060, Western Electro-Acoustic Laboratory, Los Angeles, California, February 1959.

- 9.10 Ward, W. D., A. Glorig, and D. L. Sklar, J. Acoust. Soc. Am., 31, 791 (1959).
- 9.11 Rosenblith, W. A., and K. N. Stevens, Handbook of Acoustic Noise Control, Vol. II, Noise and Man. WADC Technical Report 52-204.
- 9.12 Kryter, K. D., Progress Report No. 2 to Nat. Inst. of Neurol. Diseases and Blindness under NIH Grant B-1727, Bolt Beranek and Newman Inc. (1959).

ERRATA IN VOLUME I

PAGE	LINE	
1	7	instead of "apartments," read "compartments"
6	16,17	omit "with origin at center of propeller disc"
12	14,15	instead of "rotations away from the jet axis" read "clockwise rotations"
12	footnote, line 3	instead of "10 log," read "10 log $\eta$ "
15	5	instead of "ft/sec," read "meters/sec"
17	14	instead of "temperature," read "absolute temperature"
56	25-27	instead of "d) Stringer (longeron) spacing: 19 in., e) Stringer section: Z section, 0.75 in. web, 0.75 in. flanges," read d) Stringer (longeron) spacing: approximately 6 in., e) Stringer section: Z section 0.75 in. web, 0.75 in. flange, 0.053 in. thick aluminum alloy"
59	17	instead of "Eq (53)," read "Eq (52)"
89	5,6	instead of " $f_{\max}$ is given by Eq (12), and is about 200 cps. Therefore, the octave band containing $f_{\max}$ is the 150-300 cps band," read " $f_{\max}$ is about 650 cps. Therefore, the octave band containing $f_{\max}$ is the 600-1200 cps band."
95	2,3	instead of $10 \log \frac{Q_M = 3.0}{Q_M = 1.2} = 10 \log \frac{1400}{240} = 8 \text{ db}$ By adding 8 db to $SPL_2 \dots$ ," read $20 \log \frac{Q_M = 3.0}{Q_M = 1.2} = 20 \log \frac{1400}{240} = 15 \text{ db}$ By adding 15 db to $SPL_2 \dots$ "

PAGE	LINE	
96	2	instead of "turbojet," read "turboprop"
97		add "We must also add 0-3 db to all levels for "pressure doubling" effects at the curved fuselage surface. See page 5."
98	22	instead of "TN 3147," read TN 3417"
106	(Fig 7)	on ordinate, instead of "sound power level," read "sound pressure level"
126	(Fig 27)	instead of $T_a$ read $T_a$ $-60^{\circ}\text{F}$ $400^{\circ}\text{R}$ $-10^{\circ}\text{F}$ $450^{\circ}\text{R}$ $60^{\circ}\text{F}$ $520^{\circ}\text{R}$ $140^{\circ}\text{F}$ $600^{\circ}\text{R}$ "
130	(Fig 31)	instead of "Fig F," read Fig 30"
131	(Fig 32)	instead of $T_a$ read $T_a$ $120^{\circ}\text{F}$ $580^{\circ}\text{R}$ $-40^{\circ}\text{F}$ $420^{\circ}\text{R}$ $T_{a0} = 60^{\circ}\text{F}$ $T_{a0} = 520^{\circ}\text{R}$ "
145	(Fig 46)	on abscissa, instead of "frequency = surface wt," read "frequency x surface wt"
146	(Fig 47)	on title, instead of "(lb/ft)," read "(lb/ft <sup>2</sup> )"
152	(Fig 53)	instead of $\frac{170}{\sqrt{\frac{m_1 d}{1 + \frac{m_1}{m_2}}}}$ , read $\frac{170}{\cos\theta \sqrt{\frac{m_1 d}{1 + \frac{m_1}{m_2}}}}$ "

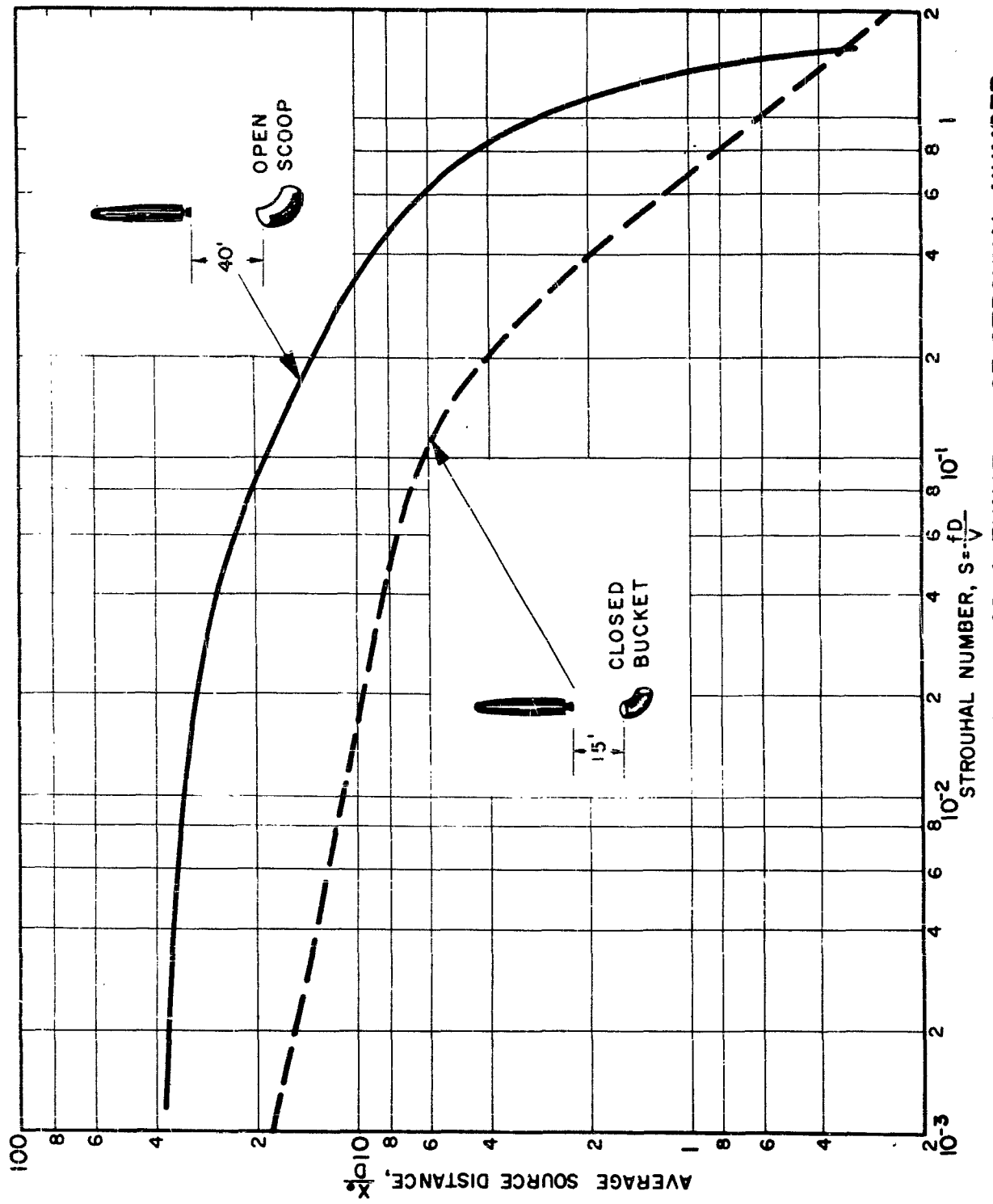


FIG. 75 SOURCE LOCATION AS A FUNCTION OF STROUHAL NUMBER.

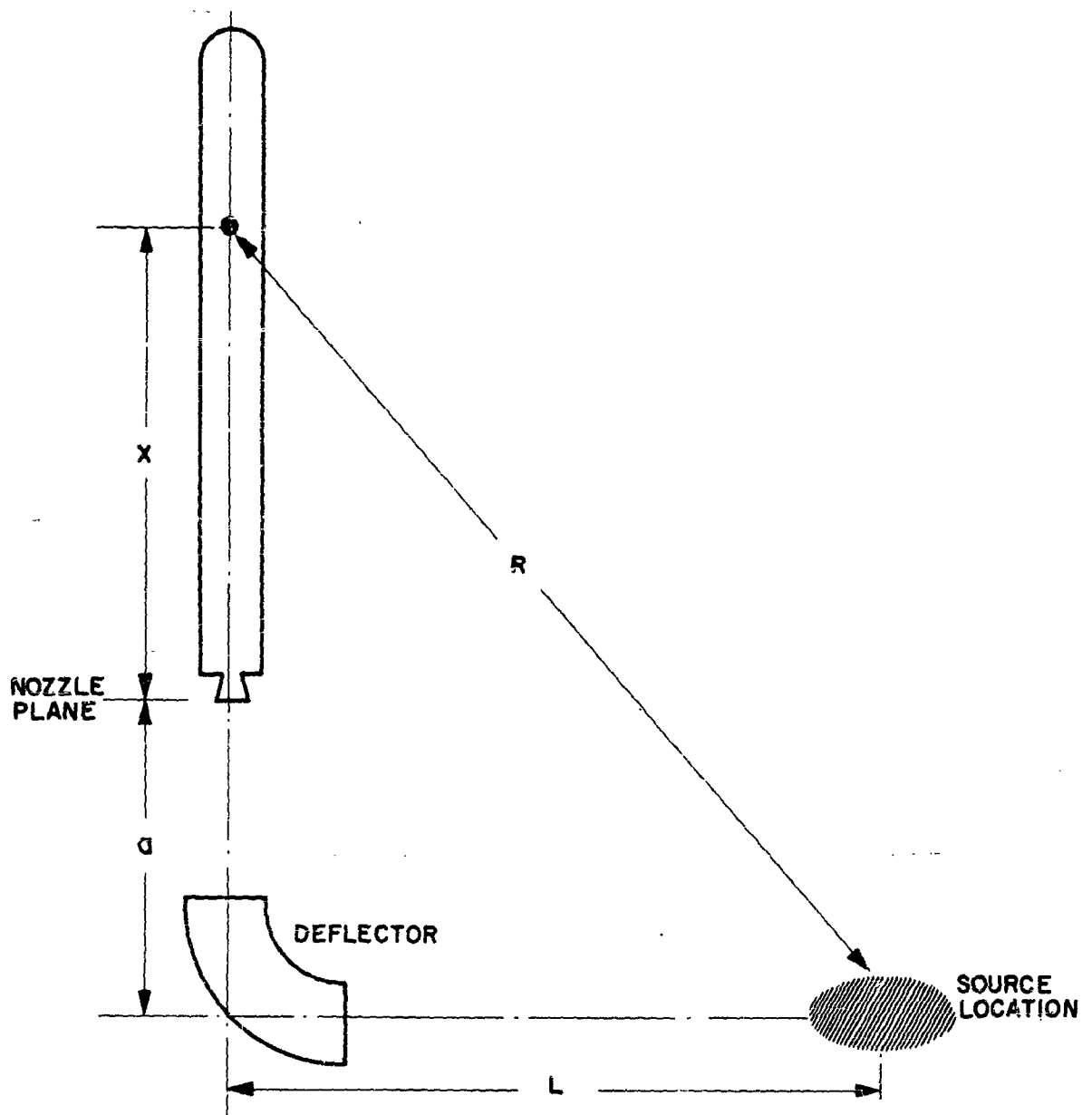


FIG. 76 GEOMETRY FOR ROCKET-DEFLECTOR CONFIGURATION.

WADC TR 58-343  
VOLUME II

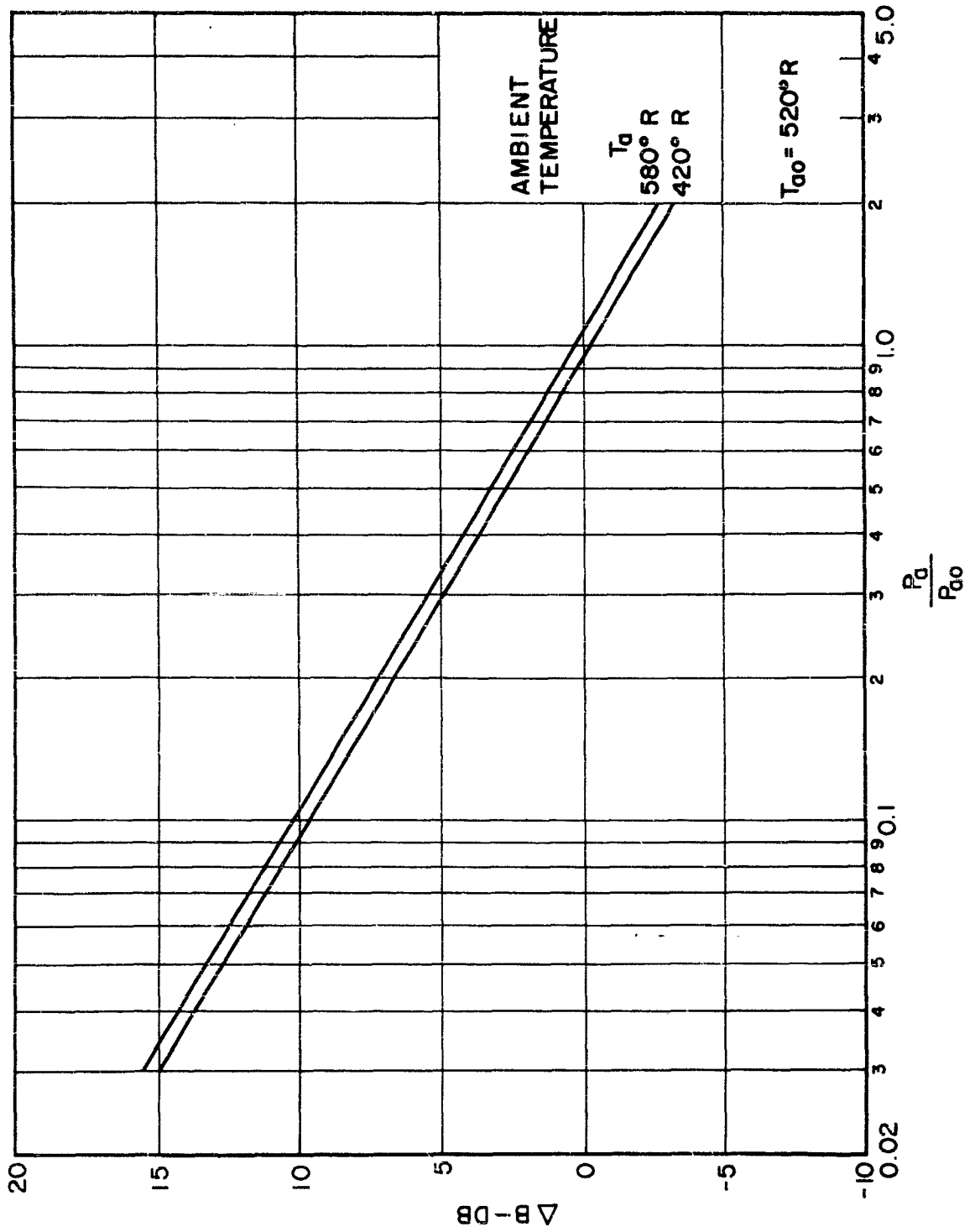


FIG. 77 CORRECTION FOR CHANGES IN AMBIENT TEMPERATURE AND PRESSURE.

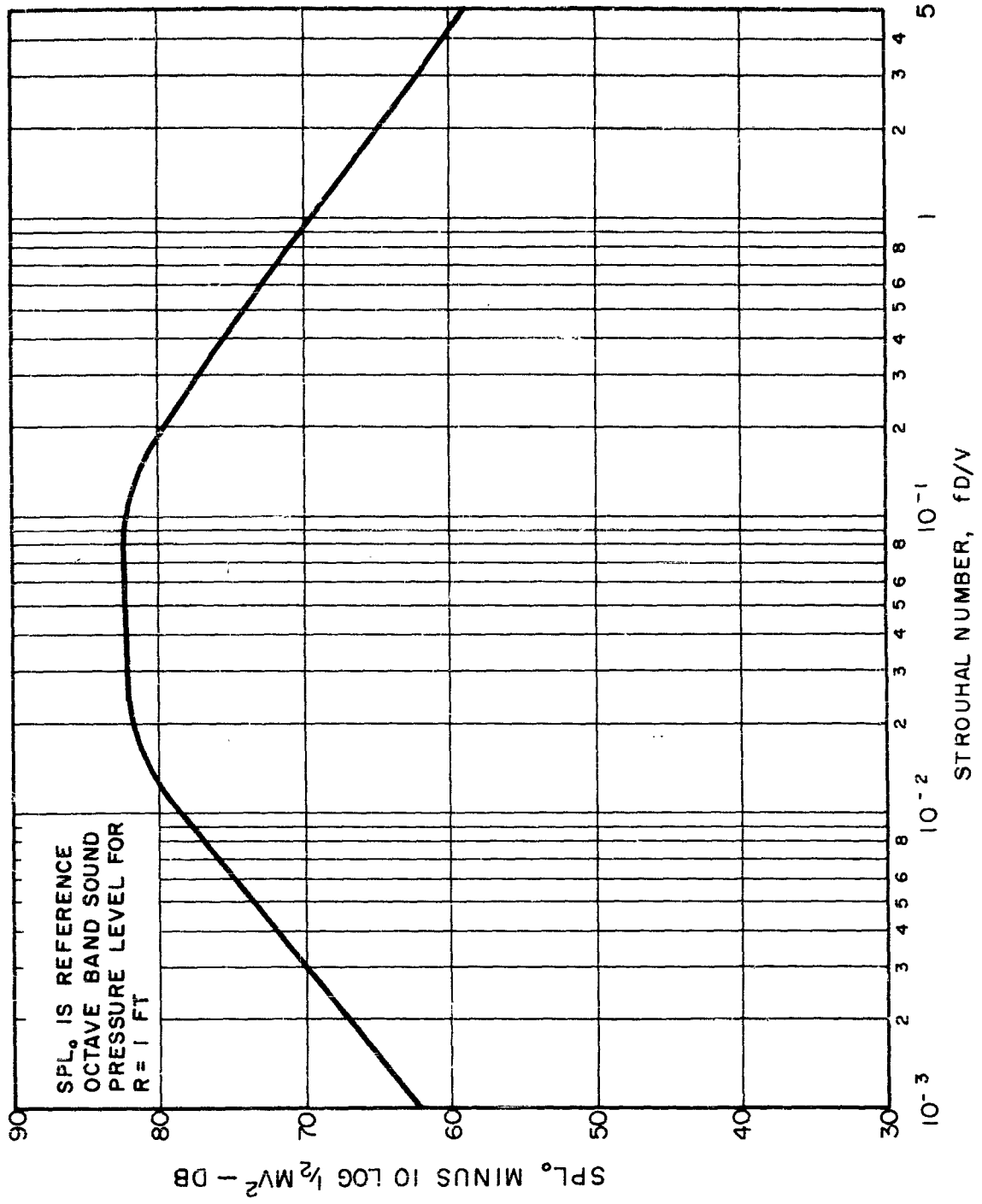


FIG. 78 REFERENCE FREE FIELD SOUND PRESSURE LEVEL AT MISSILE

WADC TR 58-343  
VOLUME II

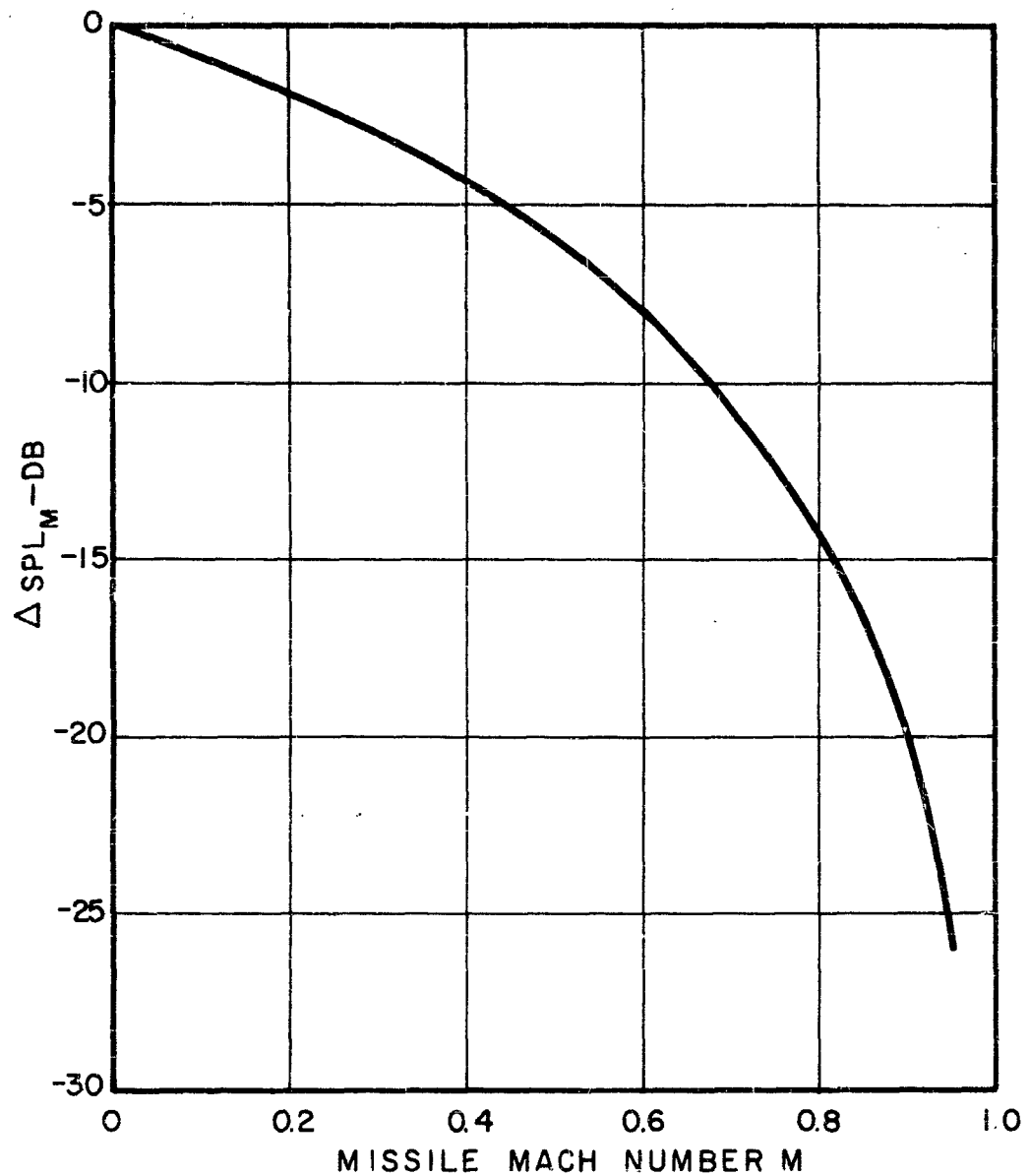


FIG. 79 SOUND PRESSURE LEVEL CHANGE AS A FUNCTION OF MACH NUMBER

WADC TR 58-343  
VOLUME II

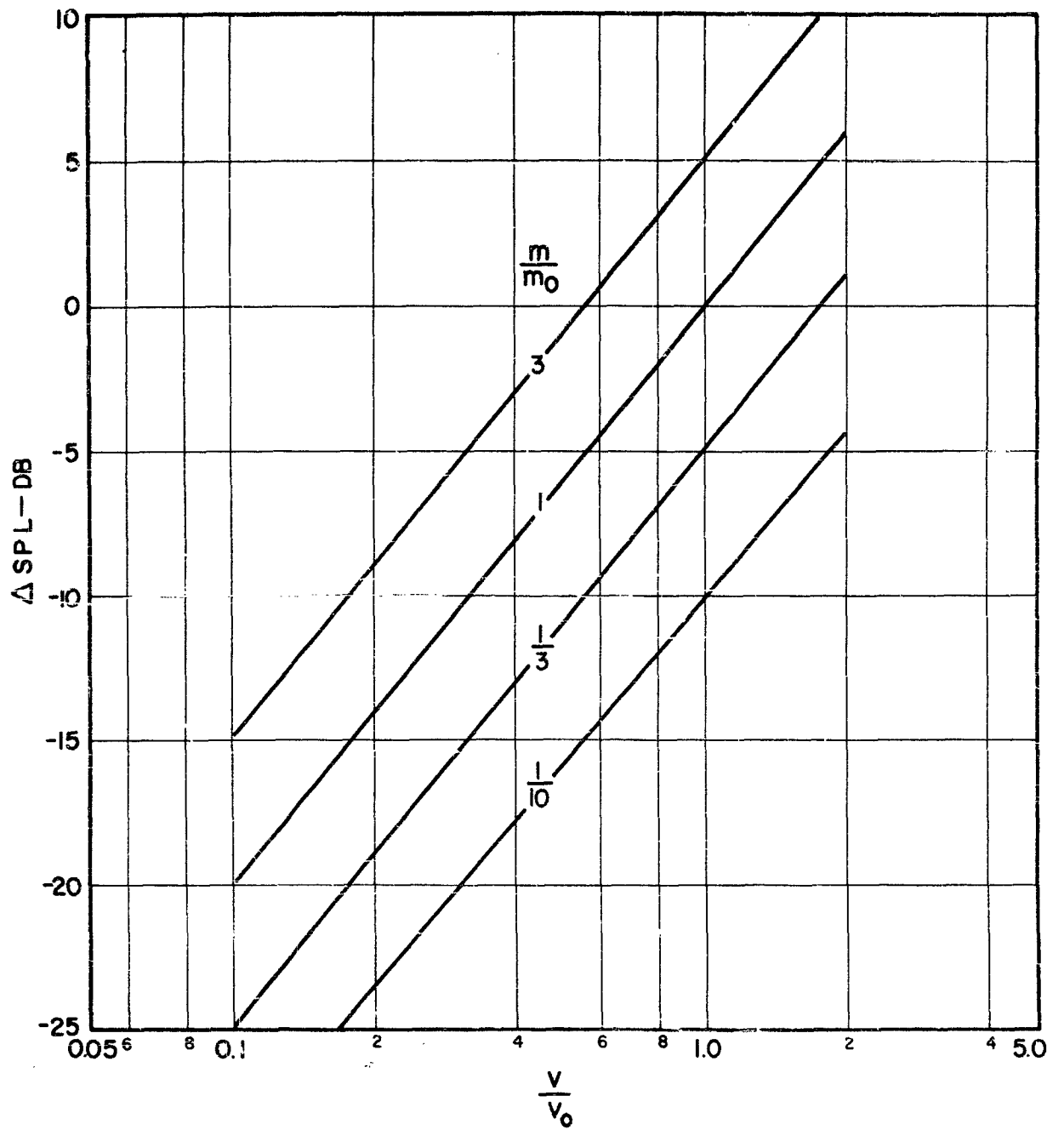
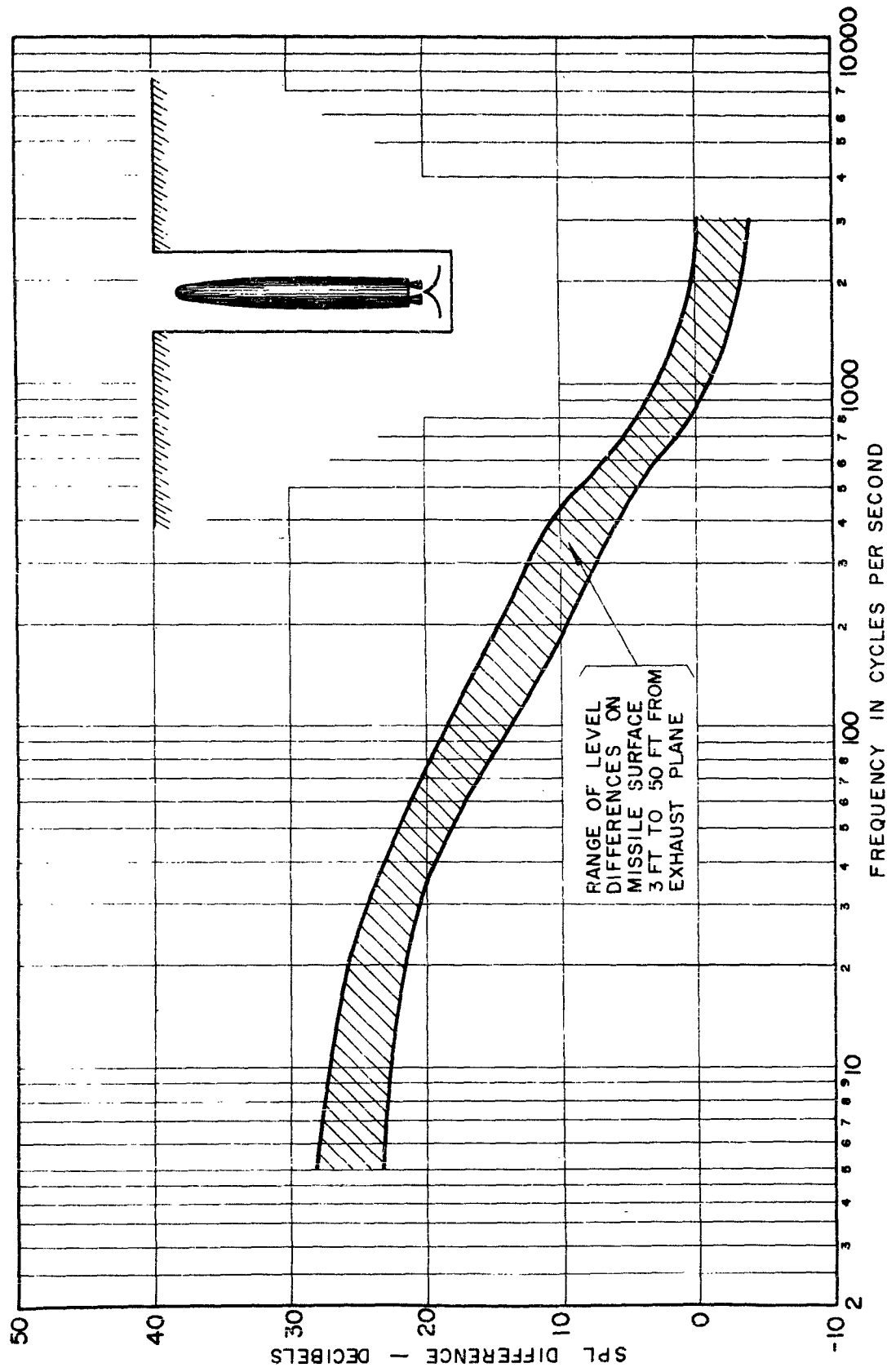


FIG. 80 CHANGE IN SOUND PRESSURE LEVEL OF LARGE ROCKETS.

WADC TR 58-343  
VOLUME II



RANGE OF LEVEL DIFFERENCES ON MISSILE SURFACE 3 FT TO 50 FT FROM EXHAUST PLANE

FIG. 81 DIFFERENCES BETWEEN HIGHEST NOISE LEVELS IN UN-LINED I-TUBE SILO AND ABOVE GROUND.

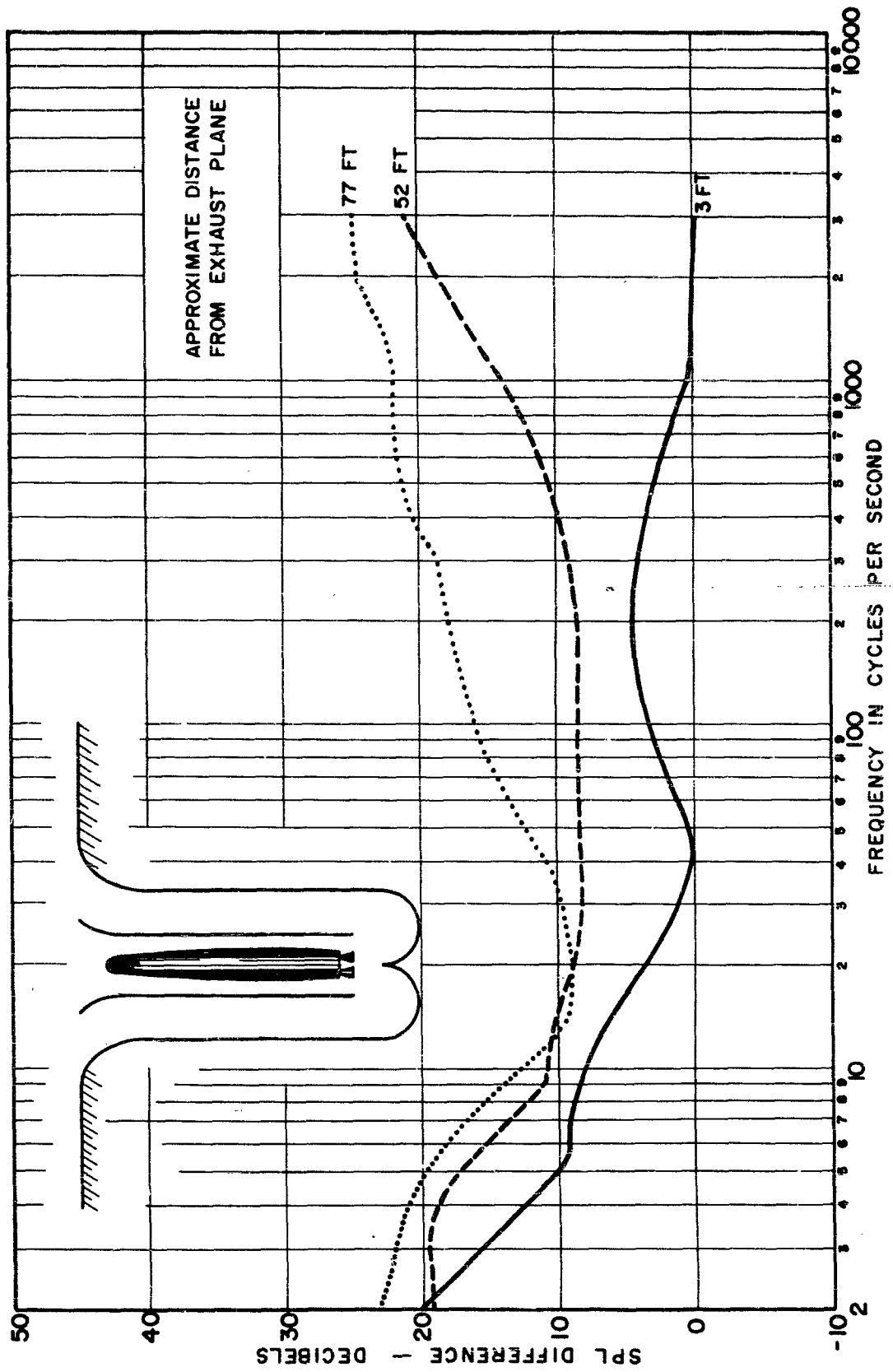


FIG. 82 DIFFERENCES BETWEEN HIGHEST NOISE LEVELS IN LAUNCH DUCT OF UNLINED DOUBLE - U SILO AND ABOVE GROUND.

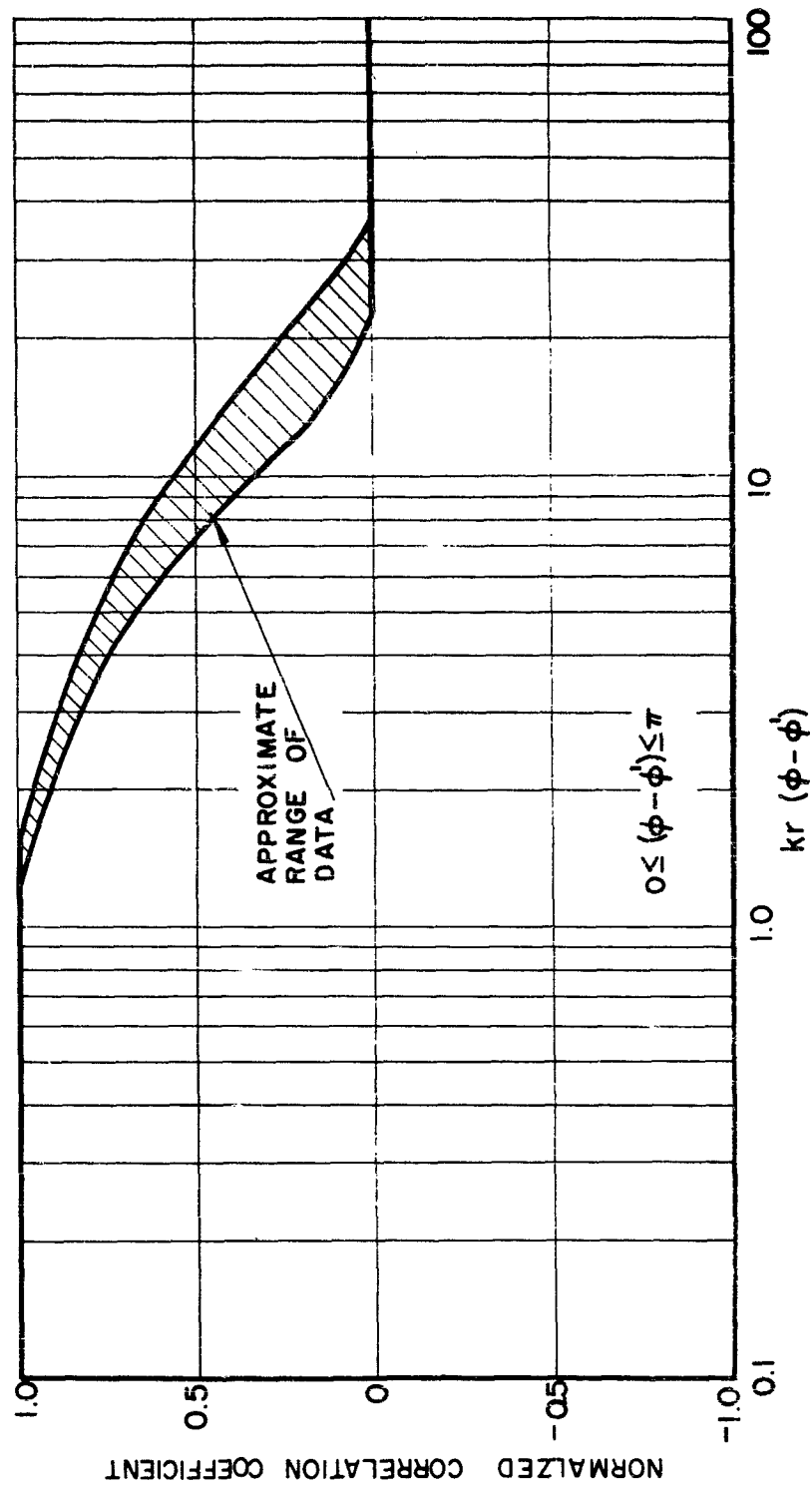


FIG. 83 ANGULAR CORRELATION AROUND MISSILE.

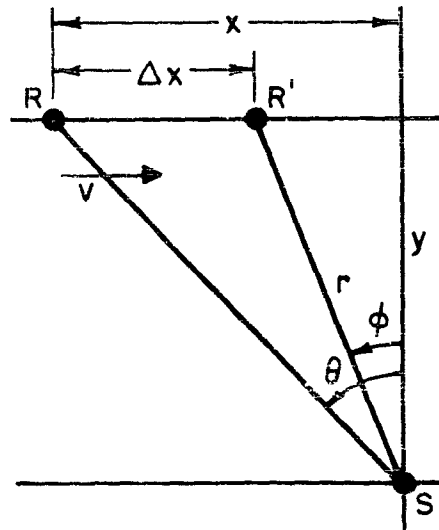
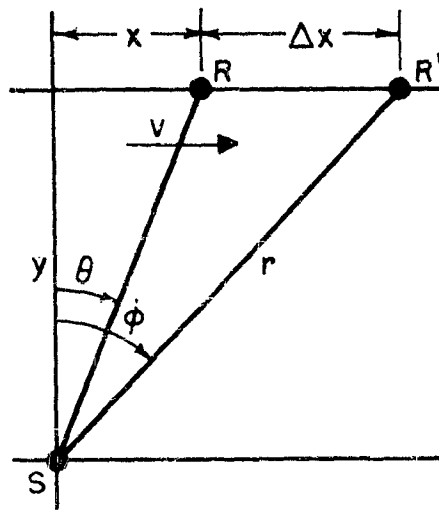


FIG. 84 EFFECTS OF FORWARD MOTION:  
SOURCE AND RECEIVER GEOMETRY

WADC TR 58-343  
VOLUME II

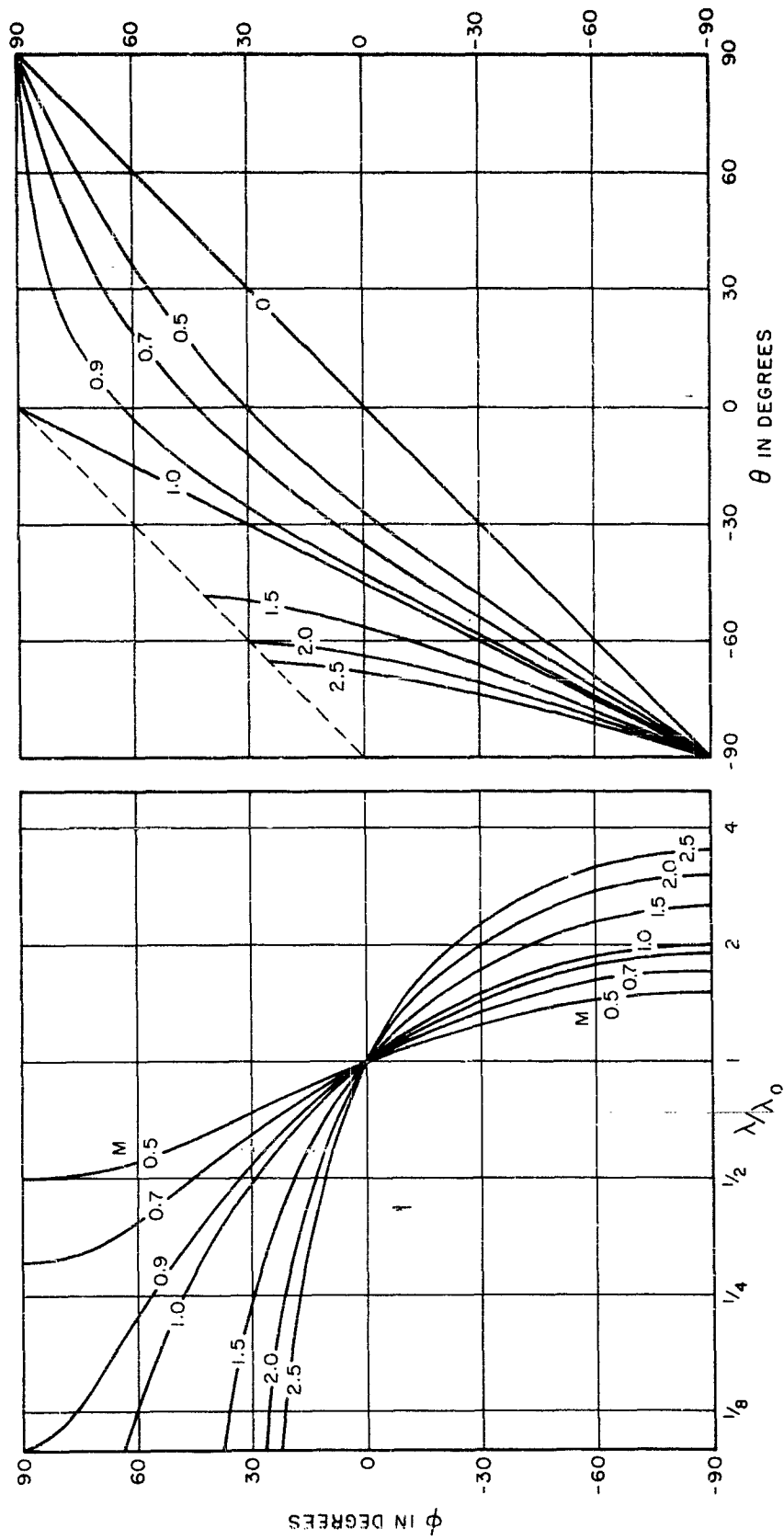


FIG. 85 EFFECTS OF FORWARD MOTION: CHANGES IN ANGLE AND OBSERVED WAVE LENGTH

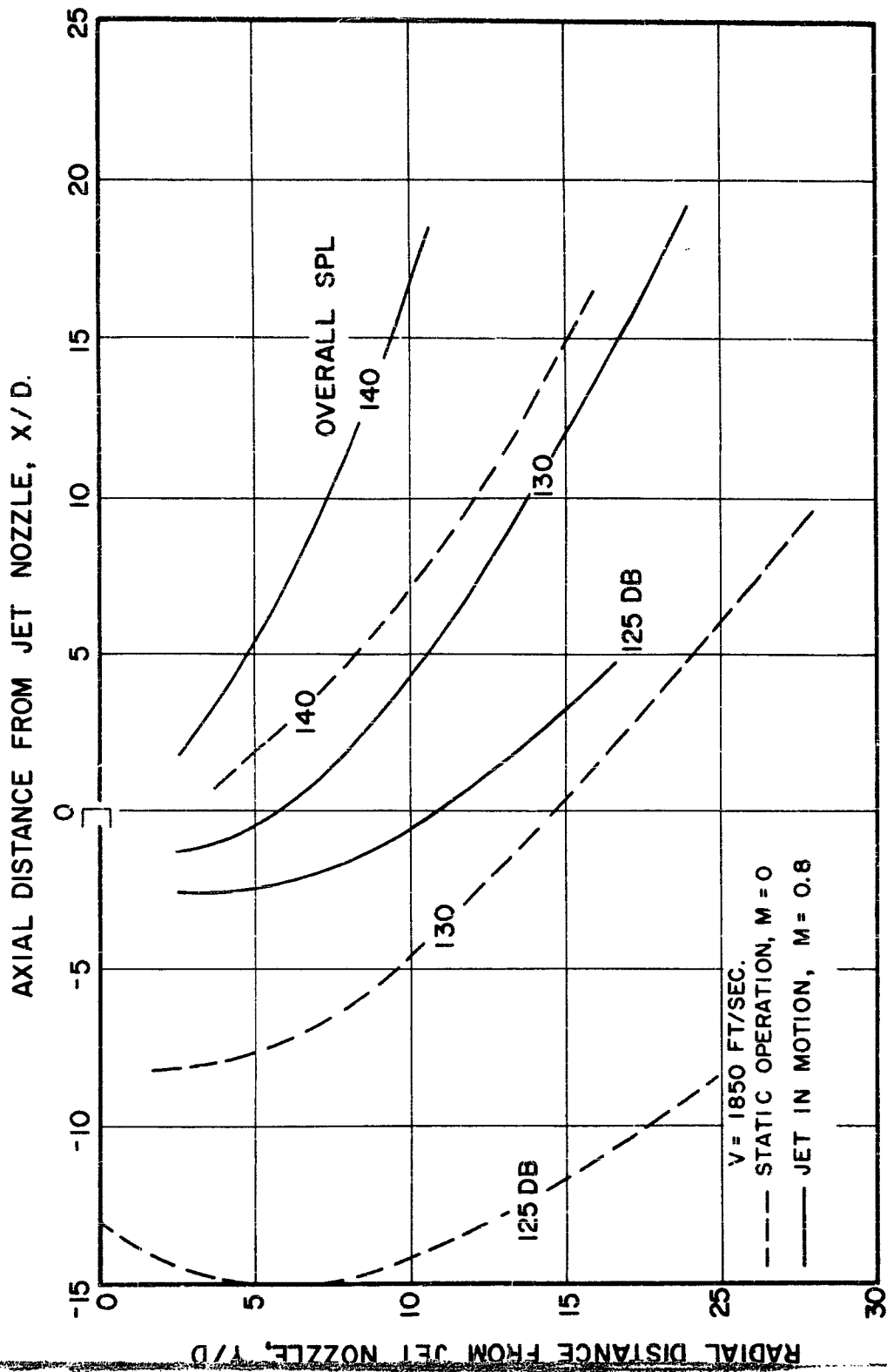


FIG. 86 EFFECT OF FORWARD MOTION ON NEAR-FIELD SOUND PRESSURE LEVEL CONTOURS OF CONTEMPORARY TURBOJET ENGINE.

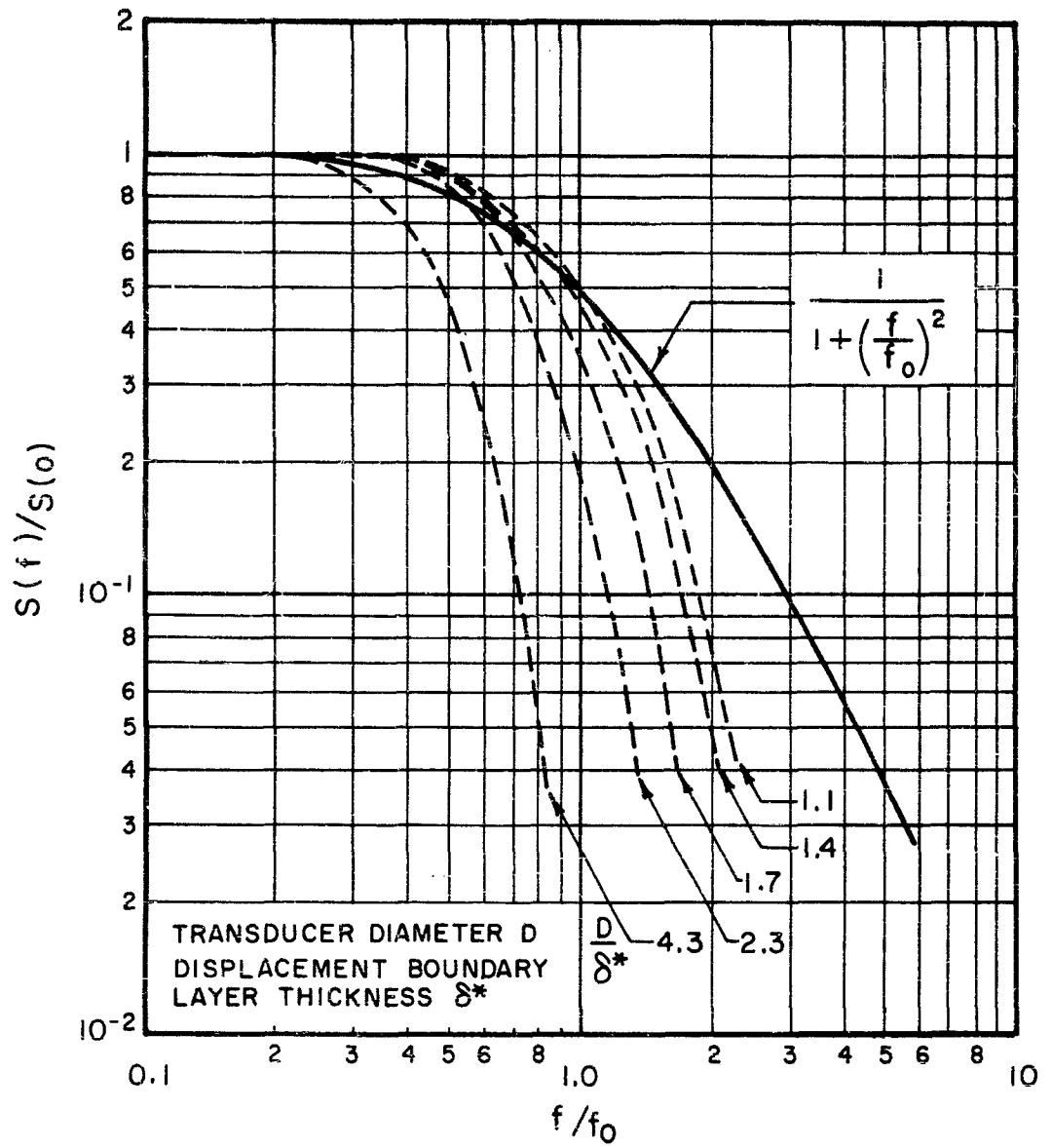
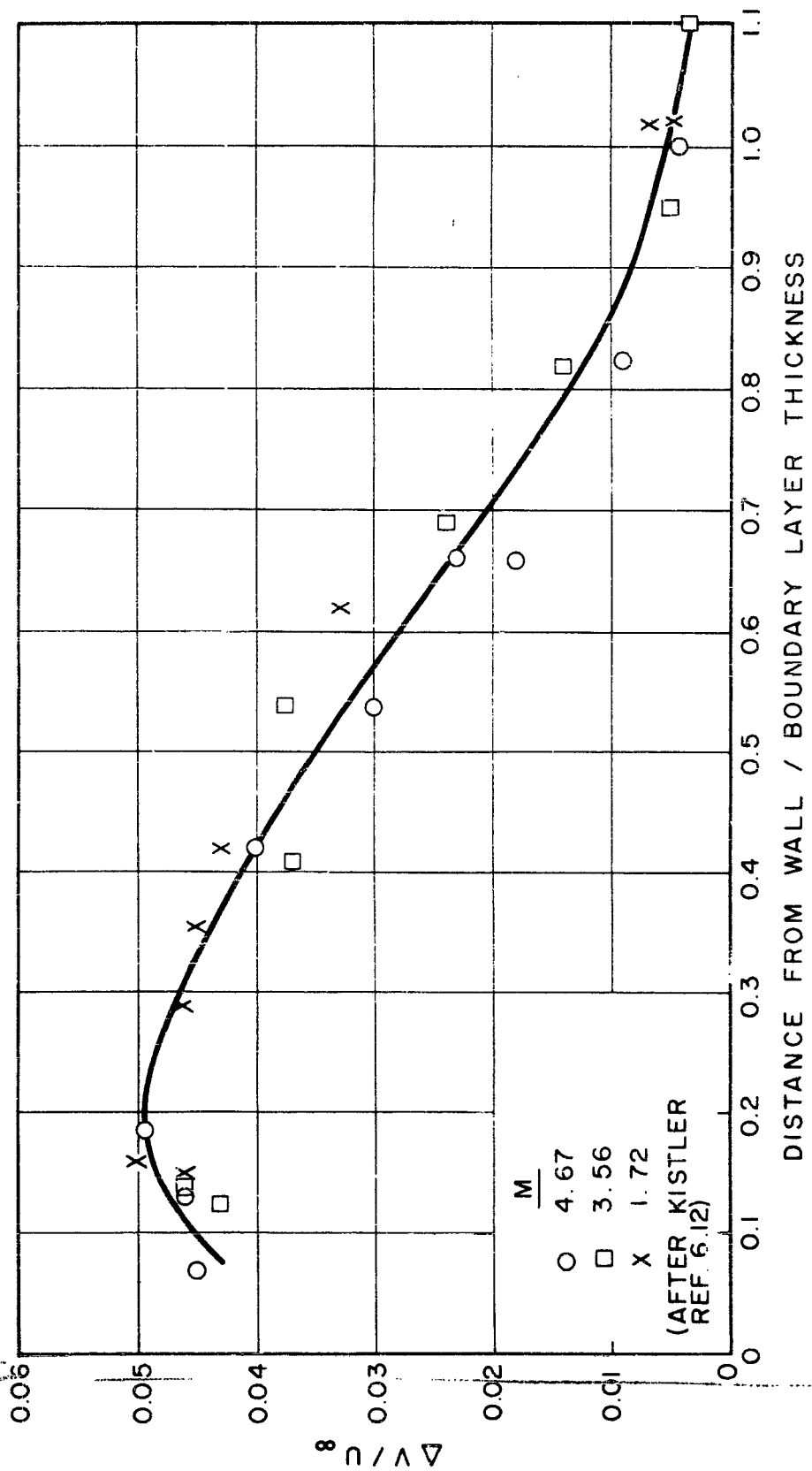
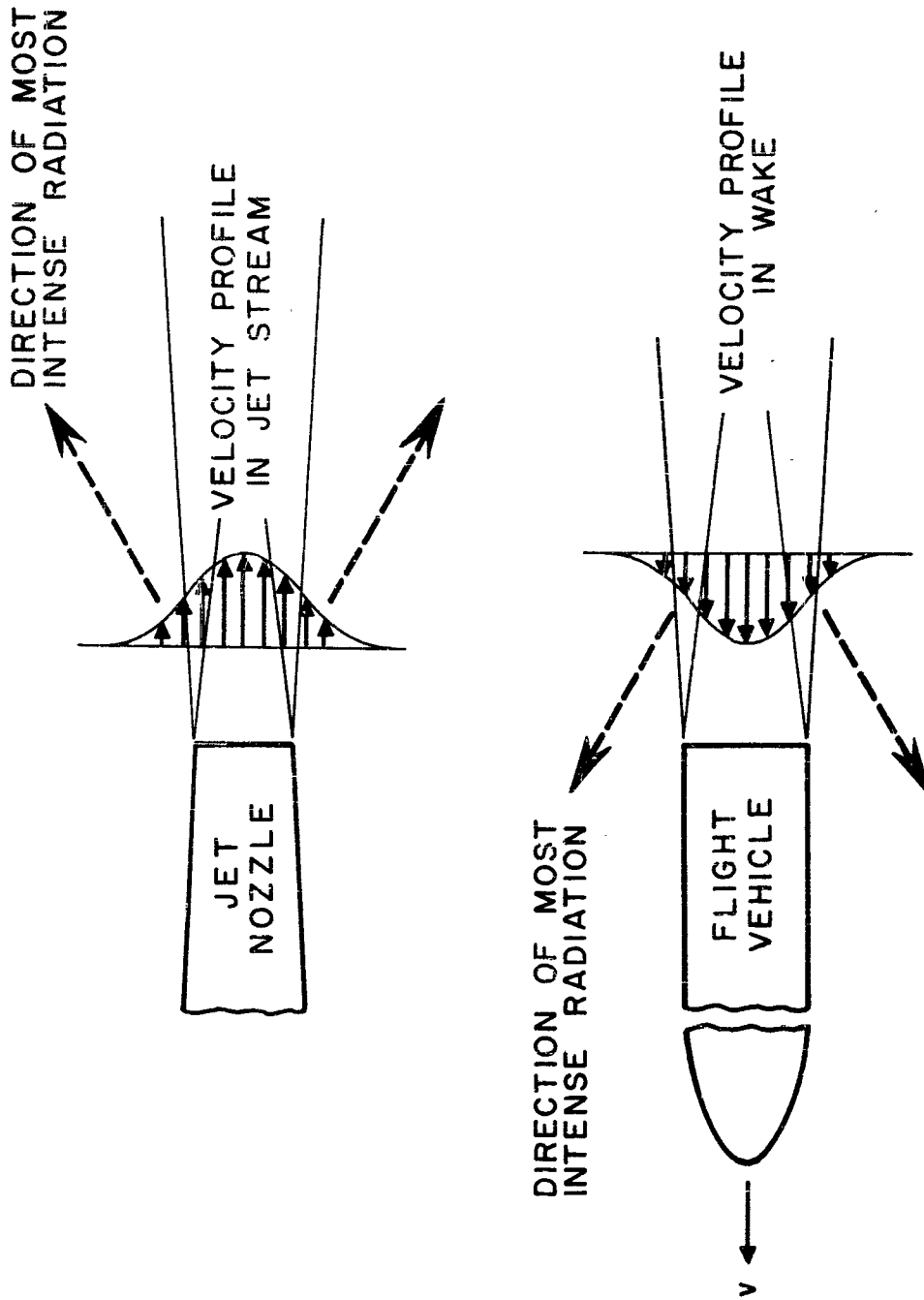


FIG. 87 BOUNDARY LAYER TURBULENCE SPECTRA



WADC TR 58-343  
 VOLUME II

FIG 88 VELOCITY FLUCTUATIONS IN SUPERSONIC BOUNDARY LAYERS.



WADC TR 58-343  
 VOLUME II

FIG. 89 QUALITATIVE COMPARISON OF NOISE RADIATION FROM A JET AND FROM A WAKE.

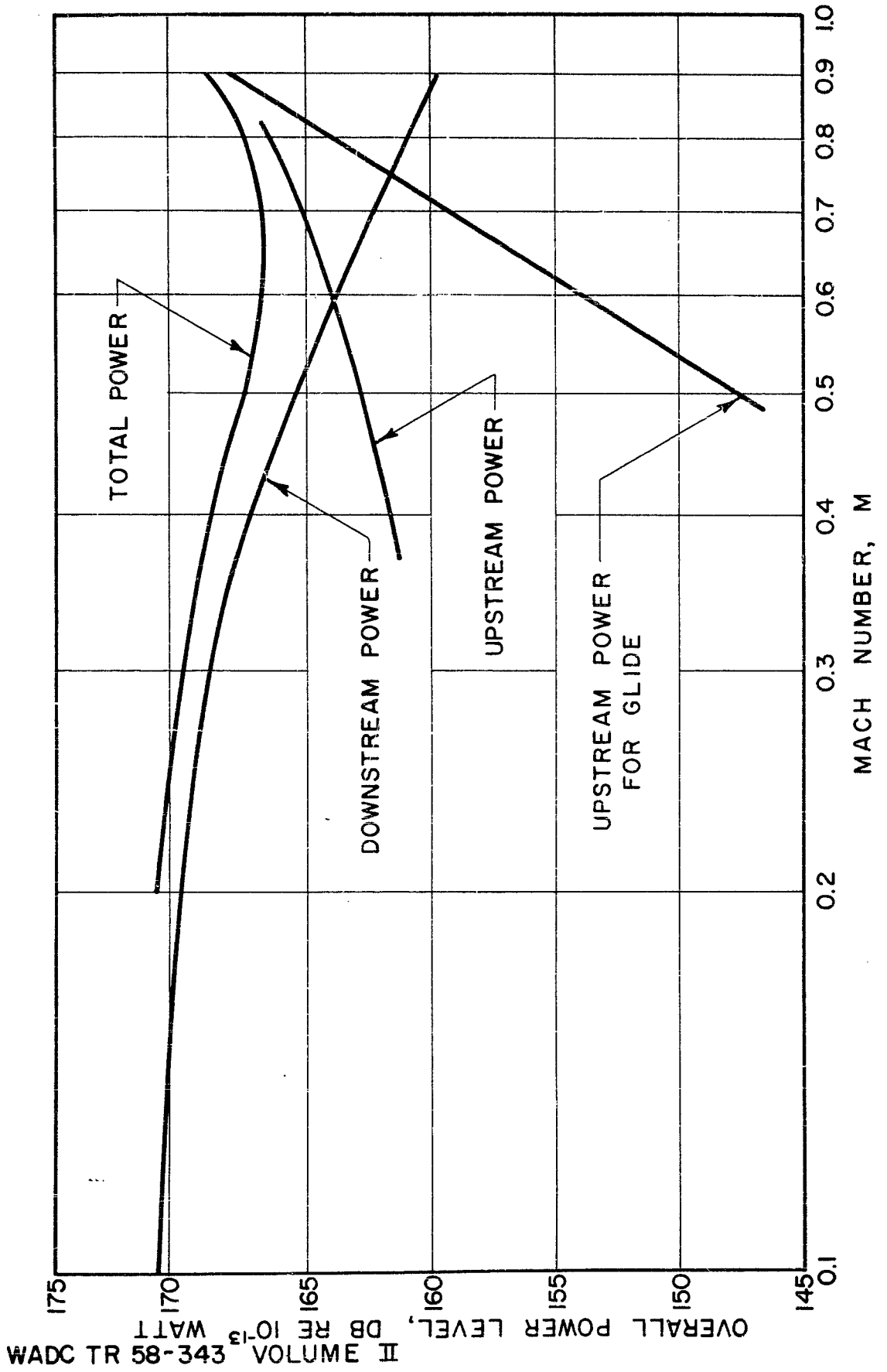
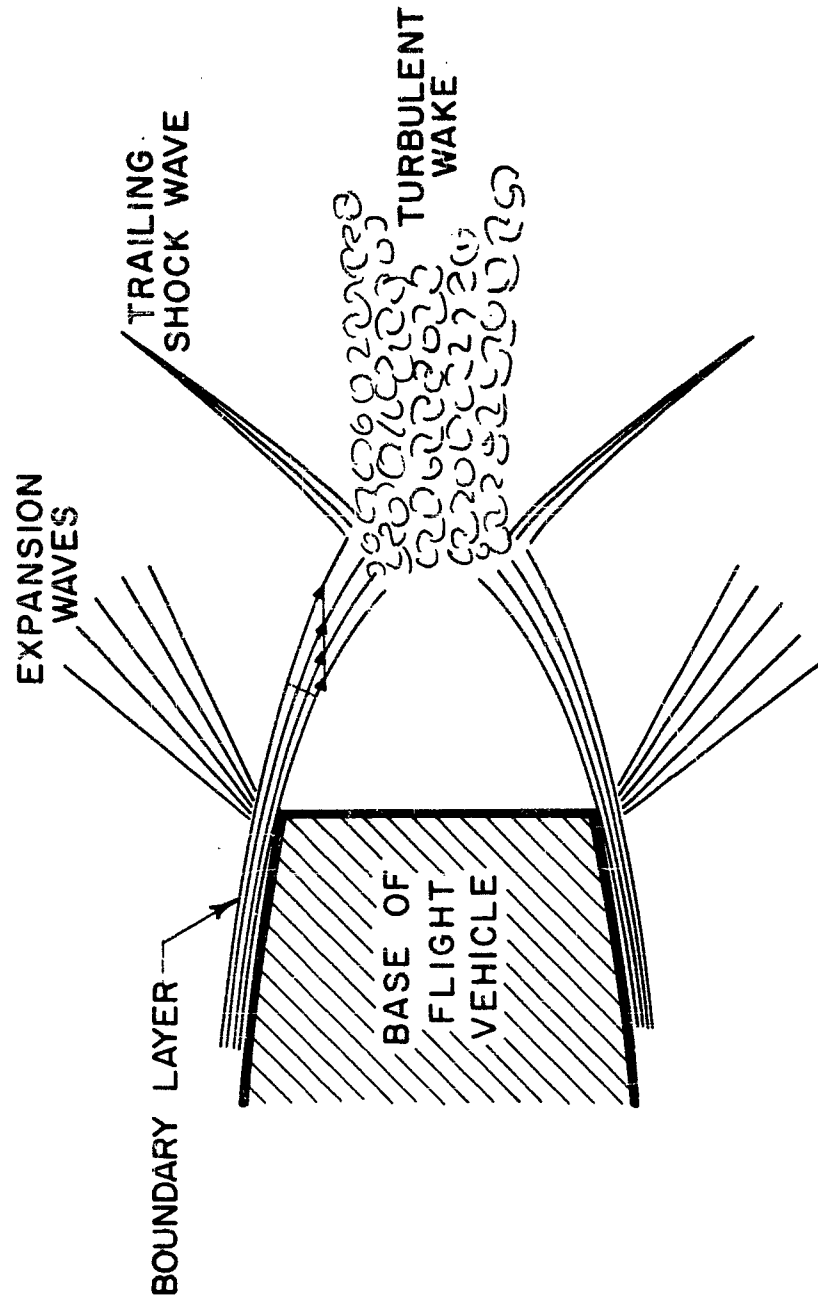
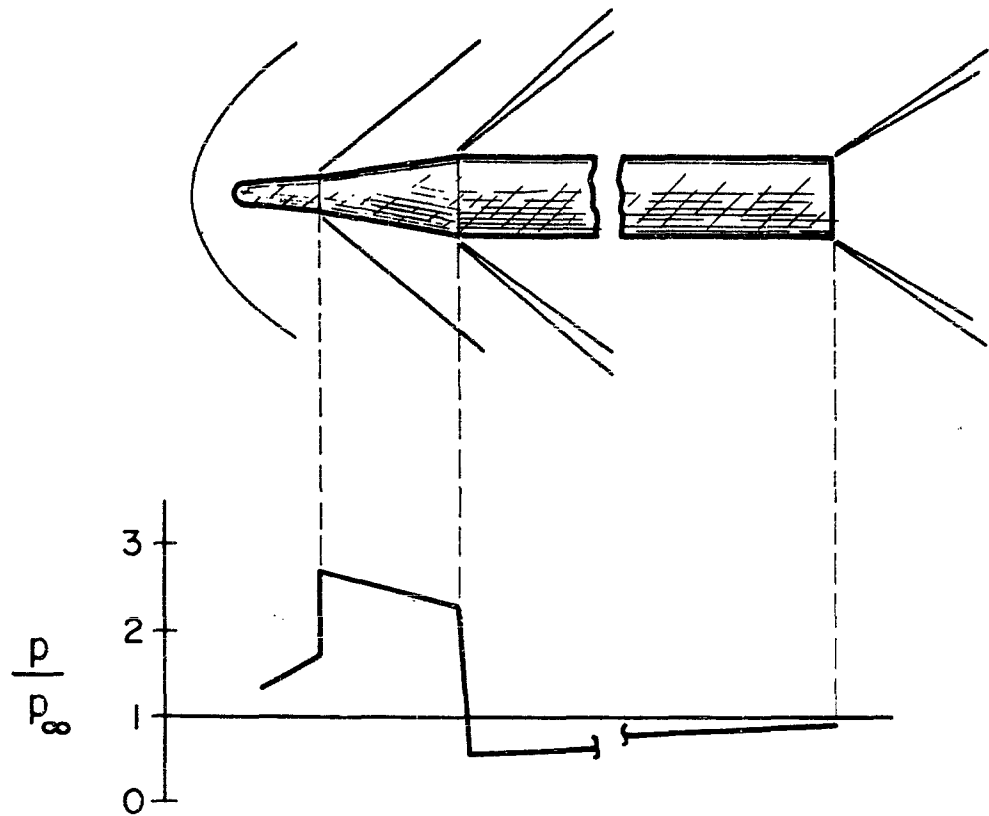


FIG.90 MEASURED ACOUSTIC POWER OF F-100 AIRCRAFT IN FLIGHT (REF.6.13)



WADC TR 58-343  
VOLUME II

FIG.91 SKETCH OF FLOW IN A SUPERSONIC WAKE.



REFERENCE  $p_\infty$  IS AMBIENT STATIC PRESSURE

FIG.92 TYPICAL STATIC PRESSURE DISTRIBUTION OVER A SUPERSONIC VEHICLE.

WADC TR 58-343  
VOLUME II

WADC TR 58-343  
 VOLUME II

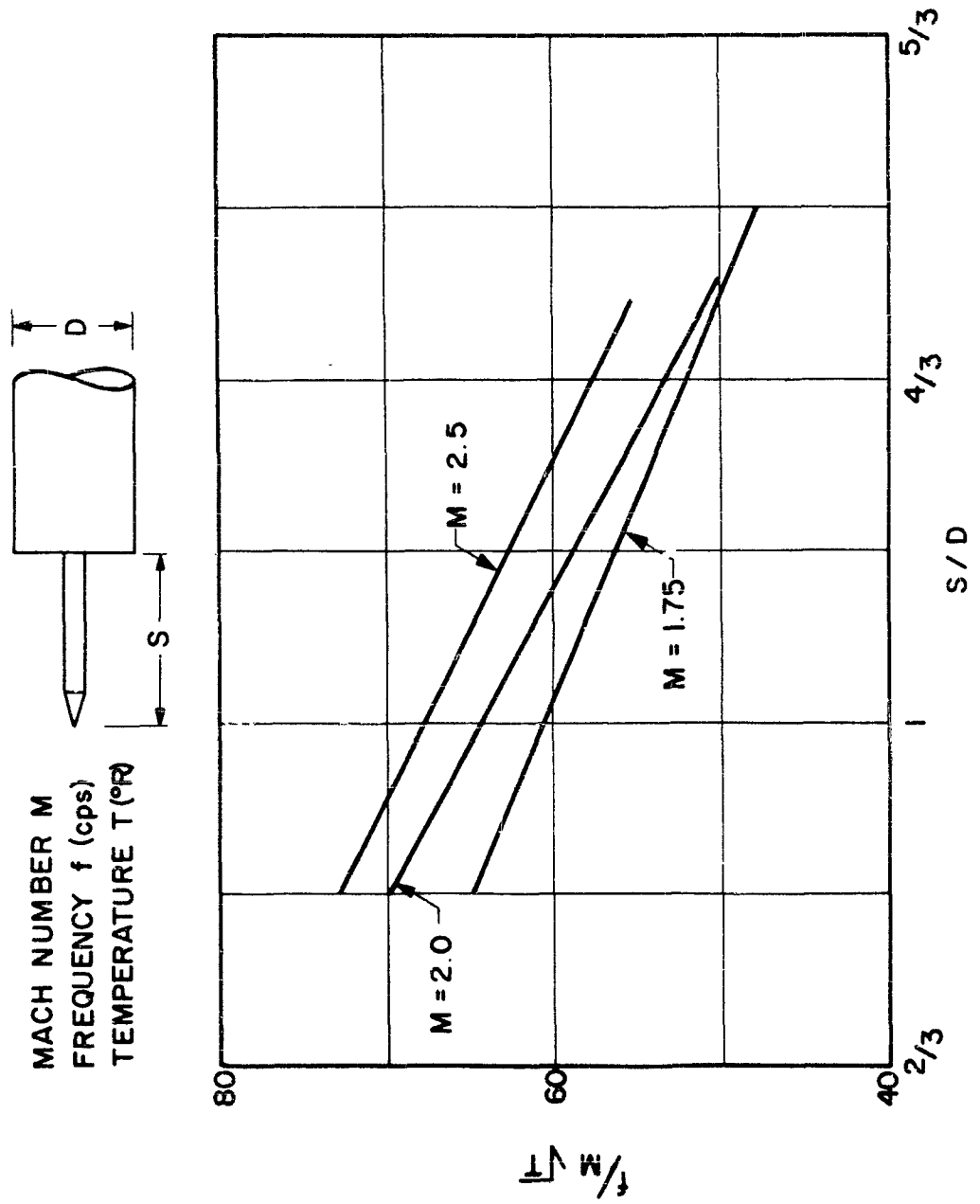
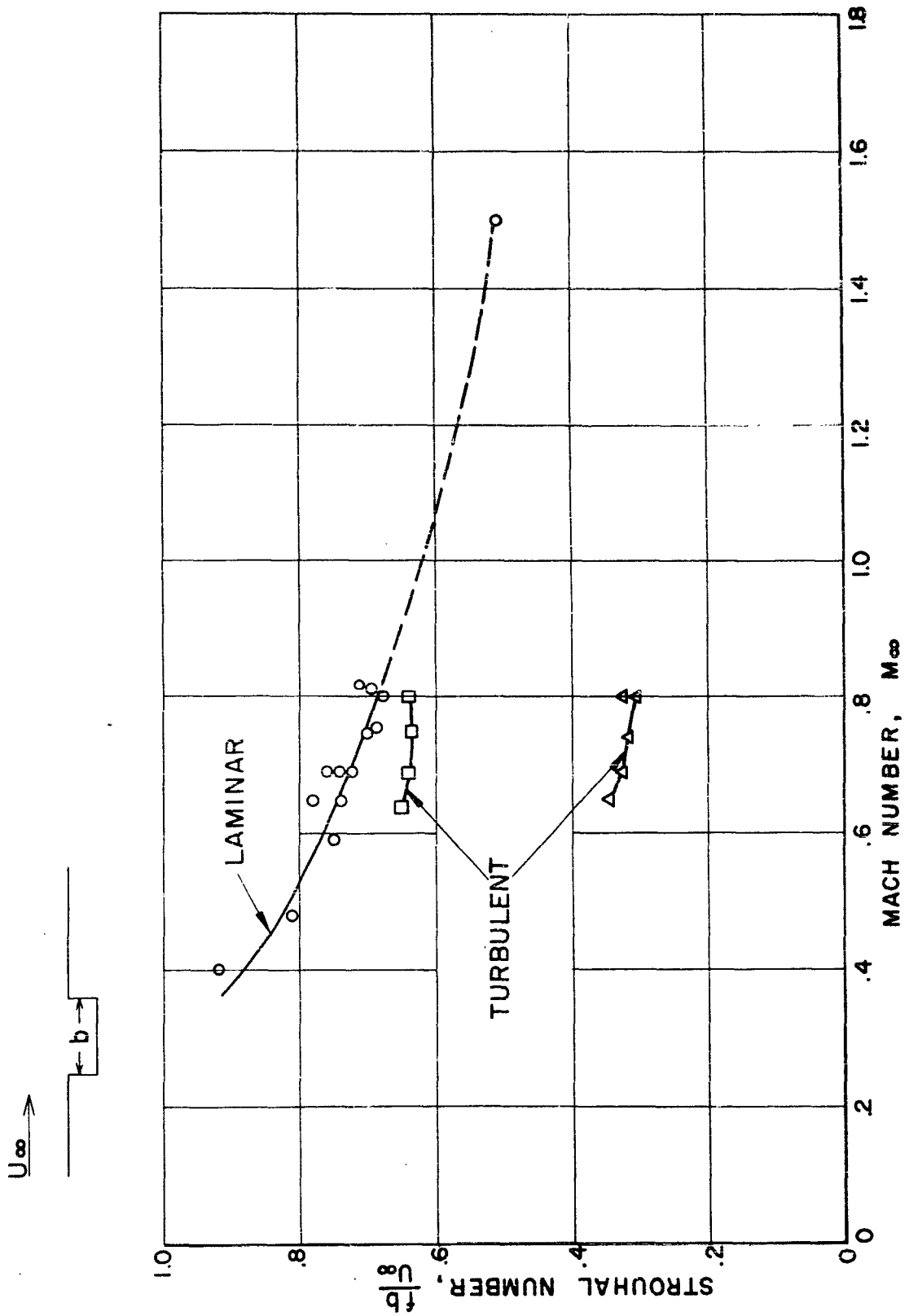


FIG. 93 FREQUENCY OF SHOCK OSCILLATIONS ON SPIKED BODIES (REF. 6.23)



WADC TR 58-343  
 VOLUME II

FIG. 94 FREQUENCY OF SOUND RADIATED IN CAVITY FLOW. (REF. 6.26)

WADC TR 58-343  
VOLUME II

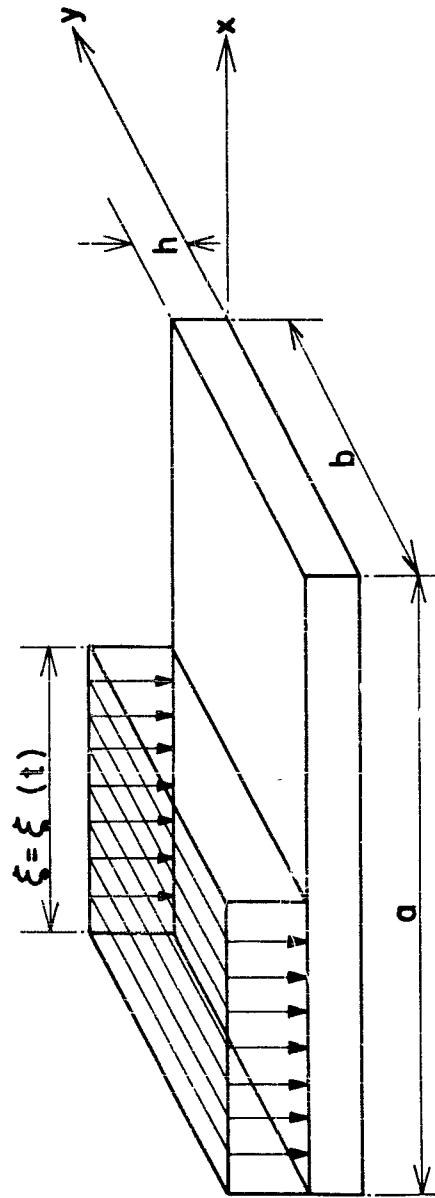


FIG. 95 PLATE SUBJECT TO DISCONTINUOUS PRESSURE.

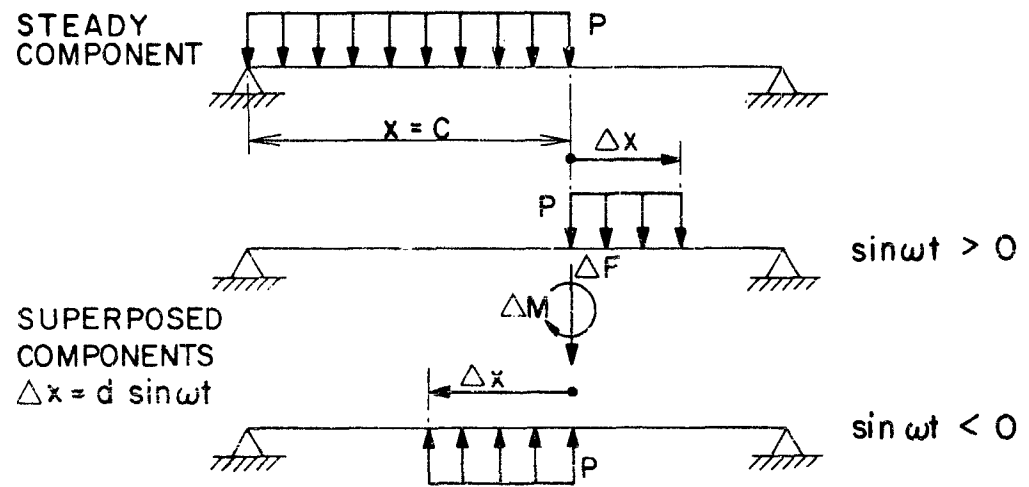


FIG. 96 STEADY AND VARYING PRESSURE DISTRIBUTIONS.

WADC TR 58-343  
 VOLUME II

WADC TR 58-343  
VOLUME II

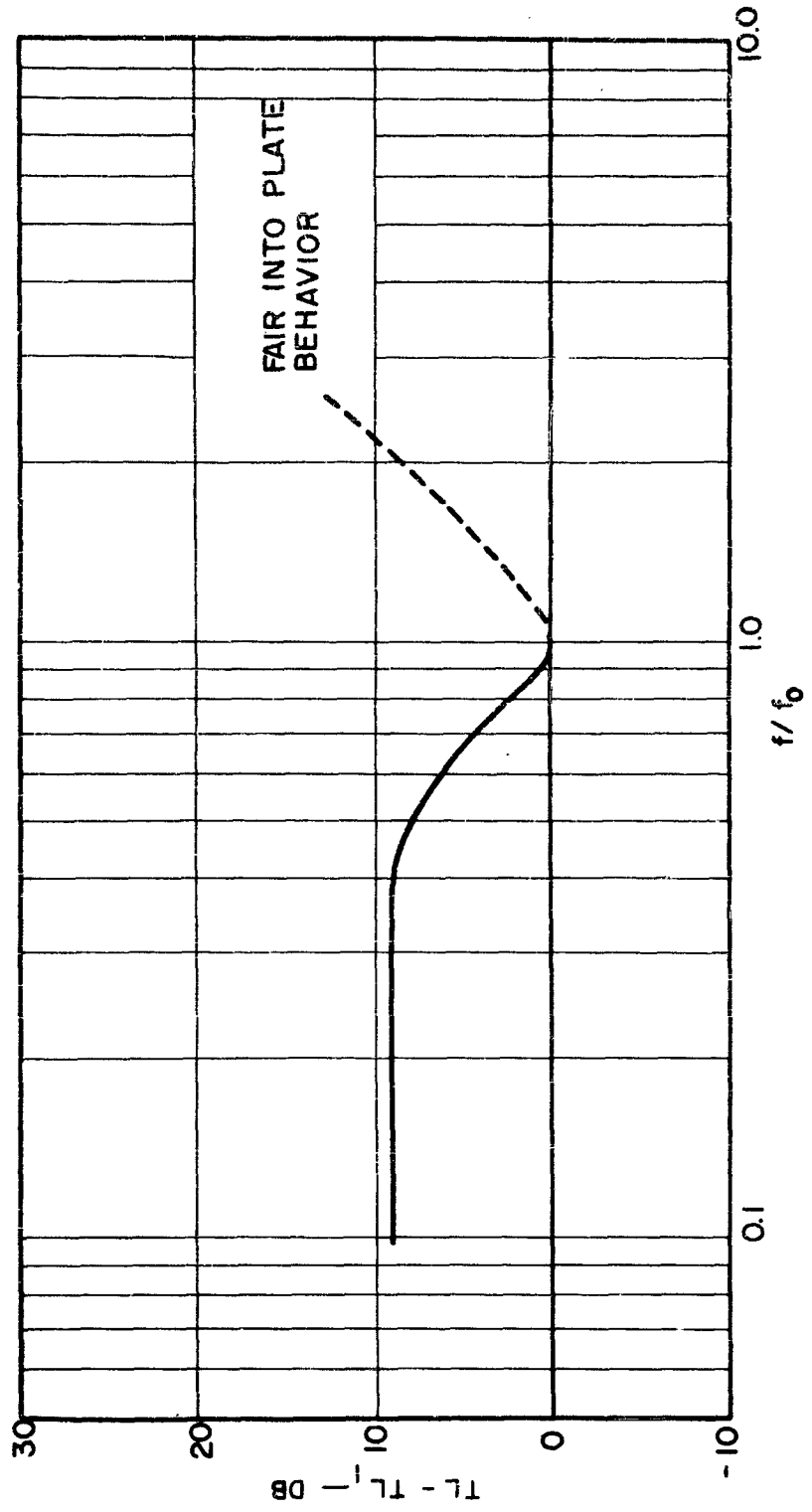
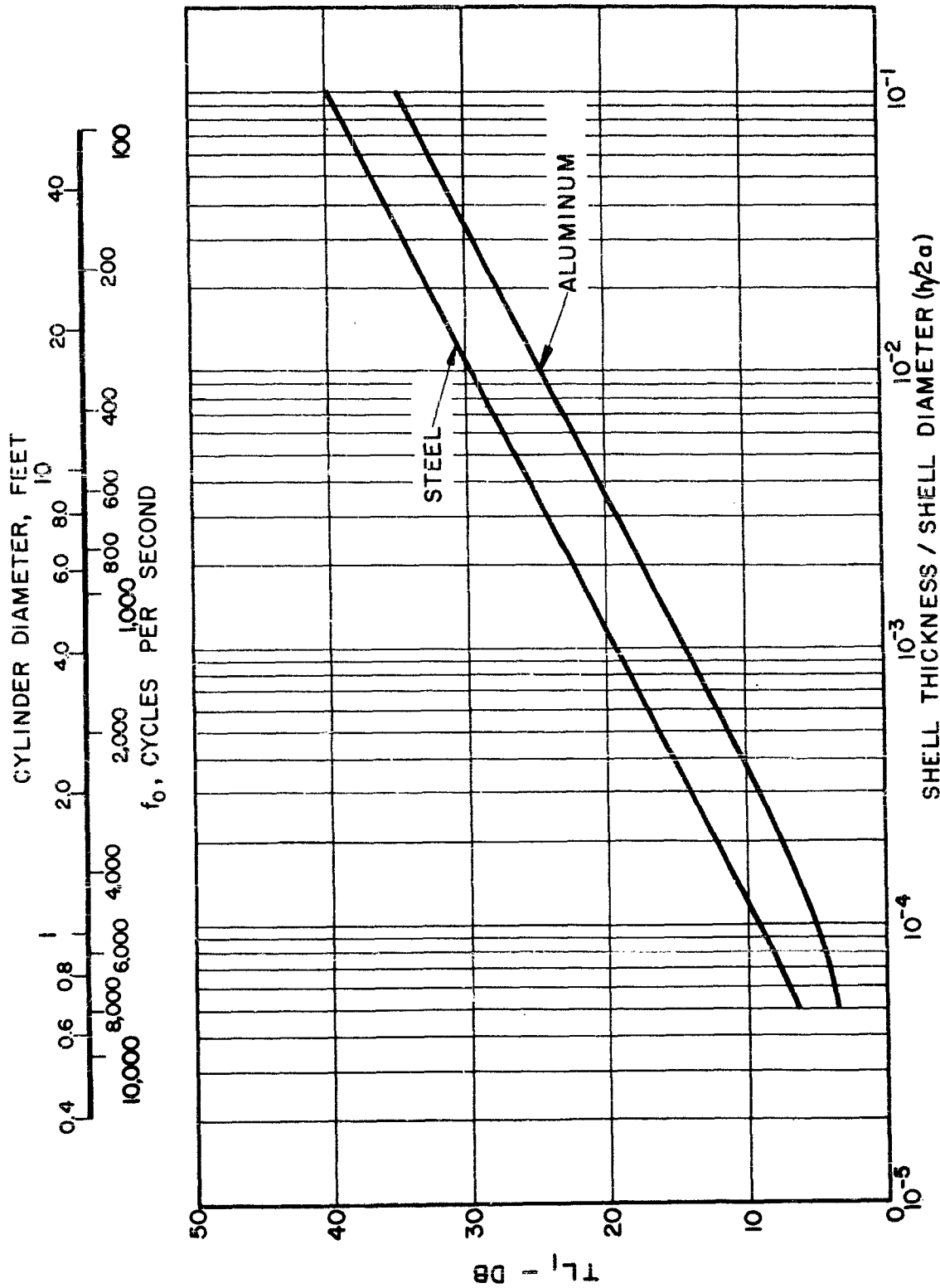


FIG. 97 PROPOSED SHAPE OF RANDOM OR GRAZING INCIDENCE TRANSMISSION LOSS OF CYLINDER (BROAD - BAND NOISE EXCITATION).



WADC TR 58-343  
 VOLUME II

FIG. 98 CHARACTERISTIC TRANSMISSION LOSS AND RADIAL RESONANCE FREQUENCY OF CYLINDRICAL STEEL OR ALUMINUM SHELLS.

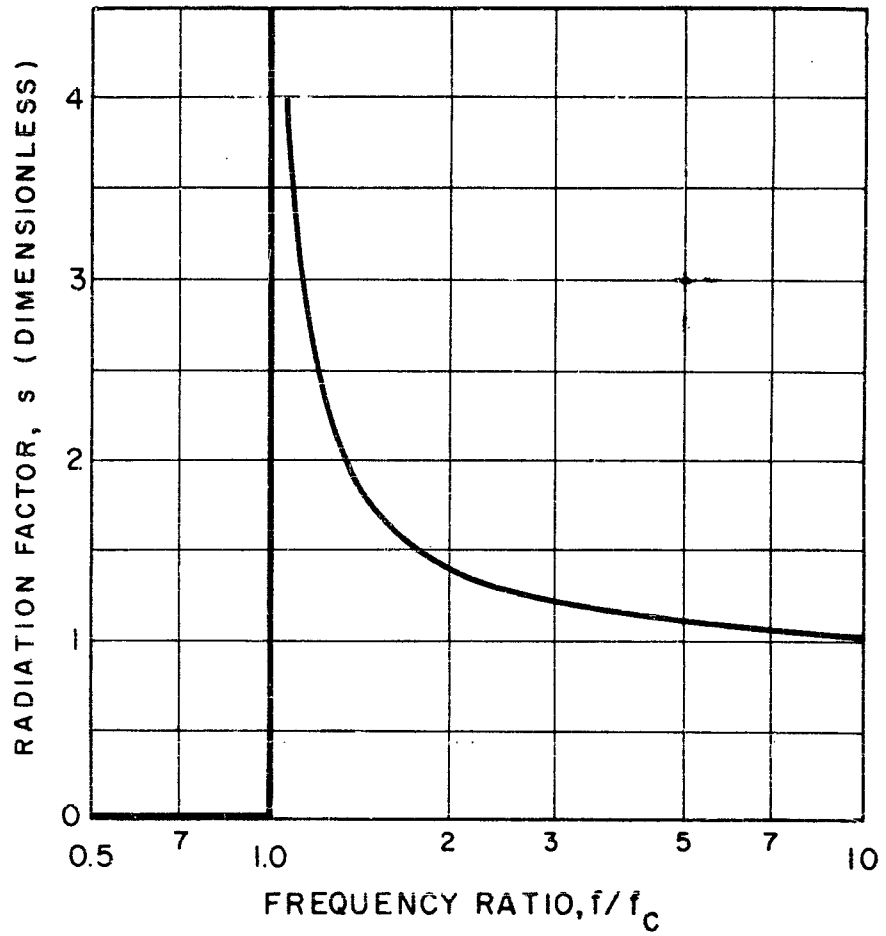


FIG. 99 RADIATION FACTOR FOR TRAVELLING WAVES ON AN INFINITE PLATE

WADC TR 58-343  
VOLUME II

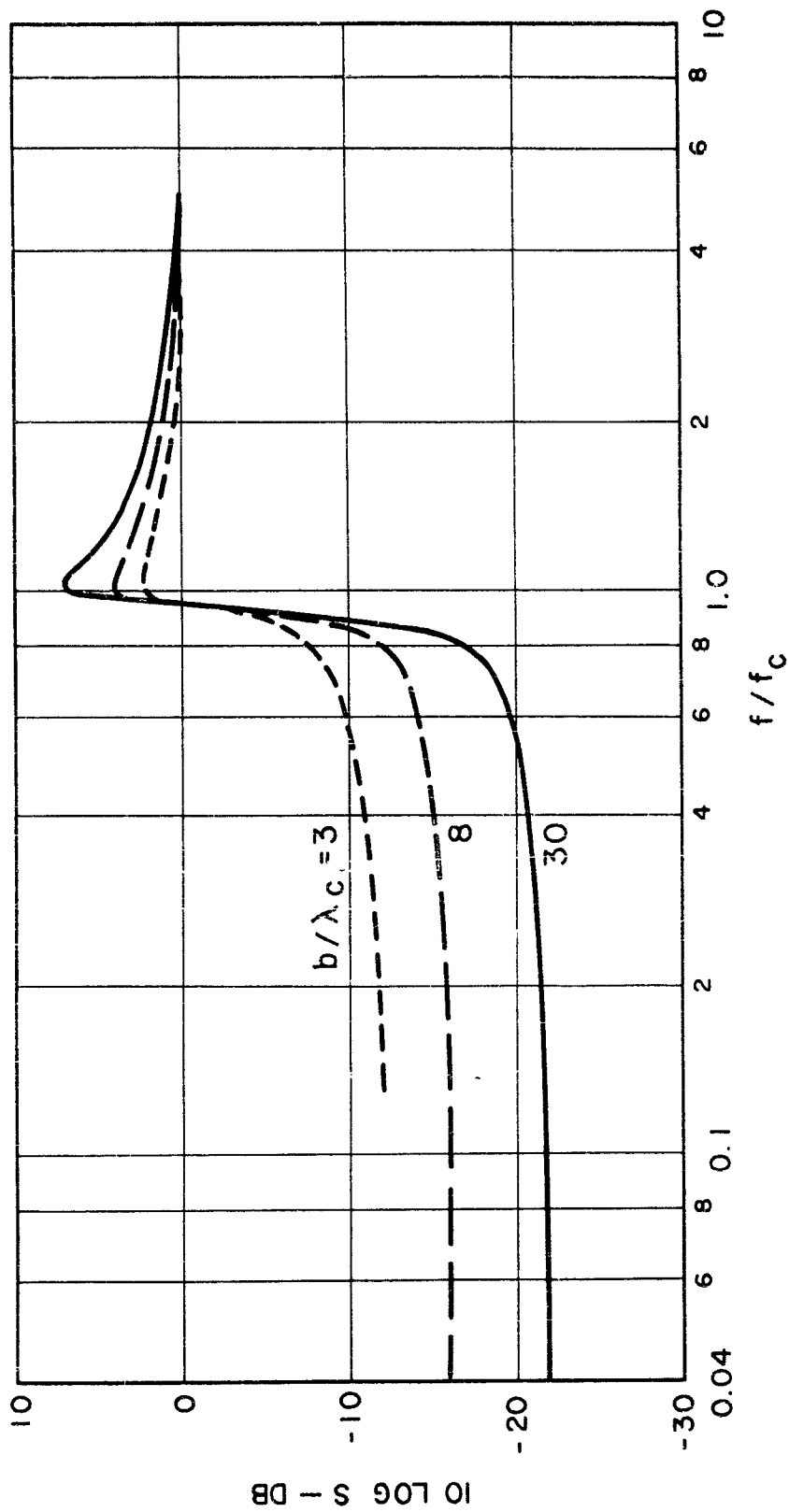


FIG. 100 RADIATION FACTOR FOR TRAVELLING WAVES ON A FINITE PLATE

WADC TR 58-343  
VOLUME II

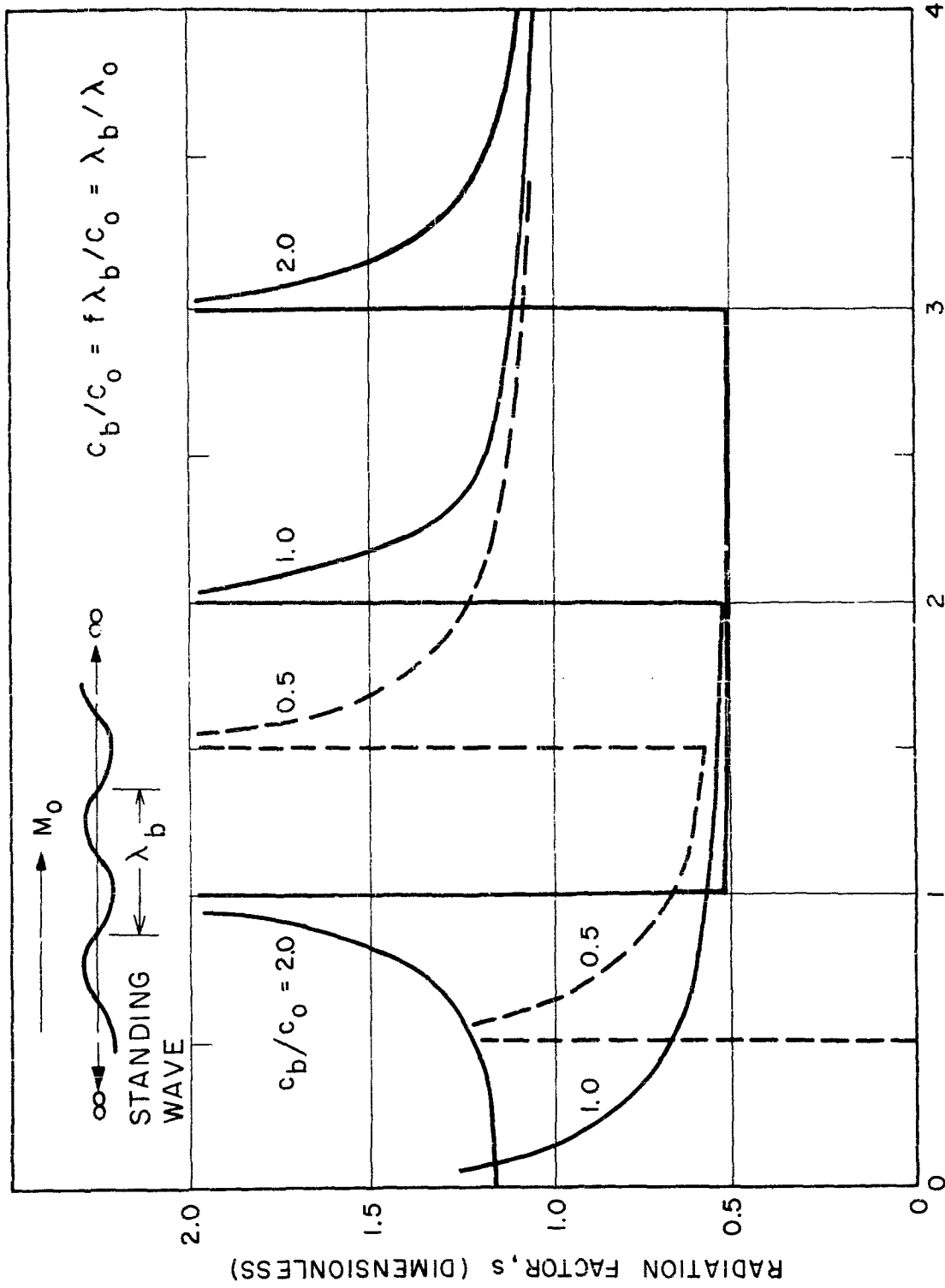


FIG. 101 MACH NUMBER,  $M_0$  OF FLOW PAST PANEL  
 EFFECT OF FLUID FLOW ON RADIATION FACTOR FOR  
 STANDING WAVES ON AN INFINITE PLATE.

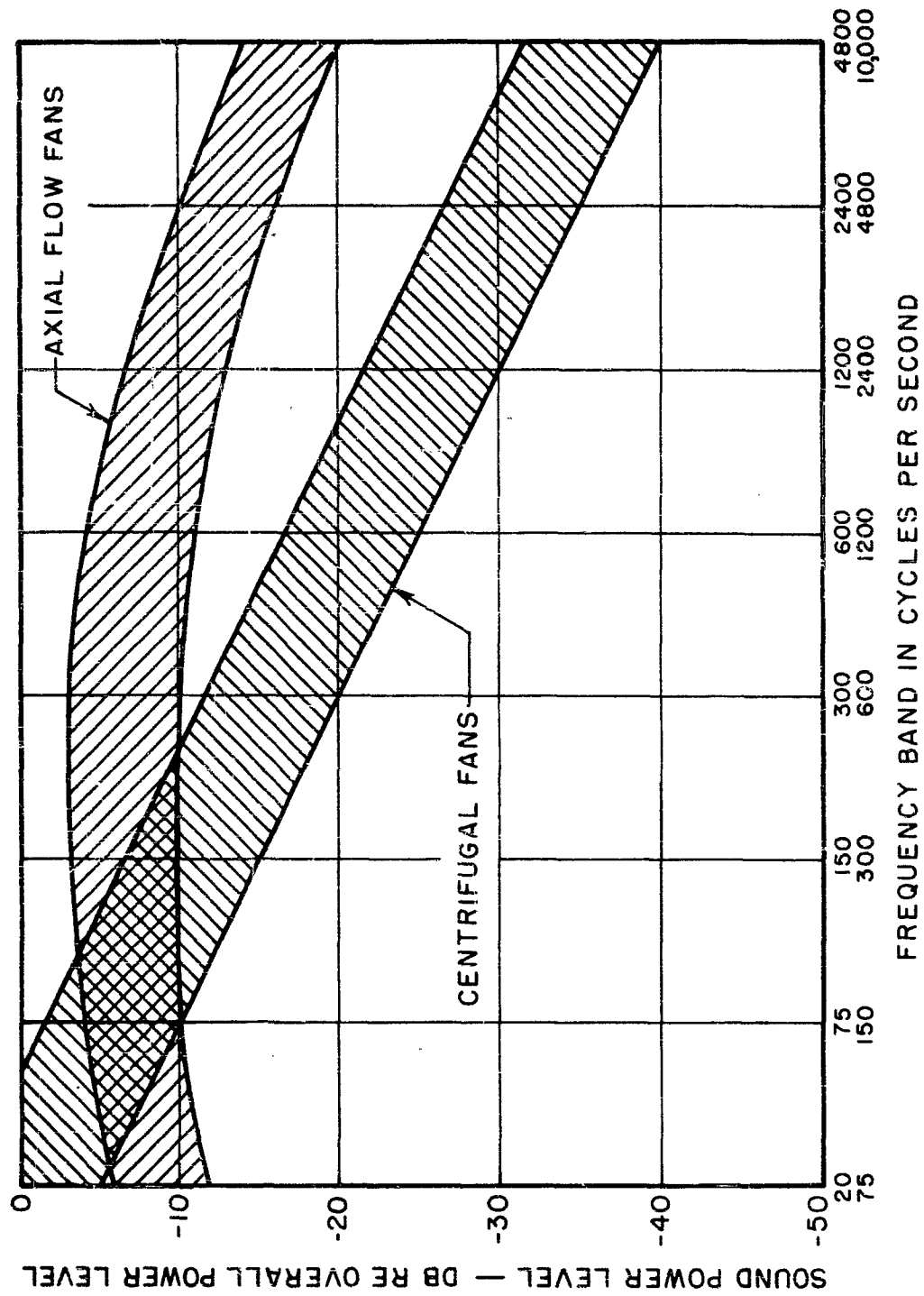


FIG. 102 FAN NOISE SPECTRA

WADC TR 58-343  
 VOLUME II

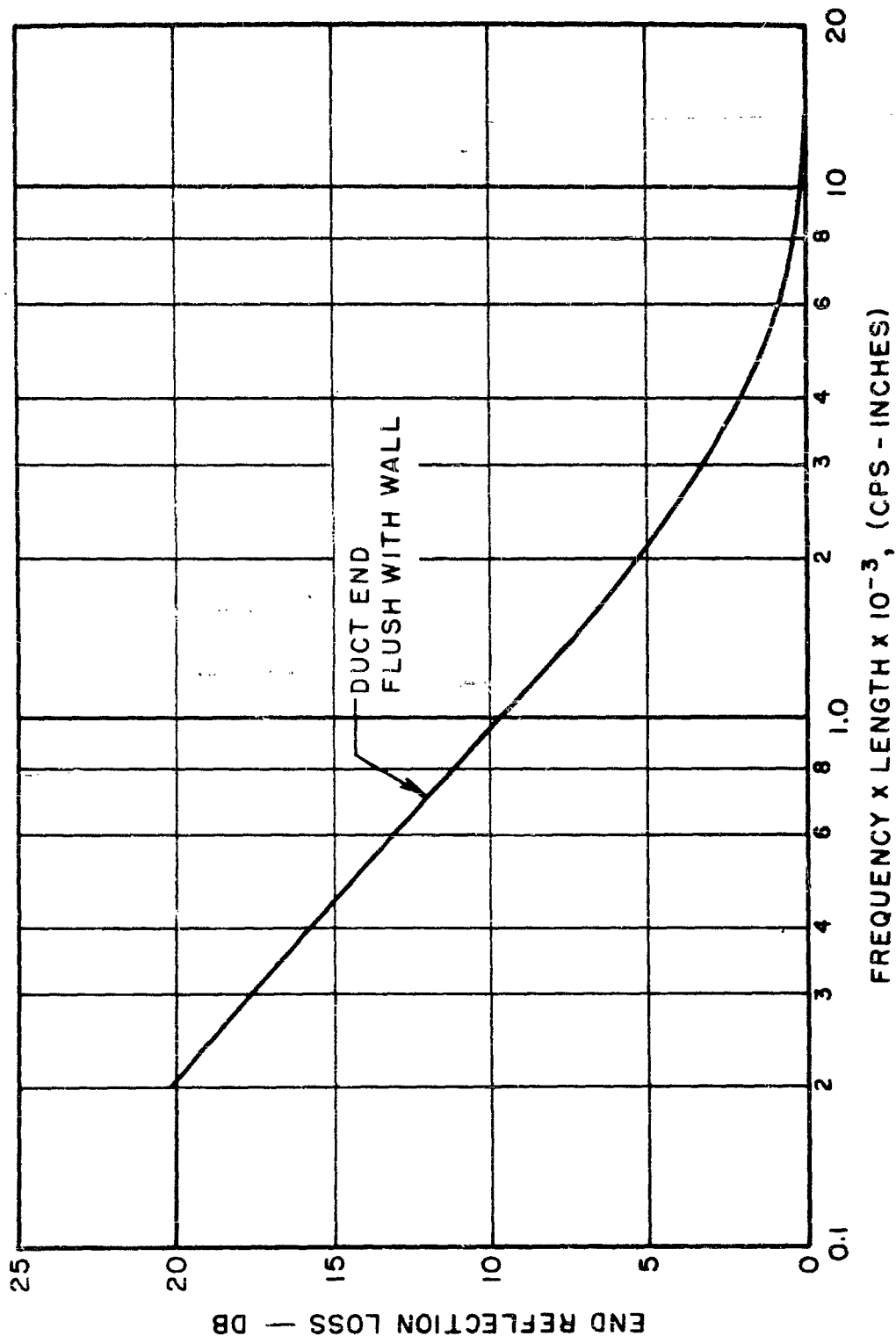


FIG. 103 END REFLECTION LOSS AT THE OPEN END OF SQUARE DUCTS

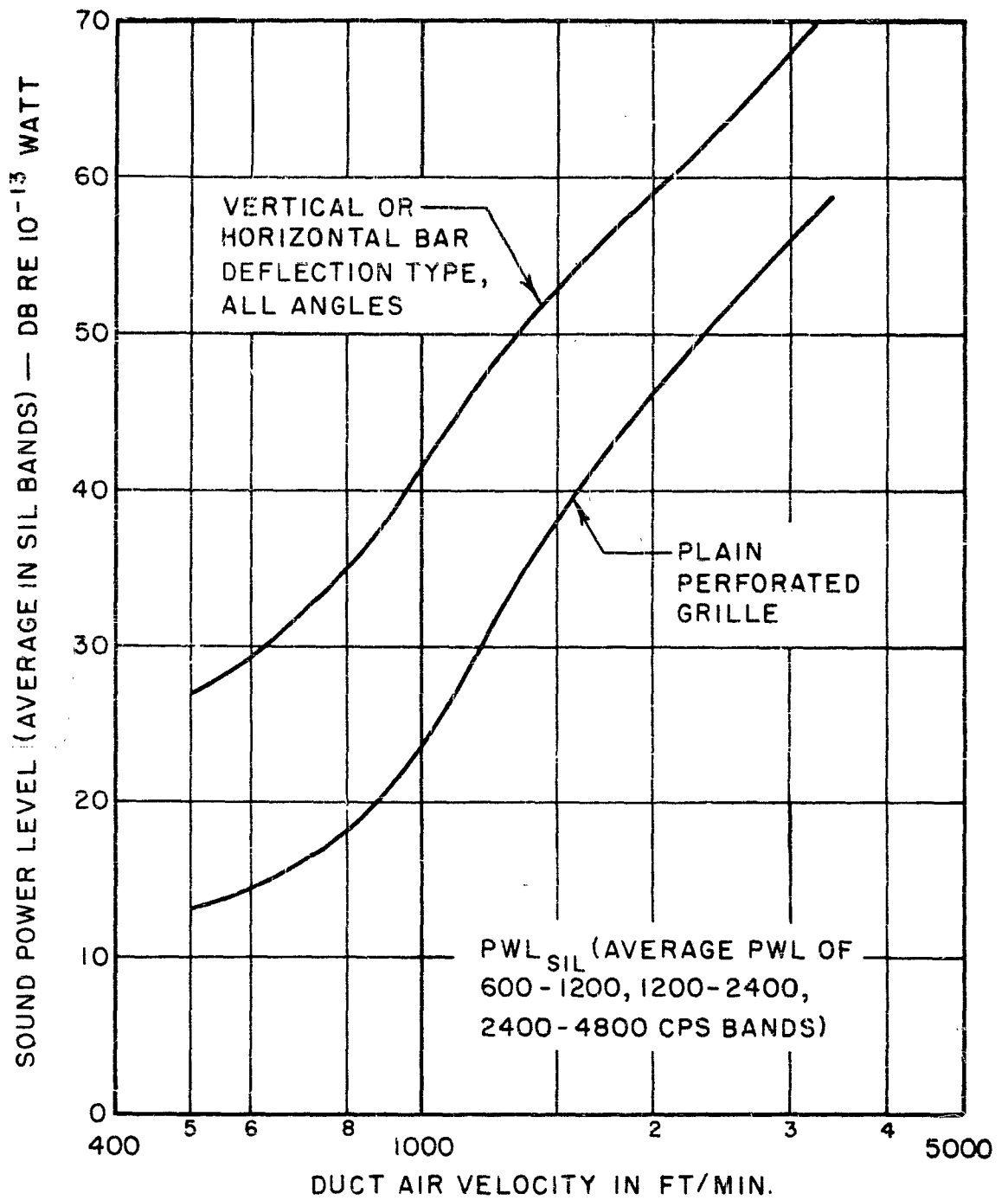
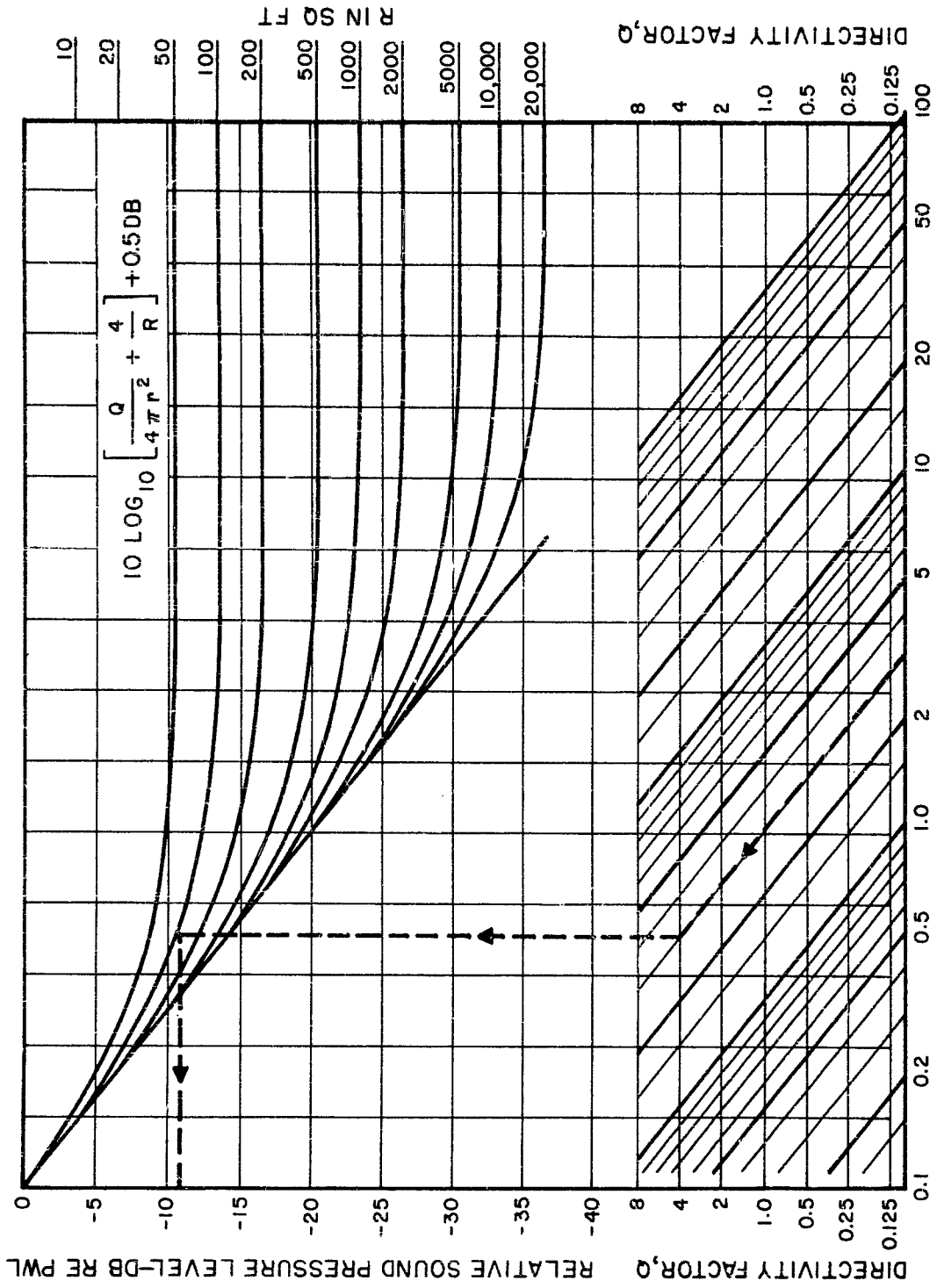


FIG. 104 GRILLE NOISE FOR CORE AREA OF 1 SQUARE FOOT

WADC TR 58-343  
VOLUME II

WADC TR 58-343  
 VOLUME II



$R = \frac{S\bar{\alpha}}{1-\bar{\alpha}}$  = ROOM CONSTANT IN SQ. FT. S = TOTAL AREA OF BOUNDARIES OF ROOM IN SQ. FT.  $\bar{\alpha}$  = AVERAGE ENERGY ABSORPTION COEFFICIENT OF THE SURFACE OF THE ROOM

FIG. 105 RELATIVE SOUND PRESSURE LEVEL IN A ROOM

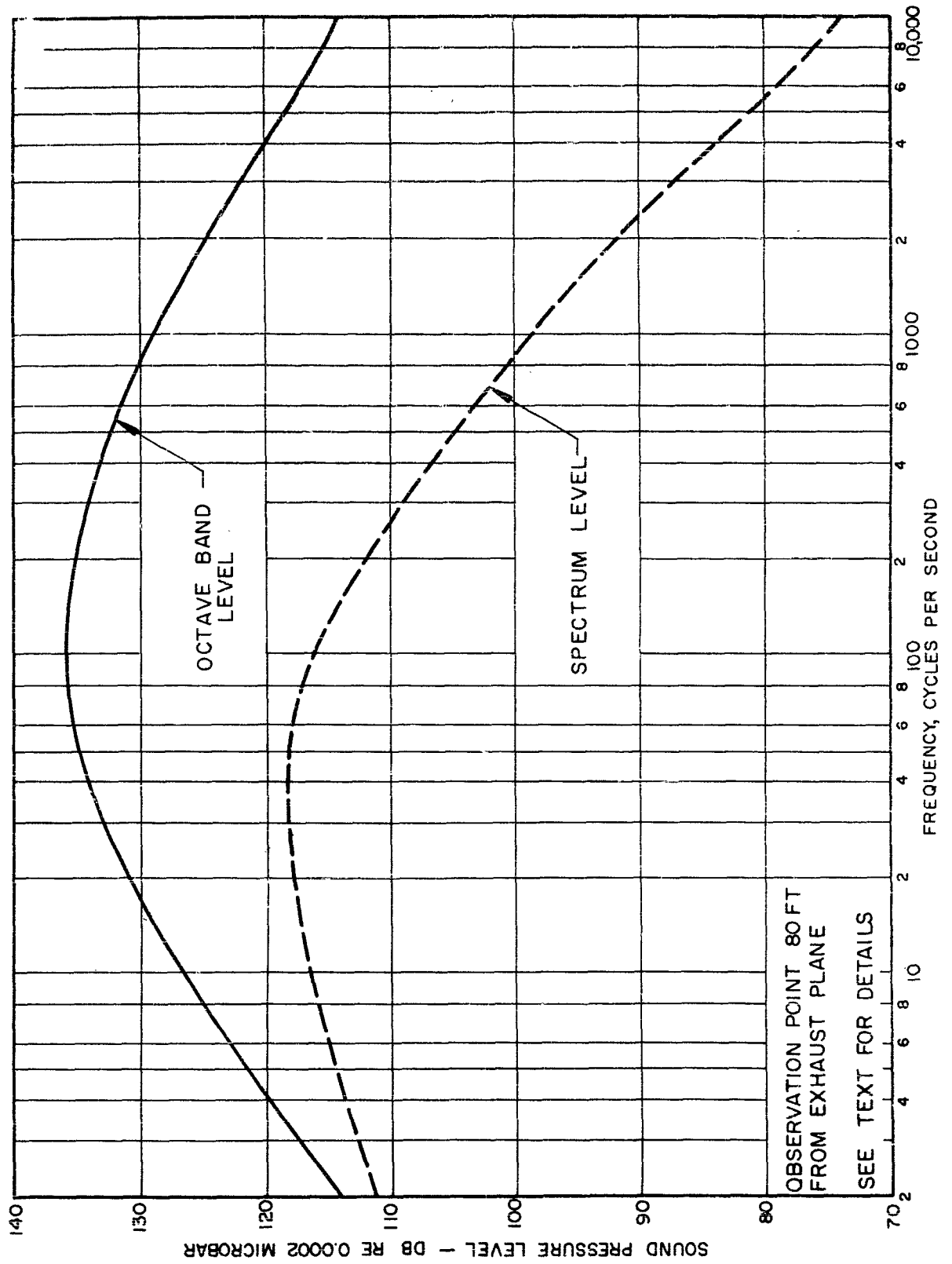


FIG. 106 "FREE SPACE" ROCKET NOISE LEVELS AT LAUNCH.

WADC TR 58-343  
 VOLUME II

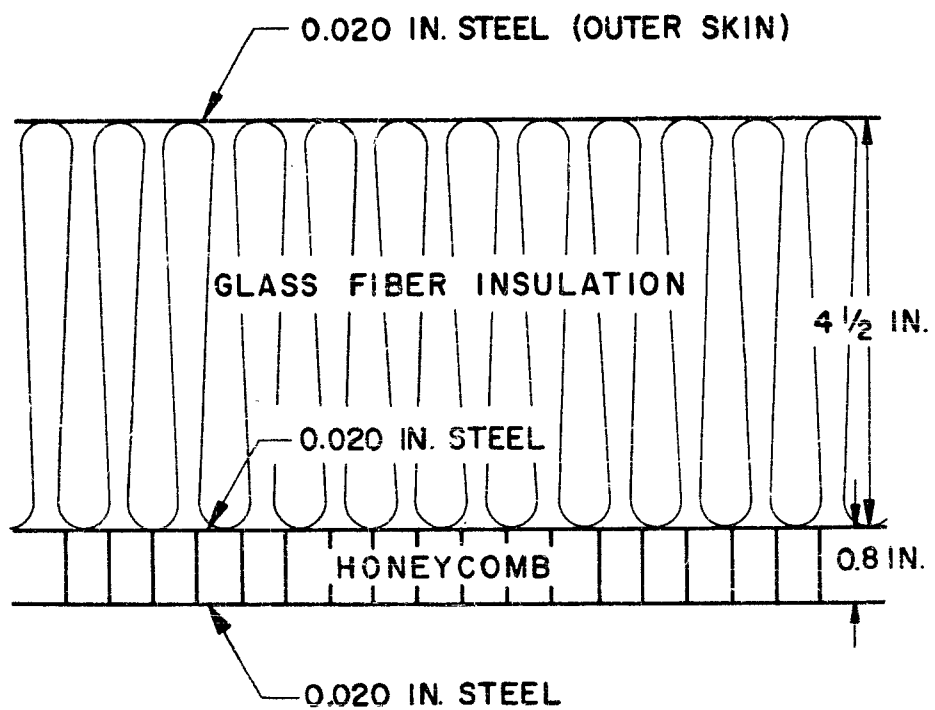
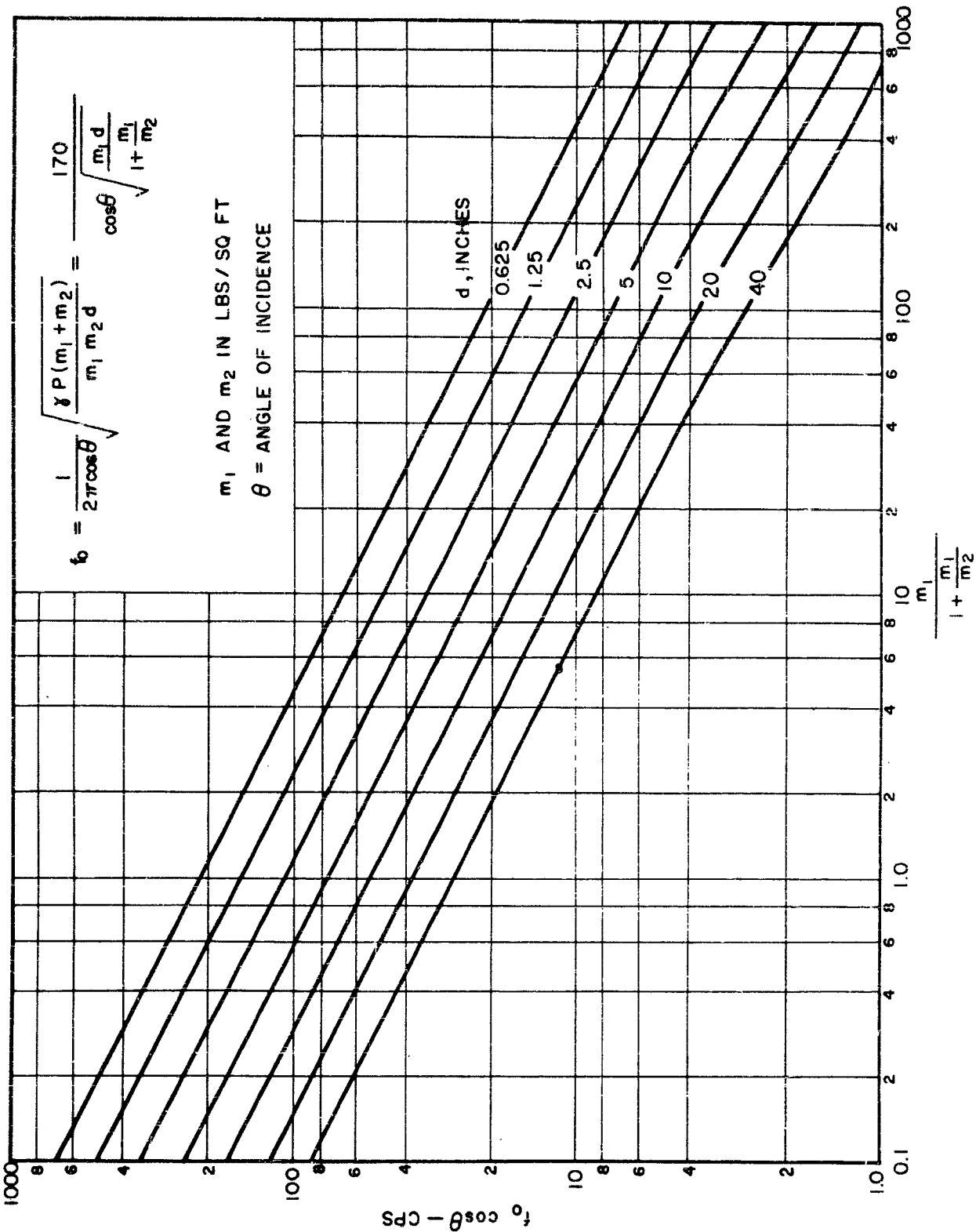


FIG.107 DETAIL OF DOUBLE WALL CONSTRUCTION IN EXAMPLE.

WADC TR 58-343  
 VOLUME II



WADC TR 58-343  
 VOLUME II

FIG. 108 DOUBLE WALL RESONANCE FREQUENCY

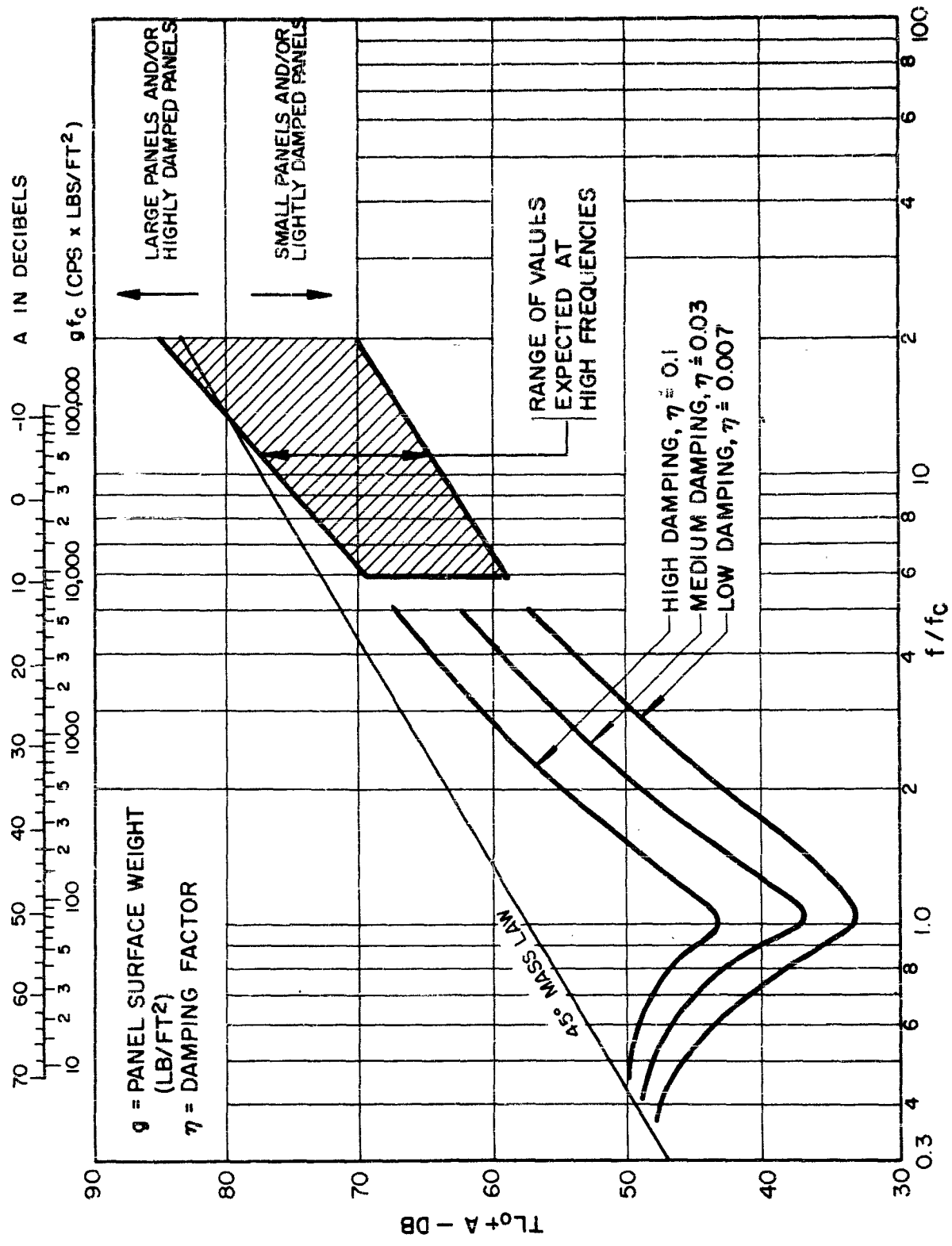


FIG. 109  $TL_0$  FOR PANELS NEAR AND ABOVE THE COINCIDENCE FREQUENCY,  $f_c$ .

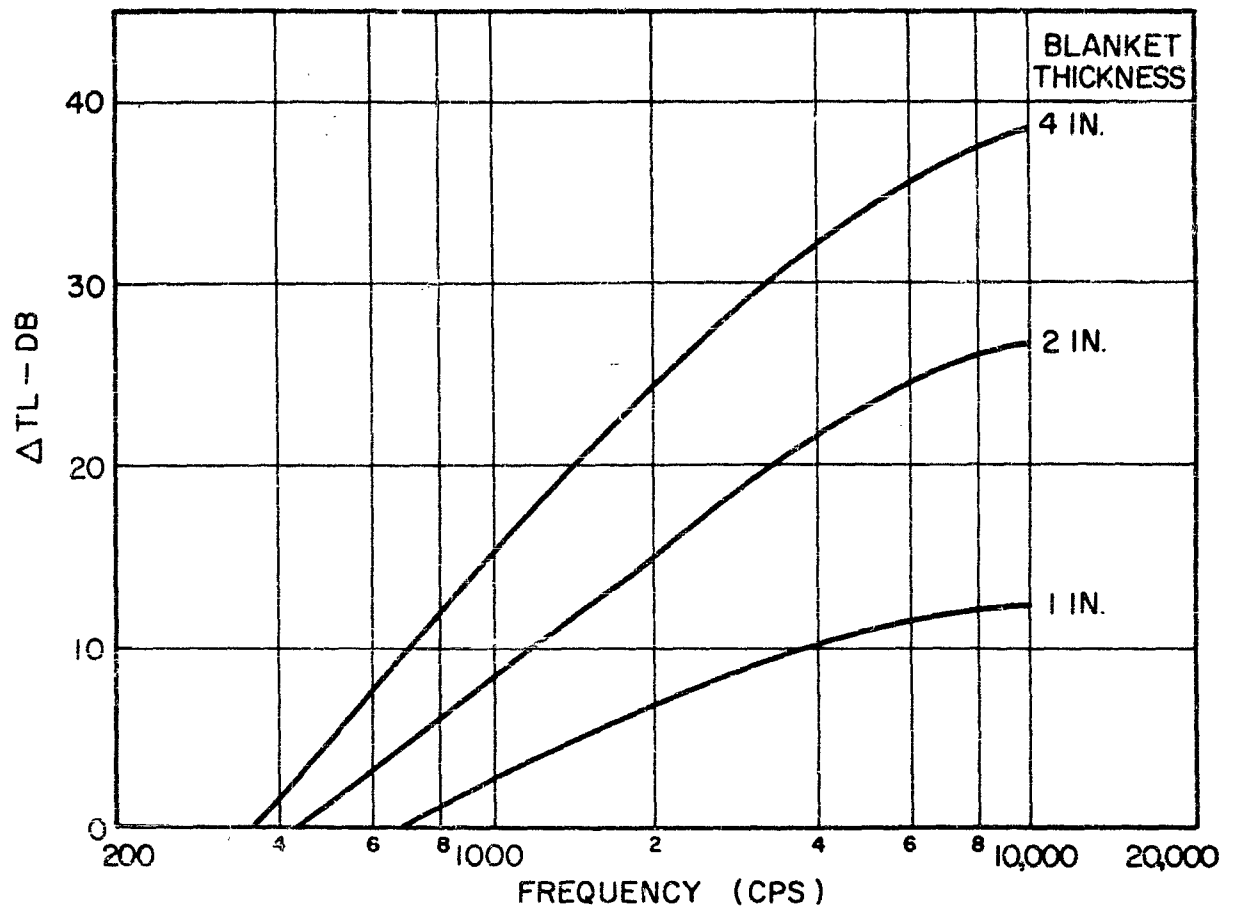


FIG. 110 APPROXIMATE TRANSMISSION-LOSS INCREASE ( $\Delta TL$ ) DUE TO ACOUSTICAL BLANKETS.

WADC TR 58-343  
VOLUME II

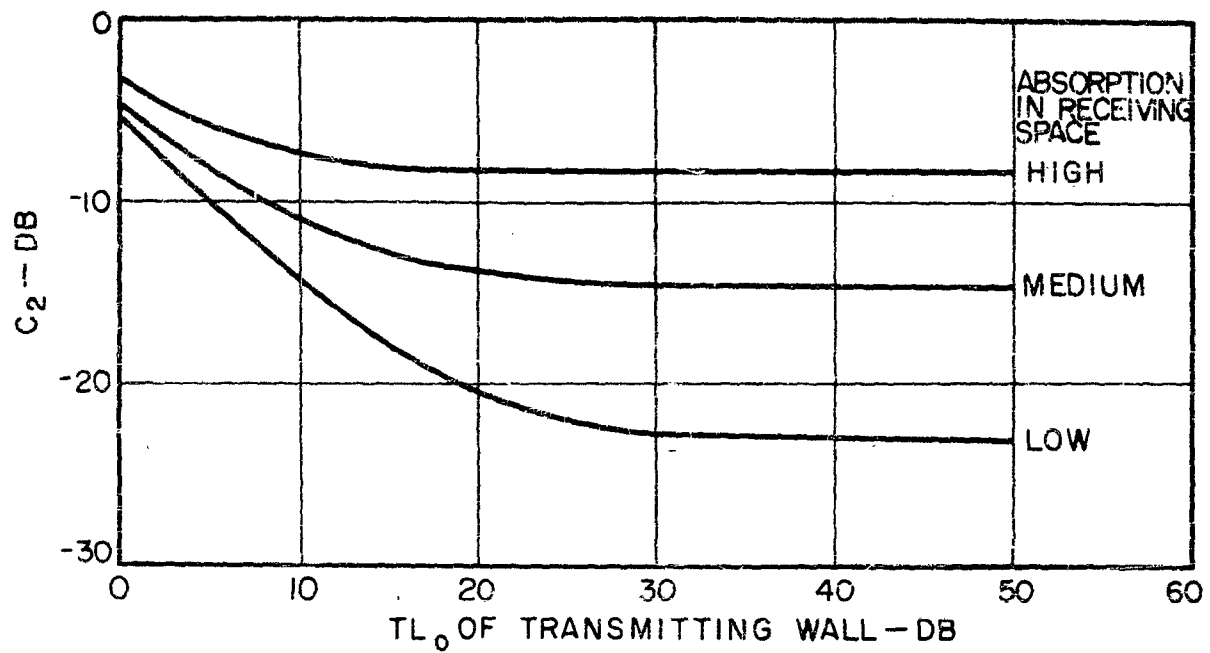


FIG. III  $C_2$ , CORRECTION TO  $TL_0$  FOR MAXIMUM EFFECT OF STANDING WAVES IN MEDIUM-SIZED RECEIVING SPACE.

WADC TR 58-343  
VOLUME II

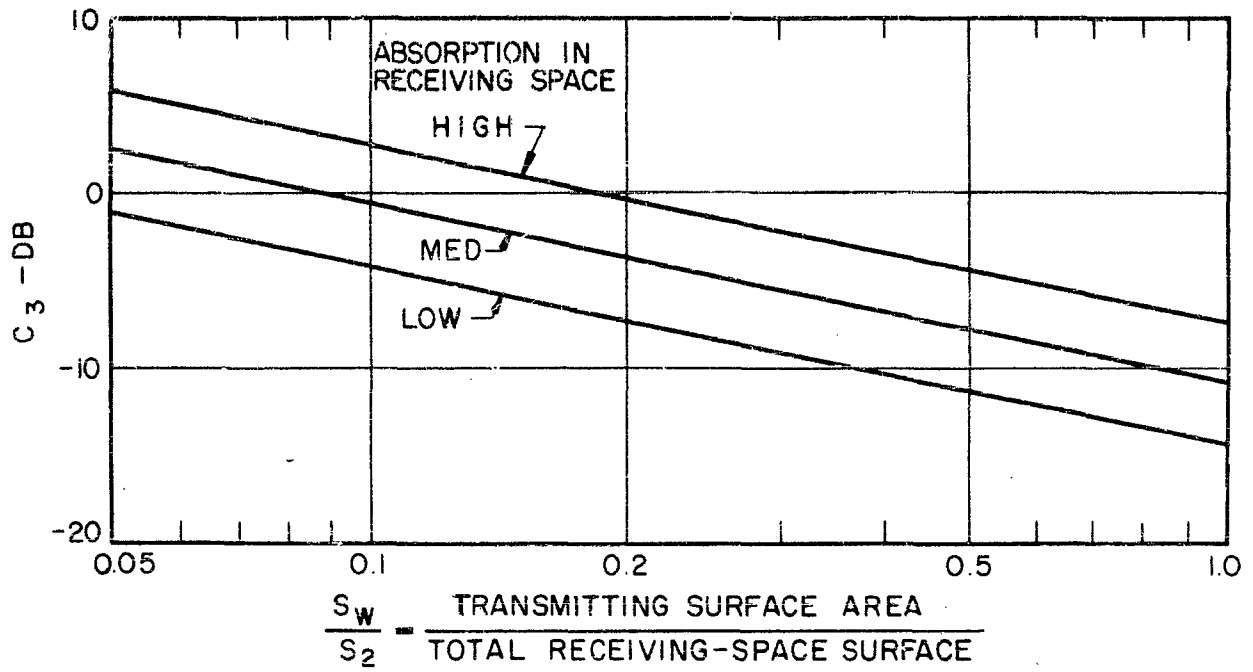


FIG. 112  $C_3$ , CORRECTION TO  $TL_0$  FOR REVERBERATION IN LARGE RECEIVING SPACES.

WADC TR 58-343  
VOLUME II

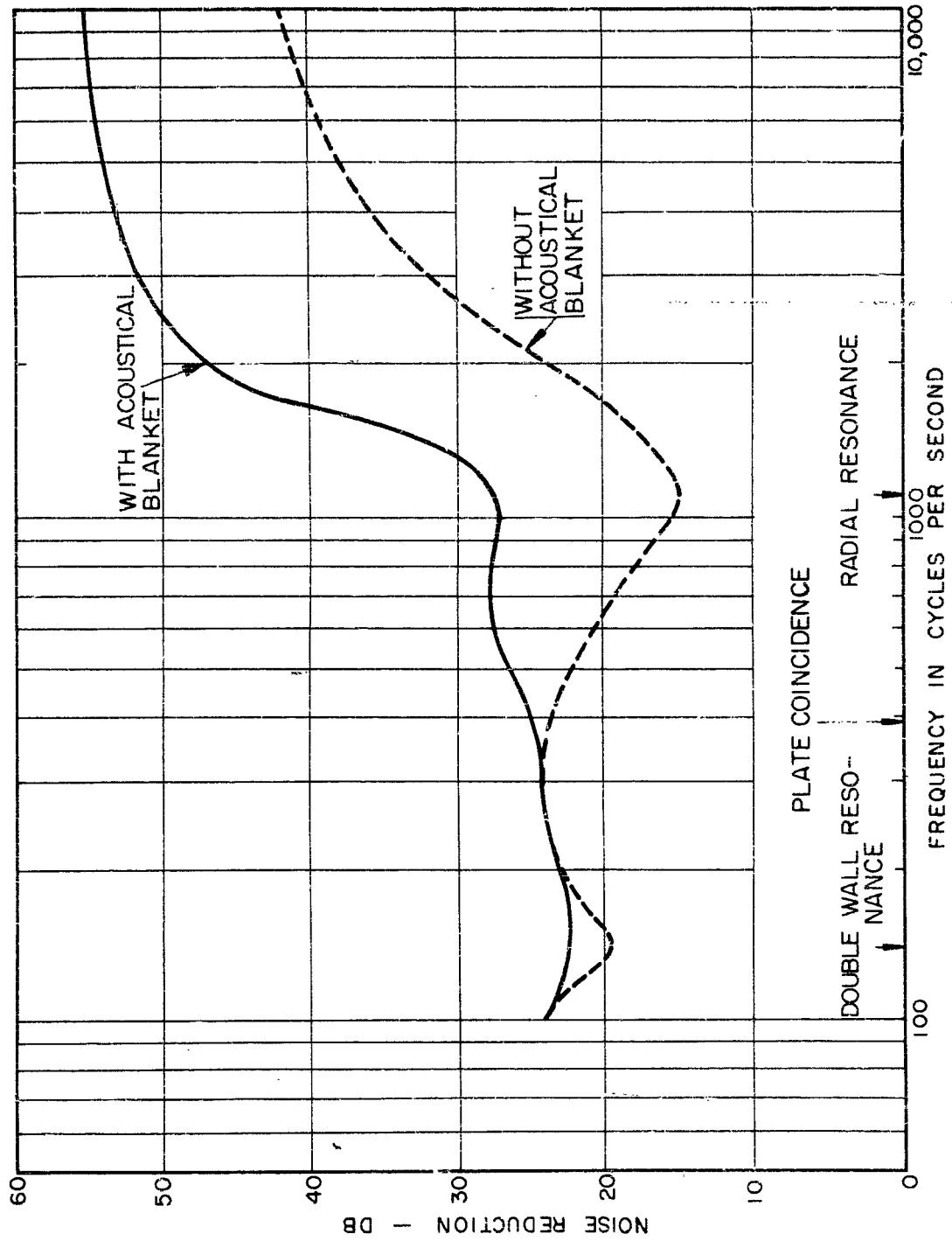


FIG.113 NOISE REDUCTION OF DOUBLE WALL IN EXAMPLE  
(SEE FIG.107 FOR WALL DETAIL)

WADC TR 58-343  
VOLUME II

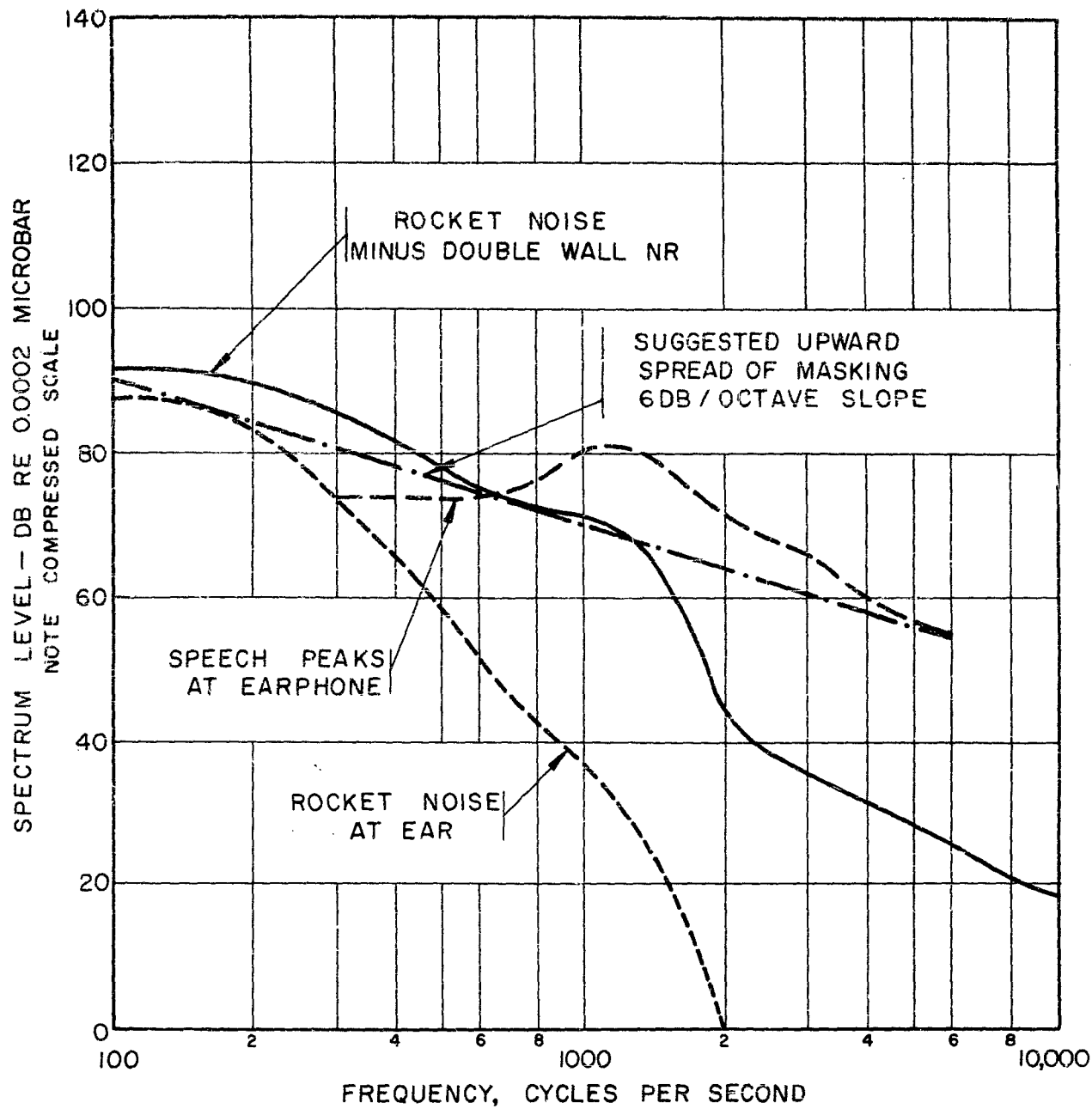


FIG. 114 INTELLIGIBILITY OF RECEIVED SPEECH DURING BOOST.

WADC TR 58-343  
VOLUME II

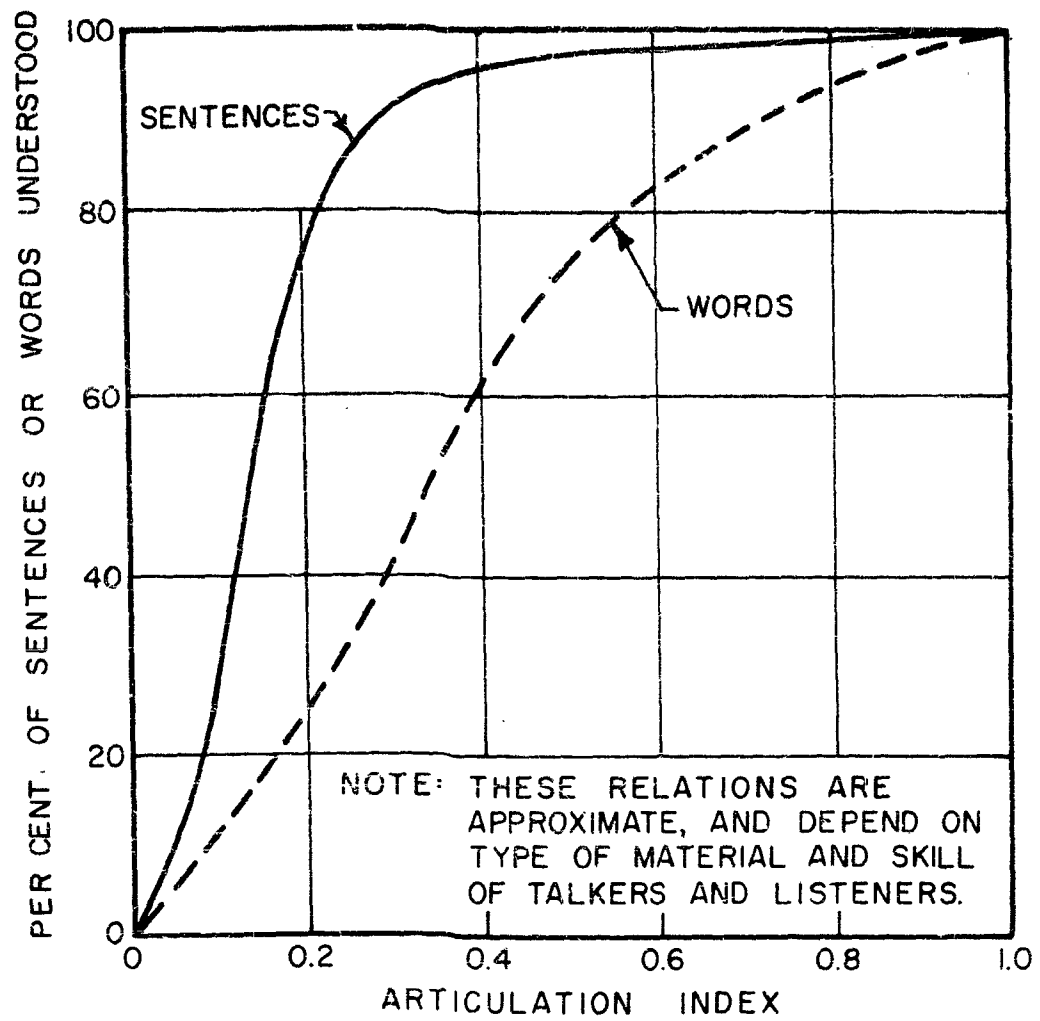


FIG. 115 INTELLIGIBILITY AS A FUNCTION OF ARTICULATION INDEX.

WADC TR 58-343  
 VOLUME II

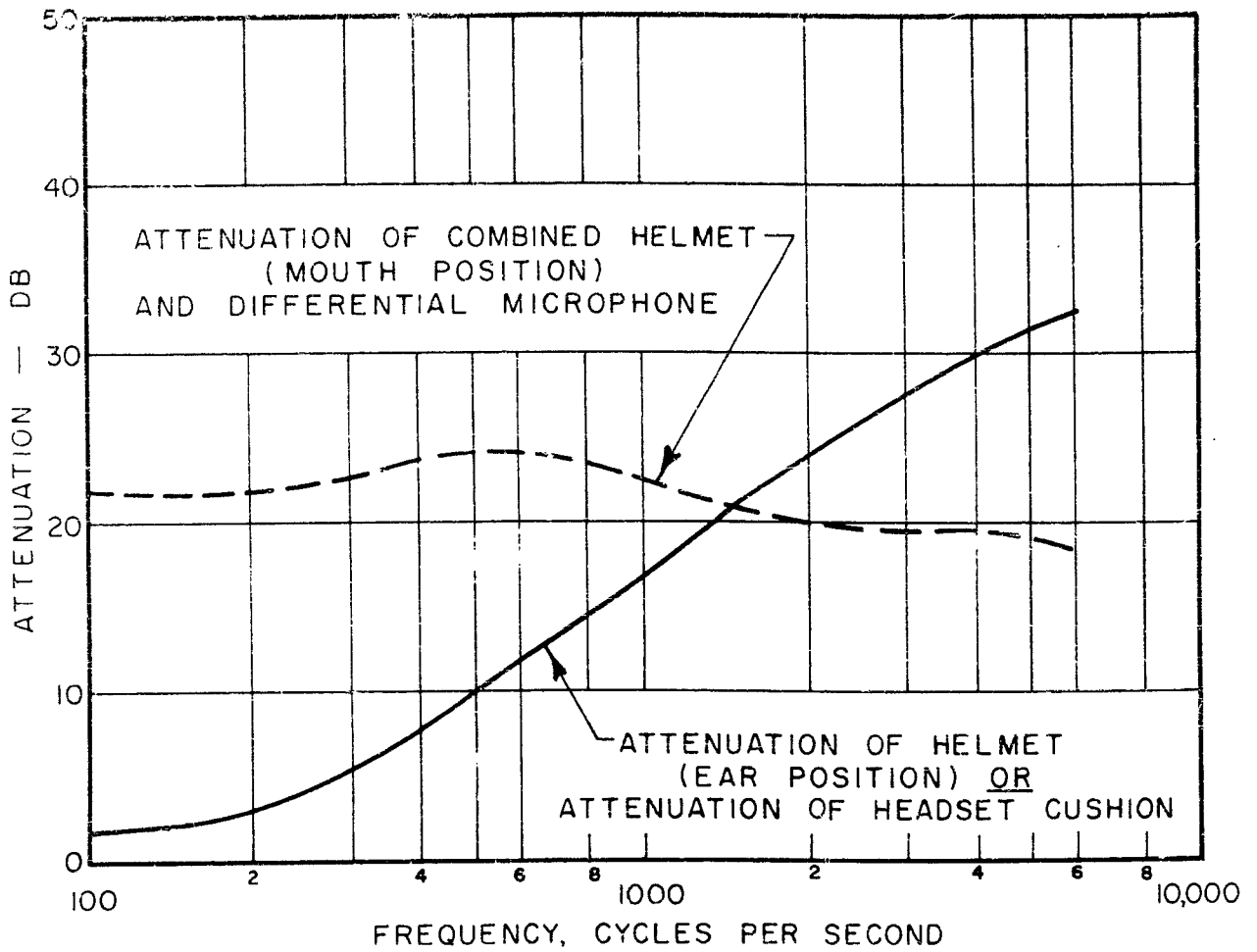


FIG. 116 NOISE ATTENUATION OF PRESENT - DAY HIGH-ALTITUDE HELMET, HEADSET CUSHION AND DIFFERENTIAL MICROPHONE.

WADC TR 58-343  
VOLUME II

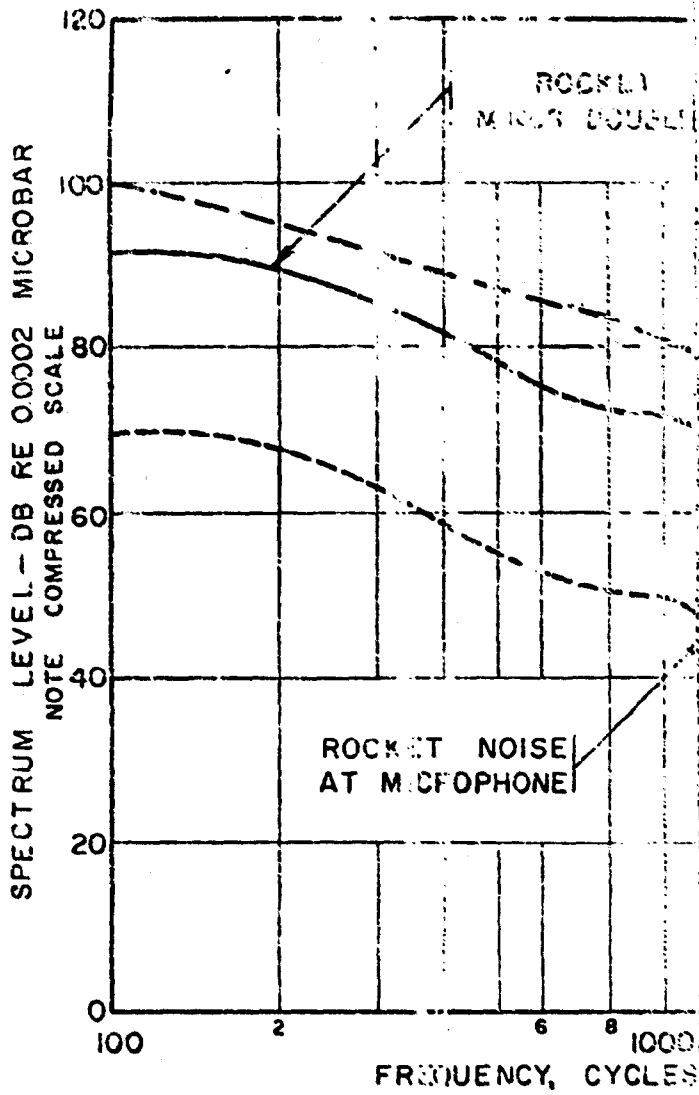


FIG. 117 INTELLIGIBILITY  
SPEECH DUR

WADC TR 58-343  
VOLUME II

Best Available Copy